UC San Diego
UC San Diego Electronic Theses and Dissertations

Title

Developmental mechanisms underlying the formation of ciliated epithelia

Permalink

https://escholarship.org/uc/item/6dk0j32m

Author

Stubbs, Jennifer Louise

Publication Date

2008

Peer reviewed|Thesis/dissertation

UNIVERSITY OF CALIFORNIA, SAN DIEGO

Developmental Mechanisms Underlying the

Formation of Ciliated Epithelia

A dissertation submitted in partial satisfaction of the

requirements for the degree Doctor of Philosophy

in

Biology

by

Jennifer Louise Stubbs

Committee in charge:

    Professor Christopher Kintner, Chair
    Professor William J. McGinnis
    Professor James W. Posakony
    Professor Nicholas C. Spitzer
    Professor Anthony Wynshaw-Boris

2008

The Dissertation of Jennifer Louise Stubbs is approved, and it is acceptable in quality

and form for publication on microfilm:

_____

_____

_____

_____

_____
                                                                                                            Chair

University of California, San Diego

2008

iii

DEDICATION

I would like to dedicate my thesis first to my family, especially my parents Keith and

Debbie Stubbs who have given me constant encouragement, love and support.

Secondly, but just as importantly to my friends, especially to the girls who have been

there with me through the highs and lows and who have been like sisters to me.

Ramlah Nehring, Colleen Noviello, Val Vitkauskas, and Sara Hotchkiss Torgenson,

without you all I wouldn't have been able to endure this journey.

TABLE OF CONTENTS

LIST OF FIGURES

ABBREVIATIONS IN USE

Abbreviation	Definition
'	minutes
CC	ciliated cell
CCP	ciliated cell precursor
DEPC	diethyl pyrocarbonate
DMSO	dimethylsulfoxide
dnHMM	dominant negative mastermind
GFP	green fluorescent protein
GRP	gastrocoel roof plate
hpf	hours post fertilization
IC	intercalating cell
ICD	intracellular domain of Notch
IFT	intraflagellar transport
INC	intercalating non-ciliated cell
KV	Kupffer's vesicle
mGFP	membrane localized green fluorescent protein
MO	morpholino oligonucleotide
mRFP	membrane localized red fluorescent protein
μg	microgram
μl	microliter
mM	millimolar
ng	nanogram
OC	outer cell
PCR	polymerase chain reaction
RFP	red fluorescent protein
RT-PCR	reverse transcription polymerase chain reaction
s.d.	standard deviation
ss	somite stage, zebrafish embryos

ACKNOWLEDGEMENTS

I would like to thank Chris Kintner for being my mentor throughout my graduate career. Chris is unique among most mentors as he still does bench work. Having his direction and advice early on in my education was critical for my development as a scientist. He has spent countless hours sitting with me at the microscopes in the lab helping me peel embryos, teaching me to do transplants or looking at my most recent data. This is something that few students have a chance to experience and I'm grateful to have learned techniques from him firsthand. Chris has also taught me to think critically about science, not just in the fine details, but how it fits in to the bigger picture. My committee members Nick Spitzer, Bill McGinnis, Jim Posakony and Tony Wynshaw-Boris, also John Newport, whose untimely death was a great loss to our department. Thank you for all of your advice and suggestions and thoughtful questions. Finally, I'd like to thank Ed Levine, who not only taught me how to use a pipette, but also gave me a chance to work in his lab and made me realize that I did enjoy doing bench work.

I would like to thank the Division of Biology at UCSD for their constant efforts to make this the best program possible. The faculty and administration are always listening to feedback, and encouraging student involvement in order to achieve this aim, treating us as colleagues, not just as students. I also need to thank my funding sources; grants to Chris Kintner funded most of my studies, also the UCSD

I can truly say that my time in San Diego has been life changing. I have tried many new things and gone on some amazing adventures that I never imagined I would take, and I have made some wonderful friends while doing it. Thanks to Ramlah

Chapter Two is modified from the following publication.

Stubbs JL, Davidson L, Keller R, Kintner C. "Radial intercalation of ciliated cells during Xenopus skin development". Development. 2006 Jul;133(13):2507-15.

I was the primary researcher of these studies and Chris Kintner directed and supervised the research. Lance Davidson assisted in transplant assays time-lapse imaging while in the laboratory of Ray Keller.

Chapter Four, in full, consists of the following manuscript submitted for publication in the journal *Nature Genetics.*

Stubbs JL, Oishi I, Izpisúa Belmonte JC, Kintner C. "FoxJ1 specifies node-like cilia in Xenopus and zebrafish embryos".

I was the primary researcher and author under the supervision and direction of Christopher Kintner. Isao Oishi assisted with all the zebrafish experiments, including injections and analysis, under the direction of Juan Carlos Izpisúa Belmonte, whose lab provided the zebrafish. I also wish to thank Malcolm Wood for his technical assistance with TEM analysis.

Chapter Three and Appendix One consist of other projects I undertook during my dissertation research, I was the primary researcher on this project and Christopher Kintner directed and supervised the research that forms the basis for these sections.

VITA

EDUCATION

2008   Ph.D., Biology, University of California, San Diego

1999   B.S., Biology, University of Utah

1996   High school diploma, with Honors, West High School
                              International Baccalaureate Diploma

WORK EXPERIENCE

2000-2002   Research Assistant, University of Utah

PUBLICATIONS

Stubbs, J. L., Oishi, I., Izpisua Belmonte, J. C., and Kintner, C. The forkhead transcription factor, FoxJ1, specifies node-like cilia formation in Xenopus and zebrafish embryos. Submitted for publication

Stubbs, J.L., Davidson, L., Keller, R. and Kintner, C. (2006) Radial intercalation of ciliated cells during *Xenopus* skin development. Development 133, 2507-15.

Green, E. S., **Stubbs, J. L.** and Levine, E. M. (2003). Genetic rescue of cell number in a mouse model of micropthlamia.: interactions between Chx10 and G1-phase cell cycle regulators. Development 130, 539-552.

TEACHING

BIPN 144 Developmental Neurobiology, Teaching Assistant
Professor Ethan Bier, University of California, San Diego Spring 2005

BICD 131 Embryology Laboratory, Teaching Assistant
Professor Kathy French, University of California, San Diego, Fall 2003

FIELDS OF STUDY

Major Field: Biology

      Studies in Molecular and Developmental Biology
      Professor Christopher Kintner
      The Salk Institute for Biological Studies

      Studies in Genetics and Molecular Biology
      Professor Edward M. Levine
      University of Utah

ABSTRACT OF THE DISSERTATION

Developmental Mechanisms Underlying the

Formation of Ciliated Epithelia

by

Jennifer Louise Stubbs

Doctor of Philosophy in Biology

University of California, San Diego, 2008

Professor Christopher Kintner, Chair

Many vertebrate organ systems contain a specialized ciliated epithelium decorated with motile cilia, which produce a ciliary flow in order to move mucus or fluid across the tissue surface. Examples include the proximal airways of the respiratory tract, oviduct, ependyma of the brain ventricles and the embryonic node. The importance motile cilia function in these specialized tissues to organ function is evident from human diseases such as primary ciliary dyskinesia (PCD) or immotile cilia syndrome. Patients with PCD are prone to chronic respiratory infections, sinus infections, in 50% of cases have *situs inversus* and in rare cases exhibit hydrocephalus. This broad array of phenotypes due to ciliary dysfunction clearly shows the importance of ciliated epithelia to organismal survival. A great deal is known about

ciliary flow and how it relates to tissue function in relation to disease states. However, much less is known about how such tissues are formed during development, and what factors control the formation of cilia in these tissues.

In this work I first describe the morphogenesis of the ciliated external epithelium of *Xenopus laevis* embryos, a tissue that closely resembles the respiratory epithelium in form and function. Cells with motile cilia cover the *Xenopus* embryo in a characteristic spacing pattern. This pattern arises early in development when cells in the inner layer of the ectoderm are selected by Notch signaling to form ciliated cell precursors (CCPs) that then undergo radial intercalation into the outer epithelial layer to form ciliated cells. Inhibition of Notch signaling results in an overproduction of CCPs; while radial intercalation becomes limiting ciliated cells maintain their spacing in the epithelium. Transgenic and transplantation assays to mark ciliated cells and intercalating populations, respectively, indicate that intercalating cells are free to wedge basolaterally, but can only insert apically at vertices where multiple outer cells make contact, likely making apical insertion the rate-limiting step during radial intercalation. Ciliated cell spacing also appears to be influenced by several other factors including competition with intercalating non-ciliated cell populations for vertices, cell morphology, and limitations on apical insertion likely imposed by the outer layer. Suggesting that cells other than the ciliated cells themselves can affect the ciliated cell spacing pattern, and thus final tissue architecture observed in such an epithelium.

In the second part of this dissertation I describe a role for FoxJ1, a forkhead transcription factor, in the specification of node-like cilia in *Xenopus* and zebrafish embryos. Monociliate cells at the embryonic node generate a leftward fluid flow responsible for left-right asymmetry breaking in mouse, fish and *Xenopus* embryos. These cilia share features of both primary sensory cilia and motile cilia found on multiciliate cells, but how these cilia are specified in relation to other cilia is unknown. Using knockdown by morpholino injection, I show that FoxJ1 plays a conserved role in basal body docking in multiciliate cells found on the external epithelium of *Xenopus* embryos. However, in contrast to results in the mouse, I also show that FoxJ1 is required for formation of the node-like cilia in *Xenopus* gastrocoel roof plate (GRP) and zebrafish Kupffer's vesicle. Additionally, I show that misexpression of FoxJ1 is sufficient to induce ectopic GRP-like cilia on the surface epithelial cells of *Xenopus* embryos. Microarray analysis further indicates that FoxJ1 can induce ectopic cilia formation by upregulating the expression of genes required for cilia structure as well as genes required for cilia motility. Together these results indicate that node-like cilia in *Xenopus* and zebrafish are likely generated using a genetic pathway similar to that used to specify cilia in multiciliate cells. The studies presented in this dissertation shed light on the both the morphogenetic events that underlies the formation of the ciliated external epithelium in *Xenopus* embryos, but also on the specification of two different cilia subtypes that form on the epithelia of developing *Xenopus* embryo.

CHAPTER I

Introduction

INTRODUCTION

All multicellular animals develop from a single cell, the fertilized egg. The genetic information carried in that single fertilized egg directs all the developmental decisions that result in the formation of the variety of complex tissues and structures observed in the adult body plan. How organisms arise from a seemingly uniform single cell to form a complex multicellular form with tissues that have diverse functions is the root of developmental biology. One type of tissue that plays diverse roles both in development and adult function, are ciliated epithelia. Cells within such an epithelium extend elaborate microtubule based cilia from their apical surface. The beating of these cilia creates fluid flow across the tissue, which is critical for tissue function. In order to understand how ciliated epithelia are formed, we need both to understand what directs epithelial development in these tissues, as well as what directs cells to form tissue specific structures, such as the cilium.

The goals of this dissertation are first to define the morphological events that underlie the formation of the ciliated external larval epithelium of *Xenopus laevis* embryos and secondly to understand the molecular events that control the specification of cilia in a subset of epithelial cells. This chapter begins with an introduction to epithelial development and ciliated epithelial tissues, followed by a description of cilia and their roles in development and disease, and concludes with a discussion on the formation of the ciliated epithelia in *Xenopus*.

Epithelial Development

Epithelia are tissues that cover both the internal and external surfaces of the body. Epithelia serve several functions that are vital for organismal survival, including protective and sensory roles. As a protective barrier, epithelia block the entry of microbes and pathogens and also serve to protect against environmental insults such as desiccation or mechanical injury (Fristrom, 1988). Located on the external surface of an organism, they are the first cells to interact with extracellular cues such as mechanical stimuli, photons or odorants, and specializations to detect these signals are key to their sensory role (Munger and Ide, 1988). During embryogenesis epithelia undergo a variety of cell movements and reshaping events to attain their adult form (Schock and Perrimon, 2002). Thus, understanding both the morphogenetic and molecular events that control the development of epithelia and result in a specialized functional adult tissue is a key question in embryology.

Epithelial morphogenesis has been broken into several steps (for review see Schock and Perrimon, 2002). First, cells are specified to form different cell types by an array of transcription factors. Second, extracellular signals trigger morphological events within the epithelial sheet or in a subset of cells in the epithelium. Third, cells that are tuned to respond to the extracellular signals execute a morphogenetic program, which involves the coordination of cytoskeletal structure and adhesive properties. Finally, regulation of cell death and cell proliferation can affect the final outcome of morphogenetic events. The mechanisms that can lead to changes in epithelial morphogenesis include cell shape changes, cell intercalation (either lateral or radial), migration, and cell cycle changes. My research has focused on the specification of

specialized cell types in the *Xenopus* external epithelium, and their morphogenesis during radial intercalation, which shapes the final architecture of the tissue.

Epithelia are generally composed of a single cell layer and are defined by having two distinct domains, an apical domain and a basolateral domain (Fristrom, 1988). At their apical side are bands of transmembrane proteins that compose the adherens junctions (AJ). Interactions of AJs proteins within a cell provide sites of actin cytoskeleton attachment, while interactions between AJs of neighboring cells are integral to cell-cell adhesion (Perez-Moreno et al., 2003). AJs also serve to physically separate the apical and basolateral membrane domains. In vertebrates there is an additional, more apically localized, cell junction complex termed the tight junction (TJ) that acts as an impermeable barrier to prevent the passage of molecules through the extracellular space between neighboring cells, thus effectively separating the external and internal milieu (Gumbiner, 1987). Together these cellular specializations ensure that the epithelium provides a physical barrier to the extracellular environment.

Finally, epithelia serve to sense the external environment. Individual cells within an epithelium can be specialized by the expression of chemoreceptors, such as on taste buds of the tongue (Mistretta and Liu, 2006). Epithelial cells also often extend processes, such as microtubule-based cilia into the extracellular environment. These cellular extensions increase surface area and have recently been found to be key sites of cellular receptors (Pazour and Witman, 2003; Salisbury, 2004). In addition they have been shown to sense mechanical stimuli, such as the bending of stereocilia in the inner ear which are key to hearing and balance (Beyer et al., 2000), or bending

of primary cilia in the kidney tubules that sense fluid flow and effect tubule morphogenesis (Bisgrove and Yost, 2006). Epithelia are clearly necessary for organismal survival, thus understanding the mechanisms that control their specification and formation is a fundamental question in developmental biology.

Ciliated Epithelia in Vertebrates

Many vertebrate organ systems contain a specialized epithelium that produces a ciliary flow that acts to move mucus or fluid across the tissue surface. Examples include the ciliated epithelia found in the proximal airways of the mammalian respiratory tract (Stannard and O'Callaghan, 2006), brain ventricles (Banizs et al., 2005), oviduct (Lyons et al., 2006), and in the developing embryonic node (McGrath et al., 2003). In addition to cells decorated with motile cilia it has recently been shown that the majority of post-mitotic cells in mammals, and likely most vertebrates, extend non-motile primary or 'sensory' cilia during the G0 phase of the cell cycle (Wheatley et al., 1996).

The importance of these organelles to organ and tissue function is evident from human diseases such as primary ciliary dyskinesia (PCD) also known as immotile cilia syndrome. Neonates with PCD are prone to chronic bronchitis emphasizing the importance of ciliary flow in the respiratory epithelium as a first line of defense against infection (Carlen and Stenram, 2005). While some patients develop hydrocephalus, likely due to impaired cerebrospinal fluid flow in the brain ventricles (al-Shroof et al., 2001; Greenstone et al., 1984). In addition, affected individuals are often infertile as adults, not only due to sperm immotility but also likely due to defects

in ciliary fluid flow in the oviduct (Carlen and Stenram, 2005). Finally, up to 50% of affected individuals have *situs inversus*, or reversal of the left-right body axis (Eley et al., 2005). Defects in primary sensory cilia in the kidney, liver and pancreas can also cause cyst formation (Fliegauf and Omran, 2006). This broad array of phenotypes and their pleitropic effects due to ciliary dysfunction clearly shows the importance of ciliated epithelia to organismal physiology and survival. Due to the widespread presence of ciliated cells throughout vertebrates, as well as the human diseases now associated with cilia it is paramount that we understand both the morphogenetic events and differential regulation in the formation of these tissues. Thus, we must first understand cilia, including what proteins are necessary for their structure and function, as well as how those proteins are assembled.

Historical Perspective on Cilia

Cilia and flagella are microtubule based hair-like extensions of the plasma membrane that protrude from the cell surface into the extracellular environment. These highly conserved organelles perform a variety of functions and are found decorating the cells of eukaryotes ranging from unicellular green algae to vertebrates (Satir et al., 2007). In unicellular organisms beating cilia are used for movement as well as feeding (Plattner, 2002), while in vertebrate tissues beating cilia move fluid and mucus across tissue surfaces, as in examples mentioned before such as the respiratory epithelium. Furthermore, most vertebrate cells extend a single non-motile primary cilia, which is thought to act as a cellular antenna detecting chemical and

mechanical signals in the extracellular environment (Singla and Reiter, 2006; Wheatley et al., 1996).

In 1684, shortly after the introduction of the compound microscope, Antonio de Heide, first described cilia he observed in the gill of a mussel (in Latin, for review see Rivera, 1962). In 1835 Purkinje and Valentine first observed ciliary movements in the oviduct of vertebrate systems, while later that year Sharpey showed a directionality of ciliary movement in the respiratory system of birds and mammals (see Rivera, 1962). In the late 1890's two independent researchers, Henneguy & Lenhossek, identified three parts to the cilia, including the cilia proper, the basal corpuscle and the rootlets, and were the first to suggest that the basal corpuscle derived from the centrosome (for review see Rivera, 1962). Around this time robust fluid flow was observed on the skin of amphibian embryos and was attributed to the cilia extending from the surface of these epithelial cells (Assheton, 1896). Thus well over a century ago, the ciliated epithelium of frog embryos was identified as a system for studying ciliated epithelia and ciliary flow.

As indicated above microscopists have been intrigued by cilia for several centuries. Extensive studies using both scanning and transmission electron microscopy during the mid-twentieth century has provided additional clues on the ultrastructure of cilia. In 1950 Manton and Clarke first described the structure of the ciliary shaft as being composed of nine peripheral and two central filaments (Manton and Clarke, 1950). In 1954 Fawcett and Porter further described the ciliary shaft, and also noted that the plane of the two central filaments lies perpendicular to the direction

of ciliary beating (Fawcett and Porter, 1954). Using a new fixation technique,

Afzelius first described the arms and spokes that interconnect tubules and connect

outer tubules to inner tubules, respectively in 1959 (Afzelius, 1959). Additionally

Afzelius identified inherent asymmetry that allows for the numbering of the outer

doublets which is useful in identifying ciliary defects (Afzelius, 1979). The majority

of these EM studies focused on multiciliate cells in the respiratory, reproductive and

nervous system of mammals, or the spermatocytes of various organisms due to the

density of material. The large number of cilia on multiciliate cells, as well as the

dense packing of ciliated cells in these tissues made studies of cilia formation and

organization quite fruitful from a purely ultrastructural standpoint, with little

knowledge of the actual molecular components that comprise the cilium.

During this period the presence of monocilia on a variety of tissues was

known, but due to their static nature and relatively rare appearance their presence and

study was largely ignored. Then in 1971 Barnes made the first speculation that

monocilia tended to be $9 + 0$ in structure and appear within tissues of sensory function,

while $9 + 2$ cilia appeared on cells known to have motile cilia (Barnes, 1971).

Additional clues to the importance of primary cilia came from the observation that

primary cilia decorate the dendritic endings of developing olfactory receptor cells

(Menco and Farbman, 1985) and the 1987 study of Cohen & Meininger, where the

tectal primary cilia in the mouse brain were found in a key position at the interface

between ventricular fluid and the cytoplasm of bipolar cells (Cohen et al., 1987).

Recent genetic and molecular studies have shown that non-motile primary cilia are

vital for normal development and physiology in vertebrates (for review see Eggenschwiler and Anderson, 2007).

CILIA STRUCTURE

The description microtubule-based hair like extension suggests that cilia are a simple structure. However, cilia are composed of much more than a microtubule cytoskeleton and have several morphologically distinct regions including the ciliary shaft (axoneme), basal body and ciliary necklace (Figure 1.1A). In the following section I will describe the structure of these distinct regions including their role in ciliary function. Most of the structural information we have is based on analysis of classic 9 + 2 motile cilia. Many characteristics of the ciliary structure are shared among all types of cilia, however there are differences amongst cilia types and I will mention those differences when relevant.

There are two major types of cilia 9 + 2 and 9 + 0, both of which can be motile or non-motile (Afzelius, 2004). The classic motile cilium, referred to as 9 + 2, has two singlet microtubules within an outer ring of nine microtubule doublets. In contrast, the classic non-motile cilium lacks these inner microtubules and is thus termed 9 + 0. Both types of cilia share the nine-fold symmetric microtubule structure that makes up the shaft of the axoneme, whose structure will be discussed in greater detail below.

Axoneme

It has been shown through flagellar isolation and dikaryon analysis of *Chlamydomonas* that the ciliary shaft, or axoneme, contains on the order of 250 unique proteins (Dutcher, 1995; Luck et al., 1977; Piperno et al., 1977). Through

biochemical and electron microscopy studies many of these proteins have been identified and localized within the cilium leading to a clear picture of how specific components are assembled into a mature form. The major parts of the axoneme are the microtubule doublets, the inner and outer dynein arms, radial spokes and the central pair, each of which I will discuss below.

The main structural component of the axoneme is a radially symmetric array of nine microtubule doublets (Figure 1.1B). Each doublet in the axoneme is contains a complete A tubule, composed of 13 protofilaments (Tilney et al., 1973), and an incomplete B tubule composed of 11 distinct protofilaments (Sui and Downing, 2006). In addition to the microtubules that make up the outer ring of the axoneme there are hundreds of other proteins that bind to the microtubules and add structural or functional aspects to the axoneme. For example, nexin, an axonemal protein has been shown to link neighboring doublets and is thought to confer integrity to the cylindrical axonemal shaft, and to prevent buckling of the axoneme when exposed to shear stress (Bozkurt and Woolley, 1993).

The key features of all forms of motile cilia are the inner and outer dynein arms (Holzbaur and Vallee, 1994). Insight into the structure and composition of the dynein arms has come mainly from studies of *Chlamydomonas* mutants that lack specific dynein arm components (Kamiya, 2002; Mastronarde et al., 1992). Dynein arms connect each A tubule to the B tubule of the neighboring doublet with outer dynein arms (ODA) lying closer to the membrane than to the middle of the cilium and inner dynein arms (IDA) found on the luminal side of the axoneme (Figure 1.1B, C).

Dyneins are minus end directed microtubule motors and are thought, in the cilia, to mediate microtubule sliding. While the mechanism is still poorly understood the current model of ciliary motion is that activation of dyneins coupled to a subset of microtubule pairs results in microtubules sliding past their neighbors and, ultimately results in bending of the cilium (Brokaw and Kamiya, 1987; Wargo et al., 2004). Motile 9 + 0 cilia, such as those found in the embryonic node, lack the inner microtubule pair, but have dynein arms (Takeda et al., 1999). However, these motile cilia beat in a vortical motion, rather than with a whip-like stroke, which may be due to the lack of a central pair and radial spokes.

The radial spokes (RS) are projections that extend from each A tubule towards the center of the axonemal shaft, where they intermittently interact with the central pair (Figure 1.1B). Short trypsin treatments of isolated axonemes eliminate nexin links and radial spokes leaving microtubules intact. Upon addition of ATP the microtubule doublets slide past each other resulting in axoneme disintegration (Witman et al., 1978). This observation led to the hypothesis that RS prevent the tubules from continuously sliding past each other and disassembling. A second role for RS may be in controlling the rate of sliding of tubules. Dyneins, in mutants lacking the radial spoke, were shown to move microtubules at only half the rate of dyneins in cilia with intact radial spokes (Smith and Sale, 1992).

The central pair (CP) microtubules found in the center of 9 + 2 motile cilia are structurally distinguishable, and termed C1 and C2 (Figure 1.1C). Projections off C1 and C2 are not symmetric (Adams et al., 1981; Dutcher et al., 1984), yet effectively

surround the central pair, and thus are termed the central sheath (review see Smith and Lefebvre, 1997). A central bridge has also been shown to connect C1 and C2 (Warner, 1976). In many unicellular organisms the central pair has been shown to rotate during flagellar bending. During this rotation the CP must dissociate from the radial spokes, and this disconnecting/reconnecting cycle has been hypothesized as a means of regulating the waveform of the beating cilium (Huang et al., 1982; Omoto and Kung, 1980). Together the CP/RS complex is likely to act as a regulator of cilia beat frequency and waveform.

Basal Body

The nucleating center for every cilium is the basal body, a structure synonymous with the centriole. Indeed in monociliated cells the cilia must be resorbed and the centriole uncoupled from the apical domain in order for the cell to re-enter the cell cycle (Pan and Snell, 2007). The basal body is composed of nine microtubule triplets symmetrically arrayed in a circle (Figure 1.1A). Although the mechanism is unknown, the symmetrical array of microtubules in the basal body is thought to act, as a template for the nine microtubule doublets that make up the ciliary axoneme.

In multiciliate cells several hundred basal bodies must be generated in a relatively short time. Centriole duplication via the centriolar pathway is generally regulated by the cell cycle and is based on the splitting of the mother and daughter centriole pair (Delattre and Gonczy, 2004; Rice and Agard, 2002). Each individual centriole then acts as a template for a new daughter centriole to be generated

perpendicular to the existing centriole. In multiciliate cells some duplication has been attributed to the centriolar pathway. However, the majority of basal bodies (95%) are generated by means of an acentriolar pathway (Anderson and Brenner, 1971). In cells generating basal bodies through the acentriolar pathway, large electron opaque densities with numerous basal bodies at various stages of elongation can be observed in the cytoplasm (Anderson and Brenner, 1971; Sorokin, 1968). Once basal bodies are generated they migrate to the apical surface in an actin dependent fashion (Boisvieux-Ulrich et al., 1990; Dawe et al., 2007).

Basal bodies also associate with many accessory structures. These include the transition fibers, which are electron dense fibers that project from the top 1/3 of the basal body to the plasma membrane (Gibbons and Grimstone, 1960); the basal foot, another electron dense component, which projects laterally from the mid-region of the basal body and reproducibly orients in the direction of the effective stroke of motile cilia (Boisvieux-Ulrich and Sandoz, 1991; Gibbons, 1961); and finally, the striated rootlet, a conical banded filament, that extends from the proximal end of the basal body into the cytoplasm (Hagiwara et al., 1997). The rootlet projects at a 180-degree orientation with respect to the basal foot providing a second cellular read out of cilia orientation. While the precise roles of the basal foot and striated rootlet are not known, it has been speculated that they are involved in anchoring the cilia to resist shear forces during ciliary beating, or in the case of the striated rootlet, may act as scaffolds on which proteins can be moved towards the cilium. The transition fibers, in

addition to an anchoring function, may also act as a checkpoint regulating entry into the cilium.

Ciliary Membrane and Ciliary Necklace

The ciliary membrane is contiguous with, but has been shown to be selectively different, from the cell membrane. This specialization of the membrane may allow it to act as a cellular receptor by distinguishing it from the rest of the cell. Receptors and ion channels have been shown to localize to $9 + 0$ non-motile primary cilia (Corbit et al., 2005; Obara et al., 2006), but until recently it was not clear whether $9 + 2$ motile cilia also had the potential to act as cellular sensors. However two studies from the Christensen group showed that several receptor classes localize to the cilia on the multiciliate cells of the murine oviduct. These receptors include angiopoietin receptors as well as the TRPV4 channel and polycystin-1 and -2 (Teilmann and Christensen, 2005; Teilmann et al., 2006). Thus, it now appears that motile cilia, along with primary cilia, may play a role in cellular signaling.

How are ciliary membranes isolated from the contiguous plasma membrane, such that receptors and other ciliary components are restricted from the rest of the cell membrane? One mechanism might be the transition fibers providing a physical barrier at the distal end of the basal body. Evidence for a second physical barrier, the ciliary necklace (Figure 1.1A), comes from freeze-etch electron microscopy. When ciliary axonemes are examined by such techniques a structure, termed the ciliary necklace, is evident at the base of the cilium just above the transition zone (Gilula and Satir, 1972). This structure is invariable across many species, although the number of strands can

vary from two to six. No specific proteins have been identified within the membrane associated particles that make up the necklace, nor have mutants been found where the ciliary necklace is impaired. However, this structure resembles a physical barrier that that could act to delimit the two distinct parts of the cellular membrane.

In addition to generating all the components necessary to form a cilium, a cell must also transport these components into the cilium. Regardless the ciliary component, all proteins are moved into the cilium by intraflagellar transport.

INTRAFLAGELLAR TRANSPORT

The majority of cilia are generated via compartmentalized ciliogenesis. Compartmentalization requires that all building blocks must be transported from the cytosol into the developing cilium through the process of intraflagellar transport (IFT, Figure 1.2). Consequently, maintenance of cilia also requires IFT. During IFT non-membrane bound structural and signaling components, including the tubulin heterodimers that compose the axoneme itself, are transported via the IFT complex, from the base to the distal tip of the cilium along the ciliary axoneme. Once at the tip cargo proteins are released from the IFT complex, which returns to the base of the cilium, by retrograde motors where IFT particles can then be recycled and used again (for review see Rosenbaum and Witman, 2002). As compartmentalized ciliogenesis is the main mechanism in generating a cilium, it is not surprising that mutations in components of the IFT complex result in a number of diseases pointing to the importance of cilia in cellular function.

Much of our knowledge of IFT relates to the structural components and has come from studies in the green alga *Chlamydomonas*, although a growing number of recent studies have begun to add to our knowledge of IFT in animal systems. Elegant live imaging studies using differential interference contrast (DIC) microscopy in *Chlamydomonas* in the early 1990s initially captured the bi-directional movement of granule-like particles along the length of paralyzed flagella (Kozminski et al., 1993). Electron microscopy studies of the paralyzed flagella also showed lollipop-like structures, now known to be IFT particles, between the outer microtubule doublets and the plasma membrane. Measurements taken from these live images showed that anterograde transport (towards the tip of the cilia) occurs in *Chlamydomonas* at ~2μm/second, while retrograde transport (towards the base of the cilia) occurs at ~2.7-3.5μm/second, indicating the use of different motors for these two functions (Kozminski et al., 1993).

The first motor shown to be required for anterograde motor function was isolated from echinoderm embryos (Cole et al., 1993; Wedaman et al., 1996) and was found to be a heterotrimeric kinesin, termed Kif3 in vertebrates, which is composed of two kinesin related subunits and a kinesin-associated protein (KAP). Further studies on a temperature sensitive mutant of one of the kinesin related motor subunits in *Chlamydomonas* (fla10[ts]) revealed the loss of IFT in both directions following transfer to the restrictive temperature, shedding light on the necessity of anterograde transport to localize retrograde motors to the ciliary tip (Kozminski et al., 1995). Recent studies in *C. elegans* and mouse have identified a second homodimeric kinesin that is also

involved in anterograde transport, known as osm-3 or kif17, respectively (Jenkins et al., 2006; Snow et al., 2004).

The motor responsible for retrograde transport, dynein1b, was initially proposed to be the retrograde motor, as dyneins were known to move towards the minus end of microtubules (Harrison and King, 2000). However, the first molecular evidence for dynein1b having a role in retrograde transport came from loss of LC8, a cytoplasmic dynein light chain, in *Chlamydomonas*. Cilia in *lc8* mutants formed at only 50-75% of normal length and then slowly shortened over time. Retrograde transport was also greatly reduced in these mutants while anterograde transport was normal (Pazour et al., 1998). Loss of dynein1b also results in the formation of cilia with swollen tips, as intraflagellar transport components are stuck at the ciliary tip.

In addition to the motor proteins involved in transporting proteins along the length of the microtubules there are two IFT complexes, referred to as complex A and B, which are thought to mediate interactions between motor subunits and cargo. Complex A is associated with retrograde transport while complex B associated with anterograde transport. The proteins that make up the IFT complexes are often rich in classic protein-protein interaction domains such as tetracopeptide repeats, WD-40 domains, and coiled-coil domains (for review see Kozminski et al., 1995; Scholey, 2008).

THE CILIOME

The complete sequencing of several genomes in the last decade has led many researchers to take a comparative approach to identifying genes expressed specifically

in ciliated cells, or proteins specifically found in the cilium. A comprehensive review of proteomics, genomics and bioinformatics based approaches to identify cilia genes was performed in 2006 by the Leroux group (Inglis et al., 2006) resulting in the compilation of a group of genes termed the ciliome. Resulting from this comprehensive review is a searchable database available online at http://www.ciliome.com that allows researchers to look for genes that have been identified in one or more of the studies performed to identify cilia specific genes.

Bioinformatics studies have taken two approaches: First, two groups have searched the *C. elegans* genome for transcription factor binding sites, using the DNA consensus sequence of *daf-19* a factor implicated in ciliogenesis in *C. elegans*. They identified a number of novel potential cilia genes and showed through promoter driven GFP expression that these novel factors localize to cilia (Blacque et al., 2005; Efimenko et al., 2005). The large number of fully sequenced genomes now available has aided a second bioinformatics approach, comparative genomics. Two groups have reported on similar genomics approaches. In the first of these studies the *Chlamydomonas* genome was compared to other ciliated organism genomes to identify overlapping genes. The overlapping genes were then compared to the genome of a non-ciliated species, and any genes shared with the non-ciliated organism were subtracted. Validation of novel genes was again shown by localization to the basal body and cilia (Li et al., 2004). In the second study the genomes of 6 ciliated and 3 non-ciliated species were compared. Subtraction based on the presence of cilia and type of ciliogenesis, as well as whether motile cilia are present in each species

identified genes common to all ciliated organisms, only those with motile cilia, or those with compartmentalized ciliogenesis (Avidor-Reiss et al., 2004). While these bioinformatics approaches have identified several novel genes they are limited in their scope and will likely fail to identify genes found in large conserved families of proteins, or genes that are also involved in non-cilia functions.

A second method of identifying additional ciliome genes has been to look at the transcriptome, or the pool of transcribed genes, under a variety of conditions in compliment with bioinformatics data. In one example gene expression in FACS isolated ciliated neurons was compared to genes expressed in non-ciliated neurons, muscle or gut to identify cilia genes (Blacque et al., 2005). In a second approach, the Marshall group performed microarray analysis on cells undergoing flagellar regeneration (Stolc et al., 2005). These transcriptome studies have the advantage that they do not limit genes identified by their subcellular localization, and are thus able to identify cellular components not localized to cilia, but necessary for other aspects of ciliogenesis, such as tubulin folding factors and genes involved in transcription (Stolc et al., 2005).

A final method that has been utilized to identify genes of the ciliome involves proteomic analysis of isolated cilia. Studies of this type generally rely on isolation of the cilium, isolation and digestion of individual proteins separated by 2-D gel electrophoresis, and mass spectrophotometry to identify protein components. Additionally, biochemical methods allow for the sub-fraction of cilia components by compartment. Using such fractionation not only isolates novel components, but also

provides information about ciliary localization, which can help establish a functional role for novel components. Such proteomics studies have been performed in several systems (Ostrowski et al., 2002; Smith et al., 2005), but analysis in *Chlamydomonas* has been especially fruitful where identification of proteins that are of low abundance in the cilia has been achieved by using mutant strains lacking highly abundant components of cilia such as dynein arms (Pazour et al., 2005).

Taken together much progress has been made in identification of ciliary components over the last decade. The use of both classic biochemical analyses along with newly developed assays such as microarray technology have identified many novel ciliary components as well as cellular components that are involved in ciliogenesis. Coupling of these molecular, wet lab techniques, with the *in silico* experiments now possible in the genomics era has led to a great expansion in the number of genes known to be involved not only in ciliary structure, but also in formation and maintenance of the cilium.

The structural and transport components that generate a cilium are represented by no less than 250 unique proteins (Dutcher, 1995). The generation of such a large number of proteins during ciliogenesis requires strict regulation at many steps, including the regulation of protein-protein interactions, and protein translation, but also at the transcriptional level. Thus, identifying transcription factors that regulate expression of cilia genes is fundamental to understanding both how an individual cell forms a cilium and how a ciliated epithelium is generated. Recently several transcription factors have been implicated in regulating aspects of ciliogenesis.

TRANSCRIPTIONAL CONTROL OF CILIOGENESIS

The forkhead family of transcription factors is an evolutionarily conserved family of transcription factors that are involved in the development of all three germ layers with roles ranging from specification of cell types in the kidney to brain patterning (Carlsson and Mahlapuu, 2002). One forkhead family member, FoxJ1, has been shown to be required for ciliogenesis in multiciliate cells. FoxJ1 is expressed specifically in the respiratory tract (Hackett et al., 1995; Tichelaar et al., 1999), oviduct (Hackett et al., 1995) and choroid plexus (Lim et al., 1997) of mice, all tissues that have multiciliate cells covering their surface. Targeted gene knockout of FoxJ1 results in the loss of cilia from all of these tissues (Brody et al., 2000). Despite the loss of cilia, ciliated cell fates in these mice are not lost. Instead basal bodies are unable to dock at the apical membrane in multiciliate cells, thus FoxJ1 acts downstream from cell fate specification (Brody et al., 2000).

The phenotype of *FoxJ1* knockout mice has led to a distinction between cells that form $9 + 2$ motile cilia and those that form $9 + 0$ non-motile cilia. Whereas multiciliate cells are lost in *Foxj1* knockout mice, cells such as olfactory neurons that form the sensory cilia are still able to localize basal bodies to the apical cell surface and generate a cilium. However, a third type of cilia are found in the mouse node, an embryonic structure associated with the breaking of early left-right symmetry. Node cilia beat in a rotational manner to generate a leftward fluid flow over the surface of the node (Hirokawa et al., 2006). While their functionality is reminiscent of multiciliate cells in generating fluid flow, they form as monocilia, similar to sensory

cilia in other cell types. Moreover, node cilia at least in the mouse are thought to lack a central pair, thus they resemble non-motile cilia in axonemal structure (Takeda et al., 1999). *FoxJ1* null mice exhibit left-right asymmetry defects despite the presence of cilia at the node, suggesting that there may be functional defects in cilia at the node (Brody et al., 2000). Thus it is not clear how FoxJ1 effects the formation of node cilia, and if there is a distinction between motile and sensory cilia that relies on FoxJ1. Multiciliate cells on the external epithelium, as well as the monociliated cells on the gastrocoel roof plate, a node-like structure in *Xenopus* embryos, express *XFoxJ1* ((Pohl and Knochel, 2004), personal observation), suggesting that FoxJ1 may have a conserved role in controlling ciliogenesis across species.

A second family of transcription factors involved in the formation of cilia has been identified based on mutations in *C. elegans* and *Drosophila*. The loss of *daf-19*, the only RFX family member in *C. elegans,* or *dRFX*, one of two identified RFX members in *Drosophila*, results in the loss of cilia structures in sensory neurons (Dubruille et al., 2002; Swoboda et al., 2000). Furthermore, RFX transcription factors are known to bind to a consensus sequence known as the X-box (Emery et al., 1996). Examination of the upstream regions of known cilia genes in C. elegans revealed a large number of genes with X-boxes while non-cilia specific genes expressed in ciliated sensory neurons failed to have an X-box (Swoboda et al., 2000). Together these results suggest that the expression of cilia components is RFX dependent, while expression of genes necessary for cell-specific functions are not.

There are five mammalian RFX genes, RFX1-5 of which, only *RFX3* has been linked to the formation of cilia. *RFX3* is expressed in only a small subset of ciliated tissues found in vertebrates, the embryonic node (Bonnafe et al., 2004), and ciliated ependyma of the brain (Baas et al., 2006). Loss of *RFX3* by targeted mutation in the mouse results in the formation of stunted node cilia, left-right asymmetry defects (Bonnafe et al., 2004), and hydrocephalus (Baas et al., 2006). Of the remaining four family members mouse knockouts have been generated in two genes, *RFX5* and *RFX4*, which have defects in immune system and brain development, respectively (Clausen et al., 1998; Zhang et al., 2006), while no mouse knockouts for *RFX1* and *RFX2* have been described. Given their critical role in invertebrate cilia formation, it is somewhat surprising that only one RFX family member has been implicated in cilia formation. Multiciliate cells in the developing epithelium of *Xenopus* embryos express *RFX2* (personal observation), suggesting that additional RFX family members may be involved in the regulation of cilia formation in vertebrates.

CILIA IN DEVELOPMENT AND DISEASE

Left-right Asymmetry

It has been well know for centuries, based on anatomical studies, that despite the external bilateral symmetry that most vertebrates display, there is an underlying asymmetry of the internal organs. However, the links between the phenomenon of internal asymmetry and a genetic locus were first discovered only two decades ago when Brueckner and colleagues linked the *inversus viscerum* (*iv*) mouse model to a genetic mutation on chromosome 12 (Brueckner et al., 1989). Prior to these

observations it was known that patients with Kartagener's syndrome had cilia defects leading to sperm immotility, respiratory problems and *situs inversus* (Afzelius, 1976). Despite the lack of ciliary defects in *iv* mice, cilia defects in Kartagener's patient led to the hypothesis that cilia function might be required for the generation of left-right asymmetry in vertebrates.

In 1998 the Hirokawa group made a paradigm-changing breakthrough, showing that there was cilia generated fluid flow in the embryonic node. Kif3b, a component of the anterograde intraflagellar transport motor, was known to be important in the formation of cilia. In an effort to determine what the developmental role of Kif3b was the Hirokawa group generated a targeted knockout mouse. Kif3b null mice are embryonic lethal, however prior to death the embryos reach the stage at which L-R asymmetry can first be assessed. Close examination revealed that *lefty-2* expression was bilateral or missing, as opposed to being restricted to the left side of the embryo. Video microscopy of the embryonic node in wildtype embryos revealed that there was a leftward fluid flow, capable of moving latex beads across the node. While examination of the node in mutant embryos revealed a complete loss of node cilia as well as a loss of coordinated flow (Nonaka et al., 1998). This initial observation of cilia driven fluid flow at the embryonic node provided a platform to begin to understand how dynein mutations and other cilia defects could lead to L-R asymmetry defects.

The observation of motile cilia at the embryonic node, coupled to cilia linked mutations, such as the mutation of left-right dynein (lrd), now known to be the gene

associated with the *iv* genetic locus (Supp et al., 1997), and loss of cilia in the Kif3b

null mouse, led researchers to propose, in a concerted way, that cilia were involved in

L-R asymmetry. In 2002 Essner et al, in a brief communication showed that several

vertebrate model systems express *lrd* in specific locations in the early embryo, and

that monociliated cells reside in those tissues (Essner et al., 2002). These included the

node in mouse, gastrocoel roof plate (GRP) in *Xenopus*, Hensen's node in chick and

Kupffer's vesicle (KV) in zebrafish embryos. Despite this observation in 2002 it was

not until 2005 and 2007 that the KV (Essner et al., 2005) and the GRP (Schweickert et

al., 2007), respectively, were shown to mediate left-right asymmetry breaking through

leftward-generated fluid flow.

Two models have been proposed to explain how cilia generated fluid flow

could lead to L-R asymmetry breaking. The first model hypothesizes that cilia

generated fluid flow results in the formation of a morphogen gradient, by

concentration of an extracellular signal on one side of the node or by the deposition of

signaling molecules on the left side of the node (Figure 1.3A). In 2005 the Hirokawa

group (Tanaka et al., 2005) showed that small (0.3-5um) nodal vesicular parcels

(NVP) that are immuno-positive for Sonic hedgehog (Shh) and retinoic acid (RA) bud

off of nodal cells and are transported by nodal flow to the left side of the node where

they disintegrate upon hitting the far wall of the node. Based on these observations

they have proposed this as a mechanism that would account for the creation of a

morphogen gradient, even when the morphogen is lipophilic as is the case for Shh.

Such a morphogen gradient could then account for expression of downstream targets, such as nodal, on one side of the node.

A second model proposes that motile cilia in the middle of the node generate a leftward fluid flow, leading to bending of non-motile cilia on the edge of the node. Bending of these cilia leads to Ca^{2+} influx due to the opening of axonemally localized cationic polycystin-2 channels, which have been shown to be involved in mechano-sensation in kidney tubules (Bisgrove and Yost, 2006; Eley et al., 2005). This would result in asymmetric intracellular Ca^{2+} levels across the node (Figure 1.3B). The presence of Ca^{2+} in a subset of cells is then thought to lead to changes in gene expression only on the left side of the node. Evidence for this model was provided by the Brueckner group (McGrath et al., 2003) when they discovered two populations of node cilia using transgenic expression of an *lrd-GFP* fusion protein coupled with polycystin-2 immunolocalization. The more centrally located cilia are *lrd* and *polycystin-2* positive, while more anteriorly and laterally located cilia are only *polycystin-2* positive. Additionally, using a Ca2+ sensitive dye they reported increased intracellular calcium on the left side of the embryo. While the mechanism by which L-R asymmetry has still not been worked out in fine detail in all vertebrate organisms, it is clear the cilia and/or their components are key players in tissues where L-R asymmetry is first detectable in many vertebrate systems.

Primary Ciliary Dyskinesia

Primary ciliary dyskinesia (PCD) is also referred to as immotile cilia syndrome and includes a former group of diseases diagnosed as Kartagener's syndrome

(Afzelius, 1979). PCD has an incidence of approximately 1 in 20,000 individuals. Patients who suffer from PCD present with a wide range of symptoms that include recurrent upper and lower respiratory tract infections, sinus infections, *situs inversus*, male infertility, and in rare cases hydrocephalus or cystic kidneys. Regardless of the symptomatic manifestations all PCD patients have been shown to have immotile, dysmotile or absent cilia. Diagnosis can be linked to clinical results, such as nitric oxide levels in exhaled air, but is definitively diagnosed based on electron microscopic examination of cilia (for review see (Carlen and Stenram, 2005)). Up to 80% of effected individuals have reduced or absent dynein arms, while 10% show absence or dislocation of the central pair tubules (Jorissen et al., 2000). Due to the large number of proteins that make up the axoneme mutations in a number of genes can result in PCD (Blouin et al., 2000; Zariwala et al., 2007).

CILIATED EPITHELIA IN XENOPUS

The *Xenopus laevis* embryo provides a good model system for studying the formation of ciliated epithelia and specification of cilia subtypes. Ciliated cells with motile monocilia can be found decorating the epithelium lining the gastrocoel roof plate (GRP) immediately post-gastrulation (stages 13-19), while a second population of ciliated cells (CC), each with hundreds of motile cilia, form on the external epithelium during tailbud stages (stages 20-28) and continue decorating the epithelium into tadpole stages (stage 45). *Xenopus* embryos also lend themselves well to studies of developmental and cell biology due in part to the large size of embryos (1mm) and their rapid external development.

The GRP derives from cells contiguous with the external epithelium. Cells that give rise to the GRP lie near the bottle cells that initiate gastrulation at the dorsal blastopore lip (Keller et al., 2003). These cells follow the bottle cells into the blastopore, expand dorso-anteriorly, and finally come to lie on the dorsal side of the archenteron (Shook et al., 2004). Immediately after gastrulation (stage 14) GRP cells begin to extend cilia from their surface and over the course of several hours these cilia lengthen, move posteriorly on the cell surface, begin beating and create a leftward fluid flow (Figure 1.4A). Blocking fluid flow by injecting viscous solutions into the gastrocoel results in defects in left-right asymmetry (Schweickert et al., 2007). This observation is the first to link ciliary fluid flow with the generation of left-right asymmetry in Xenopus embryos.

The external epithelium of Xenopus laevis embryos derives from the non-neural ectoderm, and begins to take on its larval form during late gastrulation stages (stage 12). At least two specialized cell types, including ciliated cells, are selected as precursors in the inner or sensorial layer of the ectoderm through Notch mediated lateral inhibition (Deblandre et al., 1999; Drysdale and Elinson, 1993). These precursor cells undergo radial intercalation or egression, to join the outer cell layer beginning at stage 16 (Figure 1.5; (Stubbs et al., 2006)). By stage 28 ciliated cell differentiation is complete and cilia extending into the extracellular fluid are generating a vigorous fluid flow (Figure 1.4B, C).

This vigorous directed fluid flow is likely to have two functions in the developing embryo: First, *Xenopus* embryos are quite large, but do not have external

gills or means of respiration until tadpole stages, or several days after fertilization. Ciliary flow across the embryo is likely a means of moving cellular waste and oxygen poor water away from the embryo, and bringing more oxygen rich water in contact with the embryo. Second, mucus, which is constantly being secreted by the non-ciliated outer cells, acts as a first line of defense by trapping potential pathogens. Ciliary flow assists in this protective role by moving the mucus off the surface of the embryo. In this aspect, of mucociliary flow, the external epithelium of *Xenopus* embryos closely resembles the mammalian respiratory epithelium (Deblandre et al., 1999; Konig and Hausen, 1993; Montorzi et al., 2000).

Over the course of development a variety of morphogenetic events effect the formation of the *Xenopus* epithelium. Early in development during gastrulation, the embryo employs a combination of cell shape changes, along with egression of the inner cell layer, in order to undergo epiboly, a flattening and expansion of the embryonic epithelium that allows cells from the involuting marginal zone (IMZ) to migrate from the outside of the embryo into the interior of the embryo (Keller et al., 2003; Keller, 1980). Following gastrulation the embryo expands along its anterior-posterior axis through another well-studied cellular rearrangement, convergent extension (for review see Wallingford et al., 2002). Within the epithelium, convergent extension is mediated by lateral intercalation, whereby individual cells within a flat sheet move past each other in a lateral direction to convert a wide sheet into an elongated sheet. Later, in contrast to convergent extension movements, the post-

gastrulation external epithelium appears to mainly be remodeled by radial intercalation.

Few studies have been performed looking at radial intercalation in the formation of an epithelial sheet, as it appears to be an infrequent phenomenon during development. Studies on radial intercalation have focused on earlier stages of *Xenopus* development, during epiboly when inner cell layers radially intercalate to thin out the epithelium (Keller, 1980), or on the process of leukocyte transepithelial migration where leukocytes move through junctions in the vascular endothelium (Luscinskas et al., 2002a; Luscinskas et al., 2002b). However in the case of epiboly, inner cells do not join the outer epithelium, and in the case of leukocytes, cells only migrate through the epithelium, but fail to become integral members of the epithelial layer (Porter, 2008). By stark contrast, during radial intercalation in the post-gastrulation *Xenopus* embryo, specialized cells that originate in the inner cell layer migrate into the outer cell layer where they form adherens and tight junctions with outer cells, all while maintaining epithelial integrity.

There are two cell types that undergo radial intercalation in *Xenopus laevis* embryos, ciliated cells (CC) and intercalating non-ciliated cells (INC) (Stubbs et al., 2006). One striking feature of radial intercalation in the *Xenopus* epithelium is a spacing rule, in which no two ciliated cells lie next to each other in the outer epithelium. In addition to understanding how cells move into and become incorporated into the outer layer determining how this spacing rule is generated is equally important in understanding how this tissue develops. Notch signaling has

been shown to negatively regulate the formation of ciliated cells in the epithelium (Deblandre et al., 1999) and thus provides a starting point for studies in the formation of this epithelium.

Notch Signaling in Development

Cell fate specification is driven by signal transduction pathways that combine both intrinsic and extrinsic cues. Intrinsic cues are the transcription factors a cell expresses during its development, while extrinsic cues are the signals that coordinate cell state transitions both within and between cells. The Notch signaling pathway is one such signal transduction pathway that has been studied in detail in a number of model organisms, but has been best described in the fruit fly, *Drosophila*. Here I will discuss the components as they apply to *Drosophila*.

Notch is a membrane bound receptor that is activated by interactions with its ligands Delta and Serrate on neighboring cells. Upon activation, the intracellular domain (ICD) of Notch translocates to the nucleus where it interacts with its transcriptional co-factor Suppressor of Hairless (Su(H)) to turn on the transcription of target genes (for review see Bray, 1998; Fiuza and Arias, 2007). Since the ligands Delta and Serrate interact with Notch in *trans*, they provide a mechanism whereby neighboring cells can communicate with each other and effect cell fate specification in *trans*. Thus, Notch signaling is often involved in cell fate choices within a population of cells.

Cell fate decisions, via Notch signaling, can be modulated by lateral inhibition or asymmetric cell division. Lateral inhibition is a process, whereby a group of cells,

all with the same developmental potential, interact such that a single cell or subset of cells adopts a specific fate. The cells that adopt the given fate act to suppress the same fate in their neighbors. One well-characterized example of lateral inhibition is the formation of the sensory organ precursor (SOP) in *Drosophila*. All the cells in a proneural cluster are competent to adopt a neural fate, but amplification of subtle differences between cells within proneural clusters results in one cell expressing higher levels of Delta, concomitant with expression of higher levels of proneural genes. Neural fates are then suppressed in neighbors by the activation of Notch signaling and downregulation of proneural genes (for review see Bray, 1998; Fiuza and Arias, 2007).

Notch mediated lateral inhibition has been shown to direct the formation of tissues with a salt-and-pepper pattern in several systems (Crowe et al., 1998; Liu et al., 2007) including the selection of ciliated cell precursors (CCPs) in the external epithelium of *Xenopus* (Deblandre et al., 1999). In the wildtype situation the ciliated cell spacing rule is likely to be partially mediated by lateral inhibition, such that CCPs inhibit their neighbors from also becoming CCPs. However, when Notch signaling is blocked and ciliated cell precursors are overproduced the spacing rule still applies, suggesting that other factors, in addition to Notch signaling must effect the final spacing pattern of ciliated cells in *Xenopus*.

SUMMARY

The *Xenopus* embryo, with its external epithelium decorated with multiciliate cells (Figure 1.4C), which are negatively by the Notch signaling pathway, provides an

excellent model system for studying cell both fate specification and morphogenetic processes related to radial intercalation. The second chapter of this dissertation focuses on both these issues. I describe the cellular events that underlie the radial intercalation of two populations of cells in the *Xenopus* skin, ciliated cells and non-ciliated cells. I then go on to show that Notch signaling negatively regulates the formation of both populations and explore the morphogenetic consequences of overproducing these cell types. The observations elucidate some of the physical constraints that affect the ability of ciliated cells to intercalate, and contribute to the spacing rule observed by ciliated cells.

In the third chapter of my dissertation I further explore the role of morphogenesis in the *Xenopus* ciliated epithelium. I discuss the study of a transmembrane protein, Basigin, a protein involved in tumor cell metastasis and matrix metalloproteinase production. I show that Basigin is expressed in a subset of cells in the Xenopus epithelium, and its expression level responds to perturbations in Notch signaling in a manner that parallels the responses of intercalating cell populations. My results however fail to identify a role for Basigin in radial intercalation.

In the fourth chapter of this dissertation, I change my focus and look at specification of cilia subtypes in the developing epithelia of *Xenopus* embryos. These studies focus on *FoxJ1*, a transcription factor required for the formation of multiciliate cells, but not monociliate cells in mouse. I show that *FoxJ1* plays a conserved role in the formation of multiciliate cell in *Xenopus* embryo but that in contrast to the results

in mouse, *FoxJ1* is required for the formation of monocilia in the organs of L-R asymmetry in both Xenopus and zebrafish. Additionally, I show that *FoxJ1* is able to induce the formation of ectopic motile cilia in the external epithelium of Xenopus embryos supporting a specific role for *FoxJ1* in the formation of node-like cilia. In appendix one I discuss some preliminary experiments on *RFX2*, a transcription factor expressed in multiciliate cells in the *Xenopus* epithelium. These experiments suggest that, in contrast to *FoxJ1*, *RFX2* is not required for the formation of multiciliate cells in the epithelium. I also show that *RFX2* and *FoxJ1* do not act coordinately to generate multiciliate cells.

In the final chapter I briefly discuss the overall findings of my dissertation in the context of epithelial morphogenesis and the specification of cilia subtypes. I also discuss some of the limitations of my studies and possible future directions.
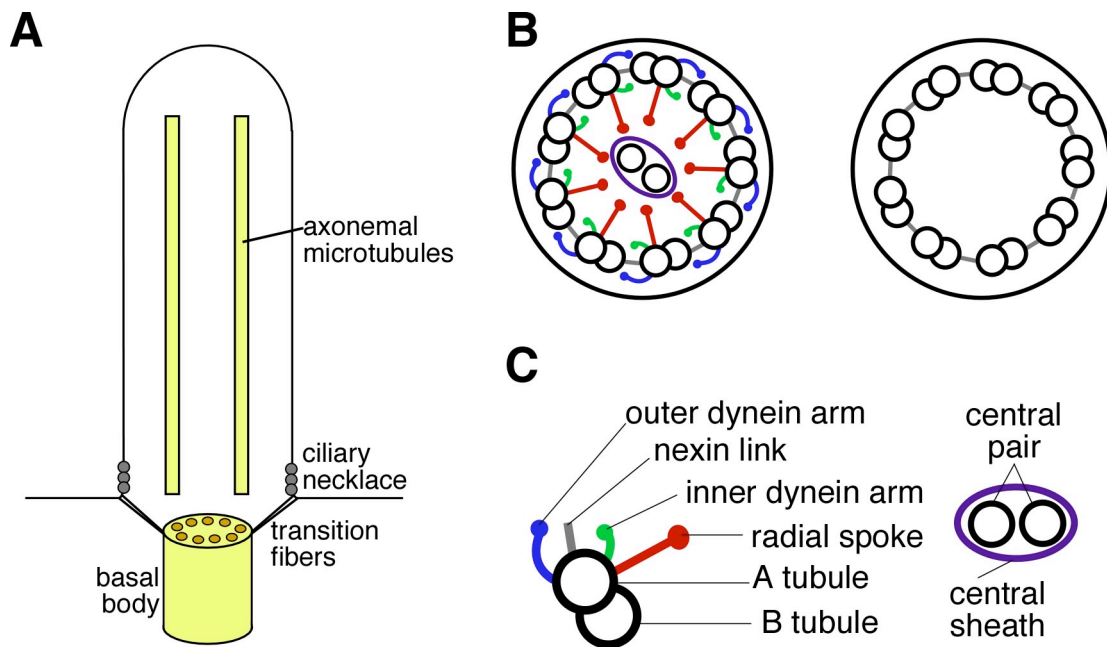
Figure 1.1 Model of Ciliary Axoneme. **(A)** Model of the main regions of the cilium. Shown are the axonemal microtubules, basal body with its nine-fold symmetry, transition fibers, and ciliary necklace. **(B)** Two main types of cilia, 9 + 2 motile, and 9 + 0 non-motile. Both types of cilia contain 9 outer microtubule doublets composed of an A and B tubule, with each pair connected to their neighbors by nexin links (gray). **(C)** Motile cilia also have outer and inner dynein arms connecting neighboring tubules (blue and green respectively). The central pair is enclosed by a network of proteins termed the central sheath (purple). Radial spoke proteins (red) connect the A tubule to the central pair. Modified from Ibanez-Tallon 2003.
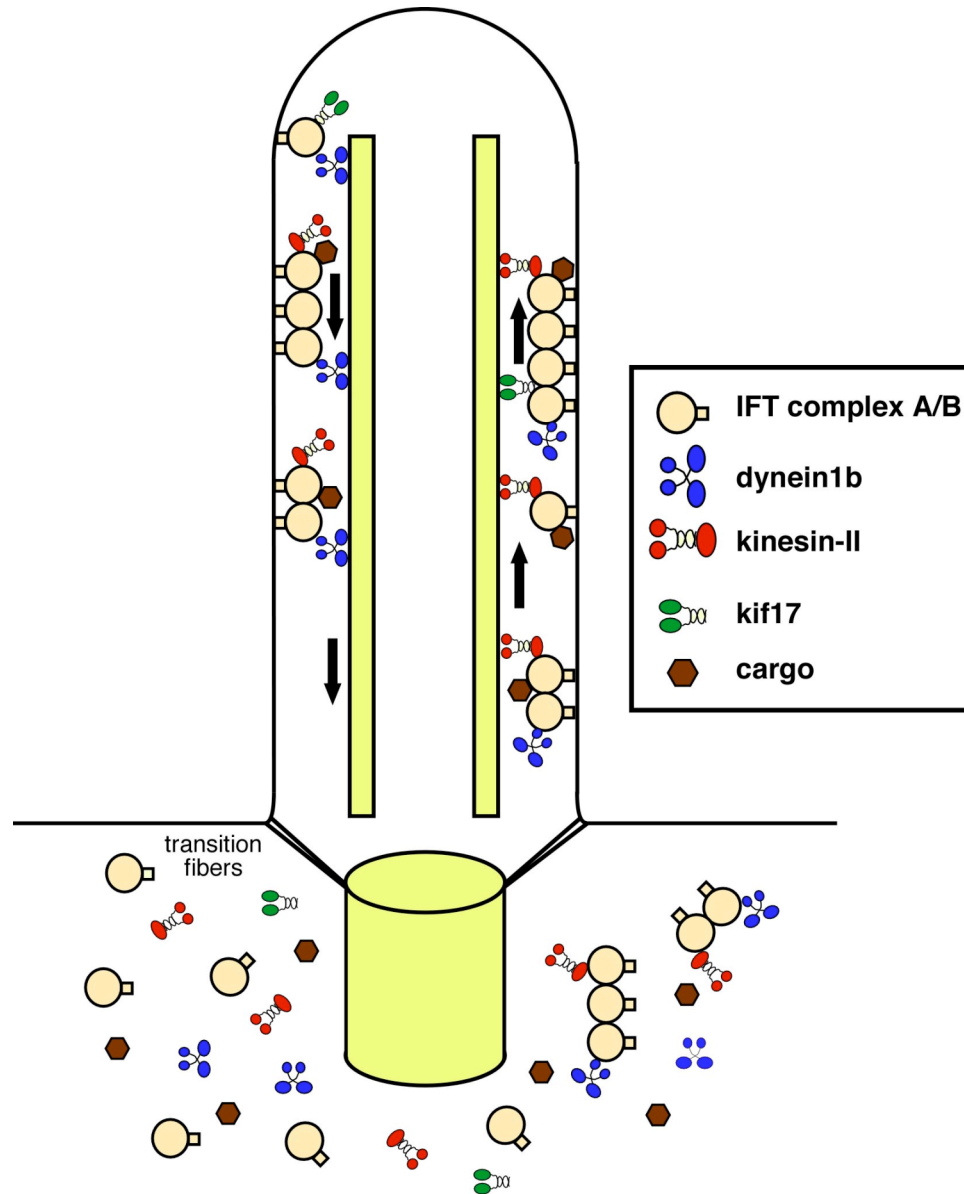
Figure 1.2 Model of Intraflagellar Transport: Model depicts intraflagellar transport along the ciliary axoneme. Anterograde transport uses kinesin-II (red) and kif-17 (green), both plus end directed microtubule motors. Retrograde transport is mediated by dynein1b (blue), a minus end directed microtubule motor. IFT complexes A and B (light yellow) mediate interactions between cargo (brown) and molecular motors. IFT particles are likely assembled in the cytoplasm before being moved into the cilium. Transition fibers, connecting the basal body to the plasma membrane, may act as a checkpoint for cargo to enter the cilium. Modified from Scholey 2003, and Rosenbaum & Witman 2002.
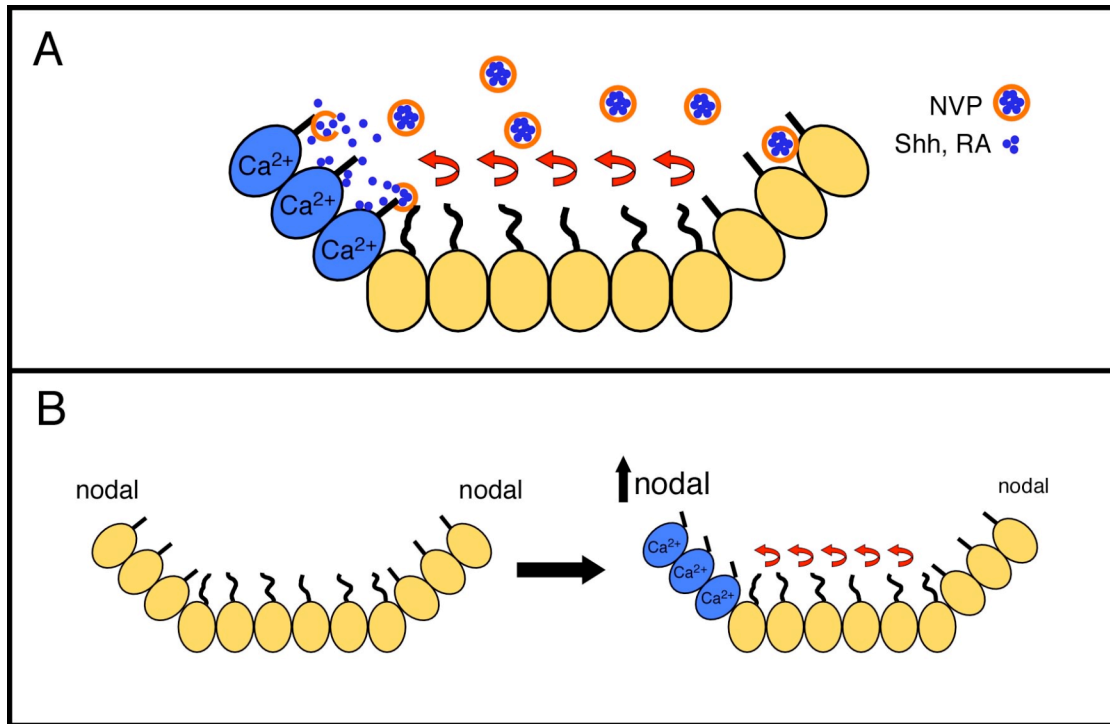
Figure 1.3 Models of L-R Asymmetry Determination: (A) Nodal vesicular particles (NVPs) containing signaling molecules Sonic hedgehog (Shh) and retinoic acid (RA) are transported across the node by leftward fluid flow (red arrows), where they are released and signal to cells on the left (modified from Tanaka 2005). **(B)** Nodal flow model where motile cilia in the center of the node cause non-motile cilia on the edges of the node to bend. Bending of cilia causes an increase in intracellular Ca^{2+} on the left side of the node, resulting in downstream signaling (modified from McGrath 2003).
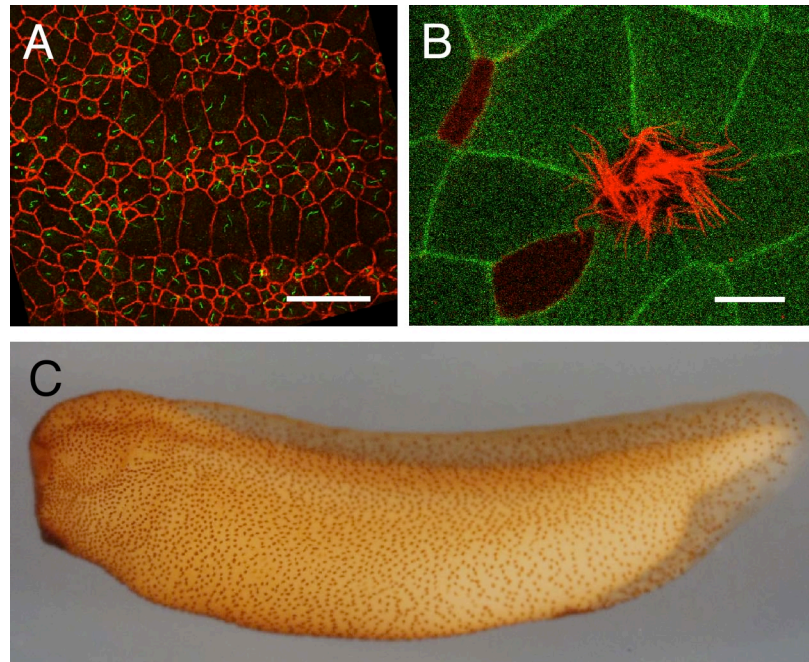
Figure 1.4 Ciliated Epithelia in *Xenopus laevis* Embryos: (A) Gastrocoel roof plate of a stage 18 *Xenopus* embryo stained with antibodies ZO-1 (red) and acetylated α-tubulin (green) to mark cell junctions and cilia, respectively. Monocilia are evident on almost all cells. **(B)** High magnification image of the *Xenopus* epithelium. Cells originating from the inner layer are labeled with membrane RFP (red), while cells from the outer layer are labeled with GFP (green). Two non-ciliated cells and one ciliated cell derived from the inner layer (red) are shown, with hundreds of cilia evident on the ciliated cell. **(C)** Whole embryo labeling of a stage 30 *Xenopus* embryo. Ciliated cells are marked with an antibody directed against acetylated α-tubulin (brown). Scale bar in (A) represent 40μm, while scale bar in (B) represents 10μm.
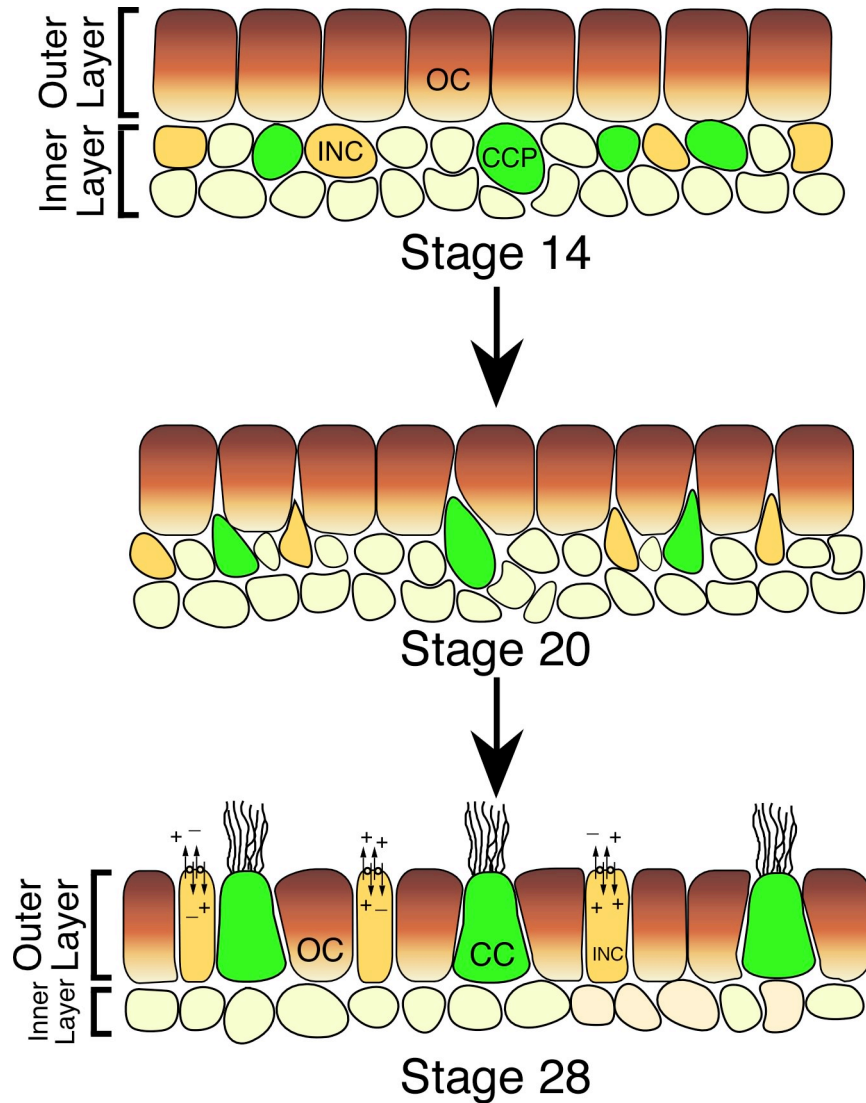
Figure 1.5 Epithelial Development in *Xenopus laevis:* At stage 14, the developing skin consists of outer cells (OC) that make up the surface occluding epithelium, and cells that make up the inner layer, including both ciliated cell precursors (green, CCP) and intercalating non-ciliated cells (yellow, INC). During stages 16-22 CCPs and INCs move into the outer layer of the epithelium. At stage 28 ciliated cells have differentiated and are generating vigorous fluid flow, while differentiated INCs are likely secreting and absorbing ions.

CHAPTER II

Radial Intercalation of Ciliated Cells During

Xenopus Skin Development

ABSTRACT

Cells with motile cilia cover the skin of *Xenopus* tadpoles in a characteristic spacing pattern. This pattern arises during early development when cells within the inner layer of ectoderm are selected out by Notch to form ciliated cell precursors (CCPs) that then radially intercalate into the outer epithelial cell layer to form ciliated cells. When Notch is inhibited and CCPs are overproduced, radial intercalation becomes limiting and the spacing of ciliated cells is maintained. To determine why this is the case, we used confocal microscopy to image intercalating cells labeled using transplantation and a transgenic approach that labels CCPs with green fluorescent protein (GFP). Our results indicate that inner cells intercalate by first wedging between the basal surface of the outer epithelium but only insert apically at the vertices where multiple outer cells make contact. When overproduced, more CCPs are able to wedge basally, but apical insertion becomes limiting. We propose that limitations imposed by the outer layer, along with restrictions on the apical insertion of CCPs, determine their pattern of radial intercalation.

INTRODUCTION

Cells with beating cilia are a common feature of many organ systems that depend on a directed fluid flow to function (Afzelius, 1995). For example, ciliated cells produce fluid flow in tissues as diverse as the respiratory tract of mammals where they clear mucous and debris, the choroid plexus where they circulate the cerebral spinal fluid into the ventricles of the brain, and the reproductive tract where they transport the egg along the oviduct. Proper development and function of these

organs, therefore, requires the formation of a specialized epithelium containing cells with motile cilia. Despite their importance to the function of many organ systems, how such ciliated epithelia develop and function remains poorly understood.

The skin of the amphibian embryo also produces a directed fluid flow generated by ciliated cells, thus serving as a model system for studying how such ciliated epithelia form during organogenesis. In Xenopus, the skin develops after gastrulation through the differentiation of two cell types that are derived from two distinct layers of the ectoderm (Fig. 1A) (Drysdale and Elinson, 1993). Cells in the outer layer of the ectoderm, also called the superficial layer, differentiate into mucus-producing epidermal cells, thus forming an occluding epithelial barrier on the embryo surface. Cells in the inner layer of the ectoderm, also called the sensorial layer, spread out underneath the outer layer during epiboly (Keller, 1980) and a subset give rise to ciliated cell precursors (CCPs) during early neurulae stages (stages 12-14) (Deblandre et al., 1999; Drysdale and Elinson, 1993). These precursors then differentiate into ciliated cells by intercalating radially into the outer layer during mid neurulae stages (stages 16-20) and undergoing ciliogenesis, allowing them to produce a directed fluid flow by late neurulae stages (stages 24-26). Ciliated cell differentiation is precisely controlled, thus ensuring that the cells are distributed across the epidermal surface at high density in an evenly spaced pattern.

In many developing tissues, specific spacing patterns of differentiated cells are generated by lateral inhibition, an evolutionarily conserved process in which cells inhibit their neighbors from acquiring the same fate using the Notch signaling pathway

(Kintner, 2003). Studies of Notch in the Xenopus skin indicate that lateral inhibition also operates during the formation of ciliated cells whereby Notch negatively regulates the number of CCPs that form in the inner layer of the ectoderm (Deblandre et al., 1999). By determining CCP number, the process of lateral inhibition could conceivably act to distribute ciliated cells evenly across the skin surface. However, when Notch is inhibited and CCPs are overproduced, the density of ciliated cells detected at tadpole stages only increases about two-fold, and moreover these cells remain spaced out (Deblandre et al., 1999). Thus, while Notch determines the number of CCPs that form in the inner layer, other factors determine the pattern of ciliated cells in the outer layer.

CCPs need to radially intercalate to become ciliated cells, raising the possibility that this morphogenetic process is a critical step in controlling the pattern of ciliated cell differentiation (Deblandre et al., 1999). If this were the case, one model is that epidermal cells in the outer cell layer effectively limit the number of intercalating CCPs, perhaps in order to maintain its function as an occluding epithelial barrier. Alternatively, ciliated cell differentiation may be limited by the extent to which intercalating CCPs can be packed into a given area without overlapping, thus resembling the honeycomb tiling of ganglion cell subtypes across the mammalian retina (Lin et al., 2004). Finally, CCPs may only intercalate when they interact with a specific number of outer layer cells. Distinguishing between these various possibilities is the first step in determining how intercalation is regulated and thus key towards understanding how ciliated cells achieve their spatial distribution.

By marking inner and outer cells with lineage tracers, Drysdale and Elinson (Drysdale and Elinson, 1993) showed that inner cells contribute not only ciliated cells but also an equal population of intercalating non-ciliated cells (INCs) to the outer layer (Figure 1A). Thus, the pattern of CCPs in the outer layer may not only be determined by their ability to intercalate but also by interactions with the INCs. To examine these issues, I used two assays to characterize inner cells during radial intercalation. I first show using a transplantation assay that inhibiting Notch leads to more CCs and INCs in the outer layer, although their number and distribution differ significantly. I then develop a transgenic assay to distinguish CCPs from INCs in order to describe the behavior of these two cell types during intercalation both normally and when they are overproduced after disabling Notch signaling. The results of these analyses reveal important morphological differences between CCPs and INCs at the earliest stages of radial intercalation. I propose that these differences along with limitations imposed on intercalation at the apical surface by the outer layer determine the pattern of ciliated cells found in the Xenopus skin.

RESULTS

Inner and outer cells during radial intercalation

In order to distinguish inner cells and outer cells during radial intercalation, I modified an assay in which outer layer ectoderm from a donor embryo was grafted onto the inner layer ectoderm of a host prior to gastrulation (Drysdale and Elinson, 1993). In this modification, host and donor cells were marked by injecting embryos at the two-cell stage with RNA encoding membrane-localized forms of GFP (mGFP) or

RFP (mRFP), respectively, allowing inner cells that have intercalated into the outer

layer to be imaged at high resolution with confocal microscopy (Figure 2.1A, B). At

stage 28, when the larval skin has fully differentiated and the embryo has undergone

axial extension, approximately half of the inner cells that had intercalated into the

grafted outer layer were ciliated cells while the other half were not (Drysdale and

Elinson, 1993). Intercalating non-ciliated cells (INCs) differ morphologically from

ciliated cells (CCs) by more than just the lack of cilia (Figure 2.1B). For example,

while CCs rarely lie adjacent to each other, INCs can often be found close to or in

contact with a CC. In addition, INCs are typically smaller than ciliated cells, perhaps

accounting for the fact that INCs on average make contact with three cells in the outer

layer while the CCs make contact with four to five cells (Figure 2.1C). Finally, INCs

are columnar in shape, while CCs have a small round apical domain and broaden

basally (Figure 2.2). Thus, the inner cell layer contributes two morphologically

distinct cell types to the outer layer in approximately equal numbers (Figure 2.4D).

To examine how cells in the outer layer respond to radial intercalation, I

imaged live grafts using low-magnification, time-lapse fluorescent microscopy (Figure

2.3). Prior to the onset of intercalation, the outer layer epithelium is organized in a

typical honeycomb pattern, as predicated by the optimal packing of epithelial cells into

a hexagonal array (Carthew, 2005). During intercalation, cell-cell contacts between

two neighboring outer cells remain intact, with little or no change in their dimensions

(Figure 2.2). Outer cell division was rarely observed during imaging (data not shown),

suggesting that division of outer cells is not necessarily associated with, and

presumably not required for, most intercalation events. The most prominent change in the outer cells during intercalation was a local rearrangement of cell borders where vertices retract between outer cells in the immediate area where an inner cell intercalates (Figure 2.2, see circled vertex). Thus, these results indicate that the outer epithelium is a relatively static structure that rearranges locally to accommodate the insertion of new elements.

INCs and CCs respond differently to Notch inhibition

The static nature of the outer layer raises the possibility that it effectively limits the total number of intercalating inner cells. If this were the case, then one possibility is that when Notch is inactive, the total number of intercalating cells remains the same, but INCs are replaced by CCs, thus explaining the modest two-fold increase in the density of ciliated cells found at tadpole stages (Deblandre et al., 1999). To test this possibility, I used the same transplantation assay but transplanted outer layer cells onto host embryos that express an inhibitor of Notch signaling (dnHMM) (Fryer et al., 2002) and then scored the number of CCs and INCs at stage 28 (Figure 2.4). Earlier stages were also assayed (Figure 2.10) but results will focus on stage 28. As expected, inhibiting Notch in the inner layer resulted in a small increase in the density of ciliated cells at stage 28 (Figure 2.4B) compared to controls (Figure 2.4A). However, inhibiting Notch did not produce a loss of INCs but rather a dramatic increase in their number (Figure 2.4D). To accommodate this increase in the total number of intercalating cells, many of the INCs were located adjacent to each other while the CCs remain evenly spaced (Fig. 2.4B). Conversely, when Notch signaling was

activated by expression of the intracellular domain of Notch (ICD) CCs were lost
(Figure 2.4C, D) and INCs were lost at early stages (Figure 2.10C, F), although an
occasional INC was observed at later stages (Figure 2.4C). Thus, these results
indicate that CCs and INCs do not represent a reciprocal population, but are instead
regulated in tandem by Notch signaling. Additionally, these results show that CCs
and INCs behave differently during radial intercalation in both the number and
spacing of cells observed in the outer layer.

Transgenic analysis of ciliated cell precursors

Since the transplantation assay cannot distinguish between CCPs and INCs
during intercalation, I developed a second assay to label CCPs using a transgenic
approach, based on an isoform of $\propto$-tubulin that marks ciliated cells (Deblandre et al.,
1999). Accordingly, a 2.5kb genomic fragment lying upstream of the $\propto$-tubulin gene
was cloned upstream of mGFP (called $\propto$-tubulin-mGFP, see Materials and Methods)
and used to generate transgenic embryos (Amaya and Kroll, 1999). Embryos
transgenic for $\propto$-tubulin-mGFP first expressed mGFP soon after gastrulation (Figure
2. 5A), within a subset of inner cells (Figure 2.5D) that resemble the pattern of cells
expressing $\propto$-tubulin RNA (Figure 2.5E). At tadpole stages, mGFP was strongly
expressed in the skin of transgenic embryos but only in cells with cilia (Figure 2C, F).
Given the perdurance of GFP, we conclude that the cells expressing the $\propto$-tubulin-
mGFP transgene during intercalation give rise to ciliated cells but not to INCs.

Using the $\propto$-tubulin-mGFP transgenic assay, I imaged CCPs during radial
intercalation using confocal microscopy both in embryos as well as in ectoderm

explanted from transgenic embryos onto fibronectin-coated coverslips (Davidson et al., 2002). In these explants, the ectoderm spreads out onto the fibronectin matrix deposited on the glass, much as it normally does during epiboly and gastrulation. This preparation provides the added advantage of allowing one to image intercalating cells from both the inner and outer surfaces.

In both embryos and explants at early-neurula stages (stages 13-16), CCPs were visualized based on $\propto$-tubulin-mGFP expression as a subset of the inner layer cells (Figure 2.6A, B, G, H). At this stage, the cell bodies of the CCPs were already wedged between the basolateral surfaces of the outer layer cells, extending processes that go up to, but not through, the apical tight junctions that seal the outer layer of cells together, as marked by staining with antibodies to ZO-1 (Merzdorf and Goodenough, 1997) (Figure 2.6A, G). Thus, inner cells initiate ciliated cell differentiation, at least as marked by $\propto$-tubulin-mGFP expression, prior to integrating fully into the outer epithelium. When imaged in explants from the basal surface, inner cells were marked by E-cadherin, the major cell adhesion molecule in differentiating Xenopus skin (Choi and Gumbiner, 1989). Basal images show CCPs were separated from the fibronectin substrate by a layer of inner cells (Figure 2.6I, J), suggesting that CCPs are not an integral part of the inner layer. Thus, CCPs appear to initiate intercalation by establishing extensive contact with outer epidermal cells by wedging between them basally, prior to apical insertion.

During mid neurula stages (stage 17/18), intercalating CCPs penetrate and join the outer epithelium as assessed by the interdigitation of GFP[+] labeled membrane

between the ZO-1 labeled, apical junctions (Figure 2.6C, D). Significantly, CCPs did

not penetrate the apical junctions randomly, but are restricted to inserting between

outer cells at vertices where multiple outer cells make contact (Figure 2.6C, see circled

vertex). In addition, by this stage, the intercalating CCPs that were embedded into the

outer layer began to take on a regular spacing pattern, even those that had not yet

inserted apically into the outer layer (Figure 2.6 C, D, arrow). Perhaps as a

consequence, intercalating CCPs were rarely if ever detected at the same apical

insertion site, and thus, avoid cell-cell contact with each other at the apical surface.

Around this stage, ZO-1 staining also revealed small apical domains that were GFP-

negative, indicating that at least some of the INCs insert apically around the same time

as CCPs (data not shown).

By late neurula stages (stages 20-24), most CCPs have inserted apically,

typically making contact with four or five outer cells (Figure 2.6E, F). Since the

vertices between outer cells involve three to four cells prior to intercalation (Figure

2.6A, G see also Figure 2.3), this observation implies that alterations of vertices to

accommodate the intercalating CCPs result in a rearrangement of outer cells, as

indicated by the time-lapse imaging described above. In regions of the developing

skin where the density of CCPs was relatively high the intercalating CCPs took on a

lattice-like pattern (Figure 2.6E, F). In explants where relatively little growth takes

place, CCPs also only inserted into vertices, and observed a spacing pattern where two

CCPs rarely shared the same apical insertion site, while associating with 4-5 outer

cells and took on a lattice-like pattern (Figure 2.6K, L). Thus the radial intercalation

of CCPs into the outer layer in both embryos and explant culture does not occur randomly but only at vertices, follows a spacing rule that precludes apical insertion of adjacent CCPs, and culminates in the association of 4-5 outer cells with each CCP.

Overproduced ciliated cell precursors are precluded from intercalation

Blocking Notch increases substantially the number of cells expressing ∝-*tubulin* RNA (Deblandre et al., 1999) but only produces a small increase in density of ciliated cells (Figure 2.4). The previous interpretation of these observations is that only a fraction of the CCPs can intercalate while the "excess" remained trapped internally. To confirm this interpretation, I followed CCPs using confocal microscopy after blocking Notch signaling in ∝-*tubulin-mGFP* transgenic embryos by injecting dnHMM RNA (Fryer et al., 2002).

When imaged from the apical surface of the outer layer at stage 16, control and dnHMM injected transgenic embryos contained approximately the same density of intercalated CCPs (Figure 2.7A, B, I). Since I was limited in my ability to detect CCPs that are located deeper than about 10 μm from the apical surface, I peeled the skin from transgenic embryos and imaged the basal side of the CCPs through the inner layer (Figure 2.7C, D). The density of CCPs detected basally in control regions was similar to that detected apically (Figure 2.7I compare control inner and outer layer), indicating that most if not all of the CCPs gain access and intercalate into the outer layer (compare Figure 2.7 A to 2.7C). By contrast, in dnHMM regions, CCP density detected basally increased at least two-fold relative to the control, with many of the excess CCPs clustered and overlapping each other making accurate quantification

difficult (Figure 2.7D, I). Thus, the total number of CCPs generated is regulated by Notch signaling but those associated with the outer layer are regulated by their ability to intercalate.

To determine whether any of the "excess" CCPs produced in Notch deficient embryos were ultimately able to intercalate, I next examined the late neurulae-stage (stage 24). In control embryos, the density of CCPs found in the outer layer was actually lower than at earlier stages (Figure 2.7I, compare 2.7A, E). Since a fixed number of CCPs seem to be generated early and all of these intercalate, I assume that these are diluted out as the outer layer increases in size during embryo growth. By contrast, in regions expressing dnHMM the density of CCPs intercalated into the outer layer remained high, while maintaining a lattice-like packing pattern (Figure 2.7F). In addition, in dnHMM-injected regions excess CCPs could be still detected in an abnormal basal position (compare Figure 2.7G and H). These excess CCPs were localized to cell clumps that were poorly attached to the inner layer (Figure 2.7H) making the size of this population difficult to measure. Thus, these observations indicate that intercalation of CCPs is limited but that additional CCPs can intercalate as the area of the outer layer grows, thus leading to an increased density of ciliated cells. Even at late stages, however, spatial limits on intercalation continue to restrict the number of ciliated cells since a lattice-like packing pattern is conserved, and at least some of the overproduced CCPs remain trapped in the inner layer.

Intercalating CCPs differ morphologically from INCs

The results above indicate that the insertion of CCPs into the outer layer is restricted during radial intercalation, thus limiting the number of ciliated cells. By contrast, the intercalation of INCs seems to be less restricted based on the transplantation assay. To explore the difference between the INCs and CCPs further, I took advantage of the transgenic assay utilizing sperm nuclei prepared from an F1 transgenic male. When injected into eggs, these nuclei produced transgenic *∝-tubulin-mGFP* expression in one half of the offspring based on the expected Mendelian distribution of a single insertion site. In addition, transgenic sperm nuclei were injected into albino eggs, thus eliminating the surface pigment and allowing for deeper imaging of intercalating cells. Finally, transgenic embryos were injected with mRFP RNA to label cell surfaces, thus allowing one to visualize outer cells and intercalating inner cells, while the transgenic mGFP expression was used to distinguish CCPs from INCs (Figure 2.8). Outer cells, CCPs and INCs were imaged in live embryos beginning at stage 16 and proceeding to stage 22 when ciliogenesis begins, and data was collected from several different regions of the developing skin at hourly intervals.

To determine when INCs and CCPs intercalate, I scored those located near the apical surface as well those wedged basolaterally at 6mm (CCP and INC) and 10mm (CCPs only, see Table 2.1). Under normal conditions, CCPs were found to outnumber INCs, even as late as stage 22 when most CCPs had intercalated (Figure 2.8A, B). Since INCs and CCPs are present in equal numbers at later stages (Figure 2.4D), INCs apparently intercalate over a more protracted period, including after CCP intercalation is normally complete. When Notch was inhibited, INCs represented a proportionally

larger fraction of the intercalating cells at early stages (Table 2.1, see t=1), although

their numbers were still modest compared to the large increase of INCs seen at later

stages in the transplantation assay (compare Table 2.1 to Figure 2.4D). Perhaps more

striking is the difference between the number of INCs and CCPs located apically

versus basally when Notch is inhibited (Table 2.1, Figure 2.8C, D). Inhibiting Notch

markedly increased the number of INCs and CCPs located basally at early stages,

correspondingly increased the number of INCs located apically at late stages, but had

little effect on the number of apically located CCPs. These findings indicate that the

ability of CCPs to intercalate becomes limiting between basal and apical insertion.

Furthermore, as apical insertion becomes limiting, INCs may compete with CCPs for

intercalation space.

The difference in the rate of basal versus apical insertion of intercalating cells

is also evident in the behavior of the outer cells. Under normal conditions, only a

small fraction of the space present around the basolateral circumference of an outer

cell is taken up by intercalating cells (Figure 2.8B, dotted lines). When Notch is

blocked most of this space becomes occupied early on by both INCs and CCPs (Figure

2.8D, dotted lines), although two neighboring outer cells were never separated by

more than one intercalating cell, except at tricellular corners (Figure 2.8C). To

accommodate the increase in intercalating cells, therefore, outer cells respond basally

by losing contact with each other and narrowing around their circumference, a change

already evident at the earliest timepoint examined (see Table 2.2, 6 μm column, t=1).

By contrast, outer cells decrease their cell-cell contacts more slowly at the apical

surface (Table 2.2, apical column) in the face of increased numbers of intercalating

cells (compare dotted lines in Figure 2.8A, C to 2.8 B, D), perhaps reflecting the static

nature of apical contacts between neighboring outer cells (Figure 2.3, see Discussion).

Thus, outer cells may limit the insertion and expansion of intercalating cells at the

apical vertex, effectively restricting the amount of space available for intercalation.

As space for intercalation becomes limiting, CCPs may be impacted more than

INCs based on morphological differences that mirror those evident at later stages

(Figures 2.1B, 2.2). CCPs take up twice as much space as INCs when they wedge

between the basolateral surfaces of the outer cells (Figure 2.8B, D, Table 2.3). As a

consequence, CCPs are much more bulb-like in shape compared to the INCs, which

tend to be more columnar in shape (Figure 2.2). Significantly, the shape and sizes of

intercalating CCPs and INCs look similar in control and dnHMM conditions (Table 2.

3), indicating that these cells do not change their morphology to increase the number

of intercalating cells.

Finally, the ability of CCPs to insert apically may also be limited by self-

exclusion at the apical vertex. During intercalation, CCPs make contact with each

other basally, but are rarely observed sharing a vertex when they insert apically (Table

2.4, Figure 2.8C, E, F). By contrast, CCPs can share a vertex with one or more INCs

(Table 2.4, Figure 2.4B). Finally, at the late phases of intercalation when Notch is

blocked and a large fraction of CCPs remain trapped below the apical surface, many of

these are positioned beneath a vertex that already contains a ciliated cell and one to

several INCs (Figure 2.8E, F arrowheads). Thus, CCP intercalation may be limited by

self-exclusion at the vertices, by competition with INCs for intercalation space, and by a limitation that the outer layer imposes on the amount of intercalation space available at the apical surface.

DISCUSSION

The Xenopus larval skin is a ciliated epithelium, evenly decorated with ciliated cells at relatively high density. A key step in the formation of this tissue architecture is a radial intercalation event, in which CCPs generated in the inner cell layer move into the outer occluding epithelium. While the trans-epithelial movement of cells has been studied in such models as germ cell migration (Kunwar et al., 2003) or the trans-endothelial migration of leukocytes (Luscinskas et al., 2002a), comparatively little analysis has been done to determine how specialized cells join an epithelial cell layer during development (Carthew, 2005). Here we analyze this process in the developing larval skin by determining the morphogenetic rules that govern radial intercalation under normal conditions, as well as when intercalating cells are overproduced.

Notch regulation of intercalation

Previous lineage studies showed that INCs and CCs are normally present in equal proportions and are often located adjacent to each other in the outer layer (Drysdale and Elinson, 1993). These findings suggested that INCs and ciliated cells might arise in pairs following the asymmetric division of a common intercalating precursor and led us to ask whether Notch signaling mediates this binary fate decision. However, our lineage analysis using α-*tubulin-mGFP* expression as a tracer indicates that ciliated cell precursors and INCs are already distinct prior to intercalation.

Furthermore, inhibiting Notch not only increases the number of ciliated cells but also, dramatically, the number of INCs. Thus, Notch may have an additional, more general role in regulating the intercalation of inner cells in parallel with its function in inhibiting ciliated cell differentiation. In line with this possibility, we have also found that ectopic expression of ICD, a constitutively activated form of the Notch receptor (Chitnis et al., 1995), suppresses the appearance of INCs in addition to CCPs, at least through early neurula stages (Figure 2.9E and 2.10C, F). The late intercalating population of INCs observed in ICD transplants may represent another separate group of intercalating cells that arise independent of Notch signaling. Similarly, INCs and CCs are also eliminated when inner cells express ESR6e (Figure 2.9C), a member of the family of bHLH repressors that acts as a Notch target gene in the skin (Deblandre et al., 1999). These results suggest a model in which Notch activity in the inner layer induces targets such as ESR6e, which in turn, repress the expression of genes required for radial intercalation.

Morphogenetic changes during intercalation

During the early phases of radial intercalation, time-lapse images reveal dynamic protrusive activity in which inner cells extend and retract processes between the basolateral surfaces of the outer layer cells, just below the apical junctional complexes (data not shown). This behavior is similar to that which occurs at earlier developmental stages during epiboly when inner cells radially intercalate between each other to thin the sensorial ectoderm (Longo et al., 2004). During epiboly, however, inner cells migrate basally, making contact with a matrix of fibronectin that

lines the blastocoel, and later on, the basal surface of the developing skin. By contrast, CCPs and INCs migrate in the opposite direction, thereby pushing up between the outer cells (wedging) and ultimately to the apical surface. Thus inner cells may initiate intercalation behavior during epiboly but a switch must then occur that directs their migration apically rather than basally.

As inner cells move into the outer layer, they first intercalate by wedging between the lateral surfaces of the outer cells (Figure 2.6), prior to interdigitating between the apical junctions to join the epithelium. During wedging, intercalating cells can be located at any point around the circumference of an outer cell (Figure 2.8), but when they insert apically, they do so exclusively at vertices: the points within an epithelium where at least three outer cells make contact. The preference for these points presumably reflects that an apical vertex is where the apical junctions between outer cells are interrupted as they pass from one cell to the next, and thus the place where the apical junctions can be disassembled to provide room for an intercalating cell to join the outer epithelium. Conversely, the vertex may also be the only place for an intercalating cell to establish new apical contacts in a manner that maintains the occluding barrier, while still allowing new tight junctions to form. The implication of this finding is that the apical vertex represents a key site for the disassembly or reassembly of junctional contacts that need to occur as cells join an epithelial layer. Similar arguments have been made in terms of how assembly of the junctional complex is regulated when cells form an epithelial sheet de novo *in vitro* (Adams et

al., 1998; Adams et al., 1996; Vasioukhin et al., 2000) or when an epithelial sheet

rearranges (Fristrom, 1988).

Maximal packing pattern of CCs

Under conditions where Notch signaling is normally active, approximately 30-

40 CCPs form per 100 outer cells and all of these, assuming no loss to cell death, gain

access to and intercalate into the outer layer. When Notch is inhibited, the number of

CCPs in a given area increases at least two-fold (Table 2.1), although we suspect that

this is an underestimation since we can only count CCPs located within 10 microns of

the outer or inner surface. Despite this increase in CCPs, the number of ciliated cells

that have inserted apically by early neurula stages is similar in dnHMM and control

embryos (Table 2.1). As these embryos grow and the number of cells in the outer

layer expands, the density of CCPs remains high in regions where Notch has been

inactivated, suggesting a model where "trapped" CCPs can intercalate when a space

opens up. Nonetheless, we can still detect CCPs "trapped" in the inner layer even at

late stages, suggesting that a certain proportion of the CCPs never make it into the

outer layer (Figure 2.7). Thus, these observations suggest strongly that limitations on

CCP intercalation largely determine the density and spacing of ciliated cells.

To determine why intercalation is limiting, we used confocal microscopy to

analyze the three principle players (INCs, CCPs and outer cells) in terms of their shape

and number, both normally as well as when Notch is inhibited. One finding that

emerges from this analysis is that intercalation is potentially limited at the apical

surface by restrictions imposed by the outer layer. Thus, outer cells initially allow

more intercalating cells to wedge between their basolateral surfaces, which they accommodate by narrowing to take up less space, and by making contact with intercalating cells around their circumference (Table 2.4). At the same time, however, outer cells seem to restrict intercalating cells apically, particularly if that cell is a CCP (Table 2.1). One possible reason for this difference is the difficulty of establishing apical junctions with outer cells, which only occurs at the apical vertex. Moreover, once an intercalating cells inserts apically, the size of its apical domain grows slowly, remaining small relative to the space it occupies basally (Figure 2.8, Table 2.3). Again this may reflect the difficulty of forming apical junctions with outer cells, but also the rate at which these junctions can form at the expense of those between outer cells, which appear static during intercalation (Figure 2.3). The picture that emerges from these observations, therefore, is one where the outer cells restrict intercalation by acting topologically as a bottleneck. As long the outer cells resist moving farther apart apically, they limit the space available for intercalating cells, both apically and basally (Figure 2.8).

If the outer layer acts as a bottleneck, then the shape and size of inner cells is likely to influence the pattern of their intercalation. CCPs and INCs have a characteristic size, regardless of whether their density is low as in the normal case, or when they pack into the outer layer as when Notch is inhibited. However, a CCP takes up about twice as much area as an INC because they are bulb-shaped during intercalation while INCs are more columnar (Figure 2.2, Table 2.3). These differences

in shape and size may impact the intercalation of CCPs more than INCs, as intercalating space becomes restricted.

The behavior of INCs and CCPs during intercalation raises the possibility that several inhibitory interactions may influence their patterns of intercalation, particularly as their numbers increase. Under normal conditions, intercalating CCPs initially outnumber INCs (see Figure 2.6), suggesting that the former intercalates more readily than the latter. However, when Notch is blocked, the proportion of INCs to CCs increases substantially, raising the possibility that INCs fill in the intercalating space available, and thereby inhibit the intercalation of CCPs. Until we find a means of eliminating INCs, we are currently unable to assess their role in limiting CCP intercalation. Nonetheless, competition between these two intercalating cells types may be significant factor, particularly when the number of intercalating cells surpasses the space in the outer layer that is available for new cells.

A second, potentially significant inhibitory interaction is one that occurs between CCPs. CCPs rarely if ever insert at the same apical vertex even when they lie adjacent to each other basally (Table 2.4, Figure 2.8). By contrast, an apical vertex often contains both a CCP and an INC, or even two INCs, indicating that multiple cells can intercalate along side each other apically as long as they are not both CCPs. These observations suggest that when CCPs insert apically they cannot overlap. This restriction may reflect the tendency of CCPs to occupy a large basal space coupled with the requirement that cells only insert apically at a vertex. In this model, since INCs are smaller, they are able to insert adjacent to each other or to CCPs.

Alternatively, another possible mechanism is that during apical insertion, CCPs favor cell-cell contacts with outer cells or INCs, but not with themselves. In this model, when CCPs are specified, they express adhesion molecules that enable apical junctions to form more readily with outer cells or INCs, but not with each other. Evidence for both possibilities comes from the finding that when CCPs are overproduced many of the trapped cells are found at the basolateral membrane of the outer layer and lie adjacent to other CCPs that have already established an apical domain.

In sum, these results indicate that during the complex process of radial intercalation, the spacing pattern of intercalating cells is likely to be influenced by several factors. Many of these factors, however, seem to relate to the pivotal role that the apical vertex plays in the process of intercalation. Intercalating cells use the vertex as the entry point for establishing apical contacts with outer cells. Modification of apical contacts occurs at the vertices, thus allowing outer cells to move apart. This separation is potentially the rate-limiting step in providing space for the insertion of new cells into an epithelium both apically and basally. Finally, the vertex is where CCPs may exclude each other during apical insertion, thus generating the spacing pattern where CCPs are only surrounded by outer cells or INCs. These observations suggest that the regulatory events that occur at the apical vertex are likely to be key in understanding the process of radial intercalation and how this process controls tissue morphology.

Chapter Two is modified from the following publication.

Stubbs JL, Davidson L, Keller R, Kintner C. "Radial intercalation of ciliated cells during Xenopus skin development". Development. 2006 Jul;133(13):2507-15.

I was the primary researcher of these studies and Chris Kintner directed and supervised the research. Lance Davidson assisted in transplant assays time-lapse imaging while in the laboratory of Ray Keller.

Table 2.1 Density of INCs and CCPs during intercalation

T=1	CCP- Apical	CCP- 6 μm	CCP- 10 μm	INC- Apical	INC- 6 μm
Control	28 ± 7	39 ± 9	41 ± 9	23 ± 7	42 ± 13
dnHMM	26 ± 10	56 ± 15	71 ± 20	31 ± 13	48 ± 21
T=2					
Control	32 ± 9	40 ± 10	42 ± 10	28 ± 11	38 ± 11
dnHMM	45 ± 18	74 ± 14	88 ± 17	49 ± 23	65 ± 23
T=3					
Control	37 ± 4	45 ± 5	47 ± 6	26 ± 9	32 ± 11
dnHMM	43 ± 11	75 ± 18	87 ± 18	53 ± 19	70 ± 24
T=4					
Control	35 ± 7	41 ± 6	43 ± 6	26 ± 9	33 ± 8
dnHMM	42 ± 20	66 ± 25	76 ± 21	54 ± 10	72 ± 17
T=5					
Control	32 ± 5	37 ± 6	37 ± 6	19 ± 9	29 ± 15
dnHMM	44 ± 16	65 ± 19	73 ± 14	55 ± 15	76 ± 34

Table 2.2 Average length (μm) of contacts between adjacent outer cells

T=1	Apical	6 μm
Control	88.0 ± 22.1	45.5 ± 21.7
dnHMM	112.3 ± 17.0	31.2 ± 13.1
T=3		
Control	76.3 ± 14.4	40.8 ± 12.3
dnHMM	80.6 ± 24.9	36.3 ± 19.9
T=5		
Control	78.6 ± 18.0	49.8 ± 16.9
dnHMM	69.0 ± 23.9	34.6 ± 10.0

Table 2.3 Average area (μm^2) of cell types measured apically and basally

T=1	CCP-Apical	CCP-6μm	INC-Apical	INC-6μm	OC-Apical	OC-6μm
RFP	59 ± 36	210 ± 75	57 ± 44	119 ± 51	783 ± 218	616 ± 150
dnHMM	41 ± 30	194 ± 68	36 ± 18	124 ± 60	831 ± 272	716 ± 149
T=5						
RFP	156 ± 65	255 ± 84	112 ± 71	127 ± 60	623 ± 193	566 ± 140
dnHMM	130 ± 60	242 ± 85	123 ± 41	125 ± 54	634 ± 191	549 ± 110

Table 2.4 Number of adjacent CCPs and INCs

T=1	CCP+CCP Apical	CCP+CCP 6μm	INC+INC Apical	INC+INC 6μm	CCP+ 1 INC	CCP+ 2$^+$ INC
Control	0.00 ± 0.00	0.91 ± 1.14	0.45 ± 0.52	2.55 ± 1.37	6.82 ± 2.23	4.82 ± 2.56
dnHMM	0.08 ± 0.29	2.08 ± 2.50	0.33 ± 0.65	2.92 ± 2.94	4.50 ± 2.75	5.42 ± 4.32
T=2						
Control	0.36 ± 0.67	1.18 ± 1.37	0.55 ± 0.82	2.50 ± 3.06	7.00 ± 3.30	3.30 ± 2.41
dnHMM	0.25 ± 0.62	4.67 ± 3.42	0.92 ± 1.31	2.92 ± 3.18	7.92 ± 4.89	7.17 ± 5.61
T=3						
Control	0.13 ± 0.35	0.88 ± 0.64	0.25 ± 0.71	2.25 ± 2.76	6.25 ± 3.24	3.50 ± 2.20
dnHMM	0.25 ± 0.45	4.92 ± 5.55	1.67 ± 2.53	3.33 ± 3.60	7.00 ± 1.76	8.58 ± 5.92
T=4						
Control	0.00 ± 0.00	0.29 ± 0.49	0.43 ± 0.53	1.57 ± 1.40	7.00 ± 4.69	2.33 ± 1.51
dnHMM	0.60 ± 0.70	3.10 ± 2.33	1.60 ± 1.43	3.20 ± 2.25	7.70 ± 3.13	8.90 ± 5.69
T=5						
Control	0.00 ± 0.00	0.60 ± 0.89	1.00 ± 1.20	2.00 ± 2.12	6.00 ± 3.16	3.00 ± 4.00
dnHMM	0.00 ± 0.00	0.91 ± 1.14	0.45 ± 0.52	2.55 ± 1.37	8.22 ± 2.91	9.00 ± 7.38
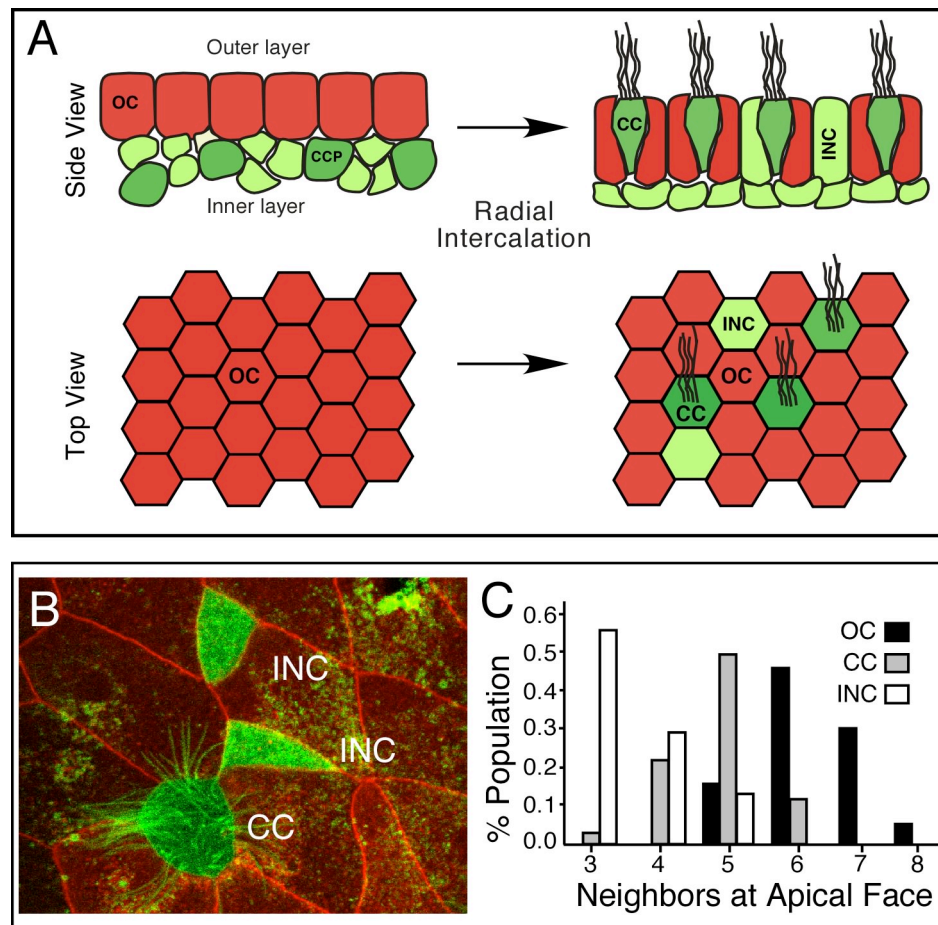
Figure 2.1 Epithelial Cell Types in Xenopus Embryos: (A) The development of the two-layered ectoderm into a ciliated epithelium. The outer layer (red) gives rise to epidermal outer cells (OC). Inner layer cells give rise to ciliated cell precursors (CCP, dark green) that become ciliated cells (CC) as well as non-ciliated cells (INC, light green). **(B)** The outer layer labeled with mRFP RNA was transplanted at stage 10 onto inner layer labeled with mGFP RNA. At stage 28, embryos were fixed and imaged by confocal microscopy. Cells from the inner layer (green) are either ciliated cells (CC) or non-ciliated (INC). **(C)** Shown is the number of neighboring cells for all three cell types in the epithelium.
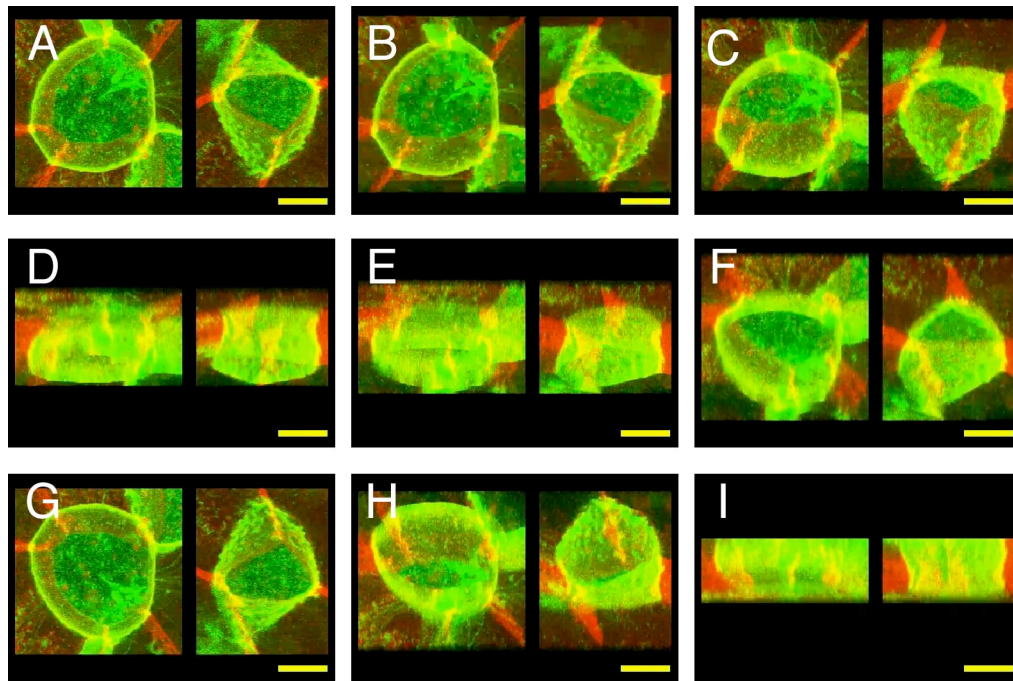
Figure 2.2 Morphology of CCs and INCs: mRFP labeled outer cells were transplanted at stage 10 onto the inner layer of host embryos expressing mGFP. At tailbud stages, transplants were imaged using a confocal microscope. Shown are still images from a 3-D reconstruction of a CC (left panes) and an INC (right panes) based on a series of maximal projections through a z-stack of images collected at 0.5μm intervals. Scale bars represent 10μm.
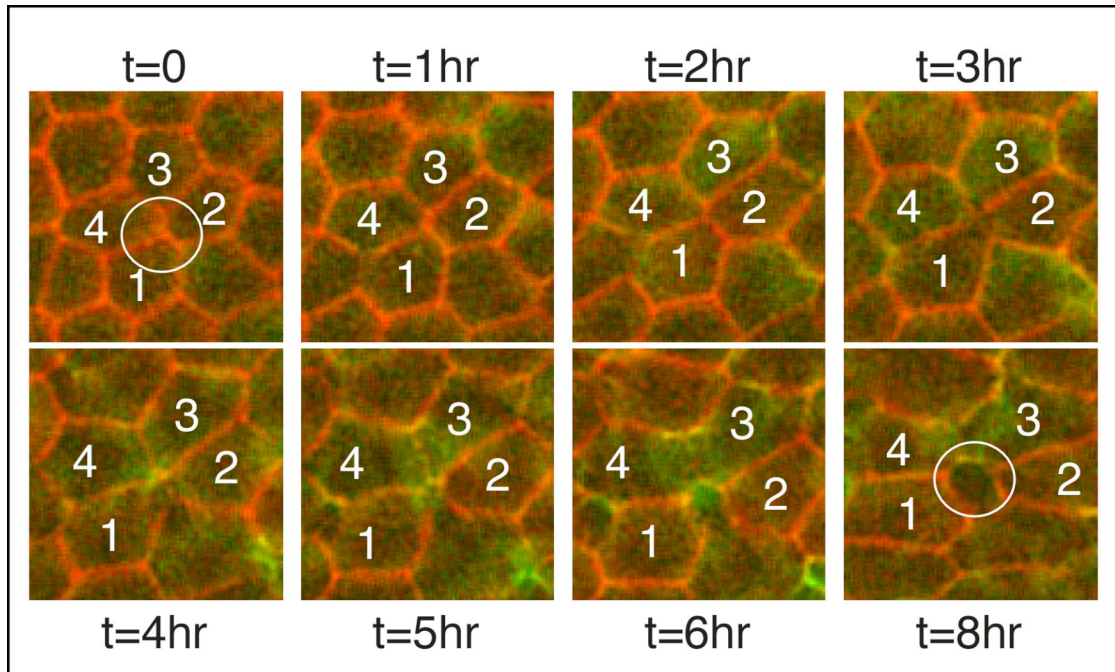
Figure 2.3 Outer cell morphology during intercalation: Time-lapse imaging of a transplant made as in figure 2.1. At stage 12, the ventral side of the embryo containing the graft was excised and placed against a coverslip for imaging under low power with a fluorescent microscope. Shown are images taken at the indicated times from around stage 14 (t=0) through stage 22 (t=8hr).
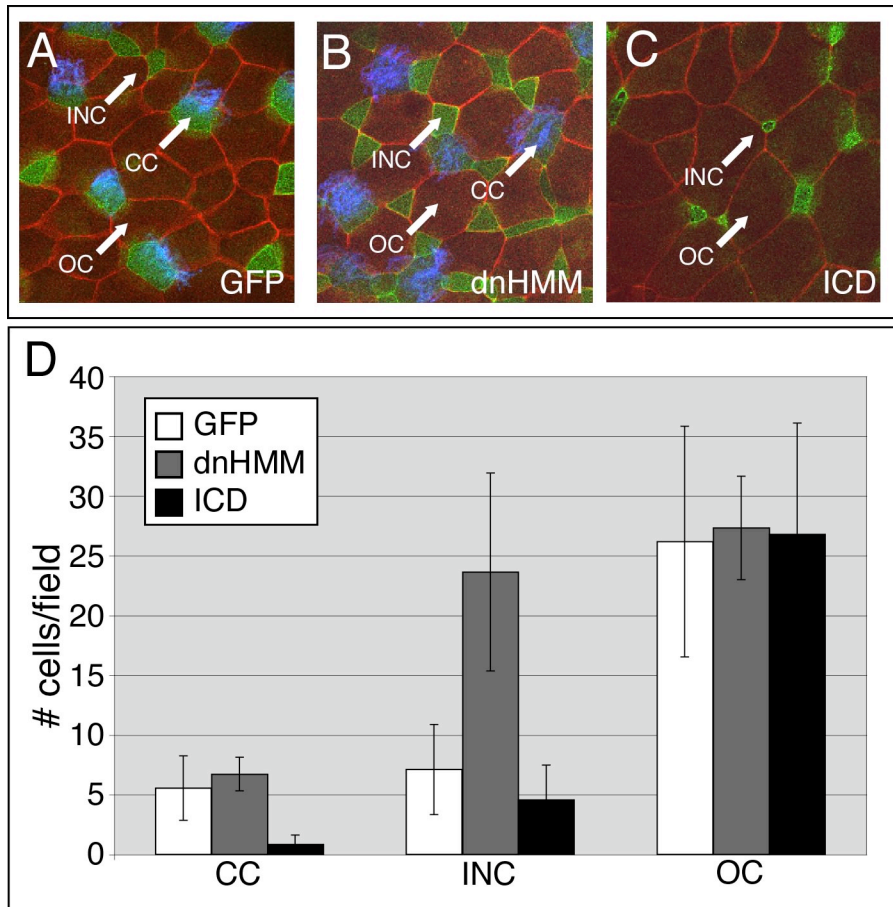
Figure 2.4 Notch signaling affects radial intercalation: (A-C) Outer layer ectoderm was transplanted onto control host (mGFP), onto host embryos expressing an inhibitor of Notch signaling (dnHMM) or onto host embryos expressing an activator of Notch signaling (ICD). Transplants were fixed at stage 28 and stained with an antibody to acetylated α-tubulin (blue) to mark ciliated cells, then imaged by confocal microscopy. Images taken through the apical surface, identifying outer cells (red, OC), ciliated cells (green/blue, CC) and intercalating non-ciliated cells (green, not blue, INC). **(D)** Quantification of the three different cell types present in ten fields from two transplants for each condition.
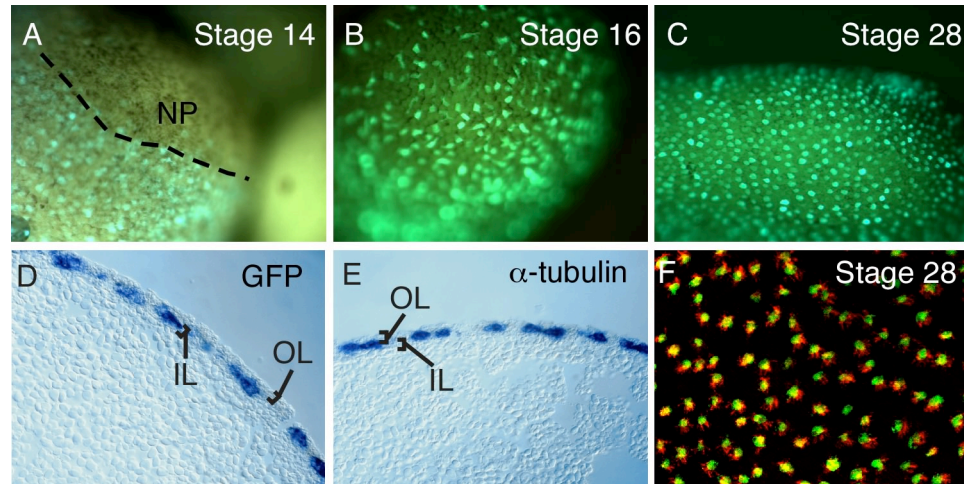
Figure 2.5 *α-tubulin-mGFP* transgene marks CCPs: (A-C) mGFP fluorescent images of live embryos that are transgenic for α-tubulin-mGFP at the indicated stages. In A, the boundary between the neural plate (NP) and non-neural ectoderm is denoted with a broken line. **(D, E)** *α-tubulin-mGFP* embryos were fixed at stage 14 and probed using whole mount in situ hybridization to detect either mGFP RNA (D) or α-tubulin RNA (E). Transverse sections of stained embryos on the ventral side with the inner layer (IL) and outer layer (OL) of ectoderm labeled. **(F)** *α-tubulin-mGFP* transgenic embryos were fixed at stage 28 and stained with an antibody directed against cilia (red fluorescence). The mGFP (green) and antibody staining overlap (yellow).
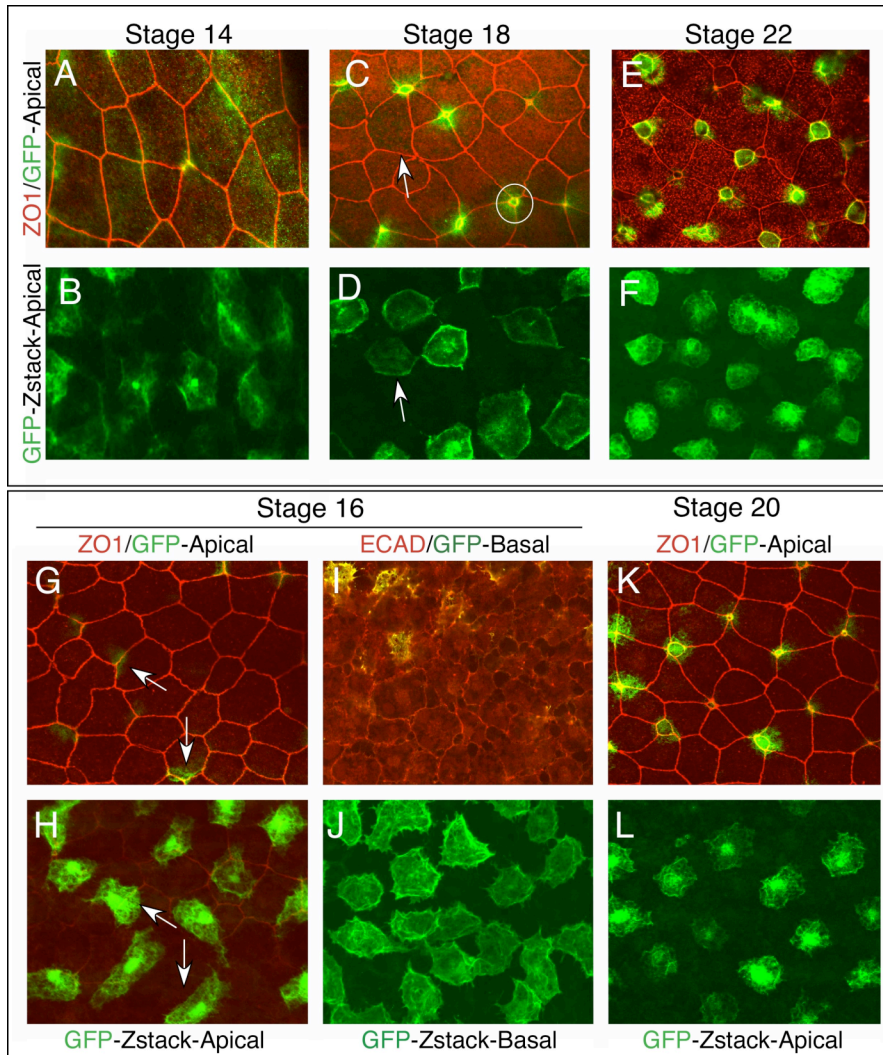
Figure 2.6 Intercalation of ciliated cell precursors: (A-F) α-tubulin-mGFP transgenics were fixed at the indicated stage, stained with an antibody against ZO-1 (red) and imaged by confocal microscopy. (A, C, E) A confocal slice through the apical surface of the outer epithelium; (B, D, F) mGFP expression in the same field below the apical surface. The arrow in B and D marks a CCP visible basally that has not yet inserted apically. **(G-L)** Ectoderm caps were dissected from α-tubulin-mGFP transgenics at early gastrulae stages and placed on fibronectin-coated coverslips. At the equivalent developmental stages shown, the explants were fixed, stained with antibodies to either ZO-1 or E-cadherin, and imaged by confocal microscopy. (G, K) mGFP (green) and ZO-1 staining (red) within 2μm of the apical surface; (H, L) mGFP-expressing cells within 6μm of the apical surface within the same fields. (I) mGFP (green) and E-cadherin staining (red) with 2μm slice of the basal surface; (J) mGFP-expressing cells within 10μm of the basal surface.
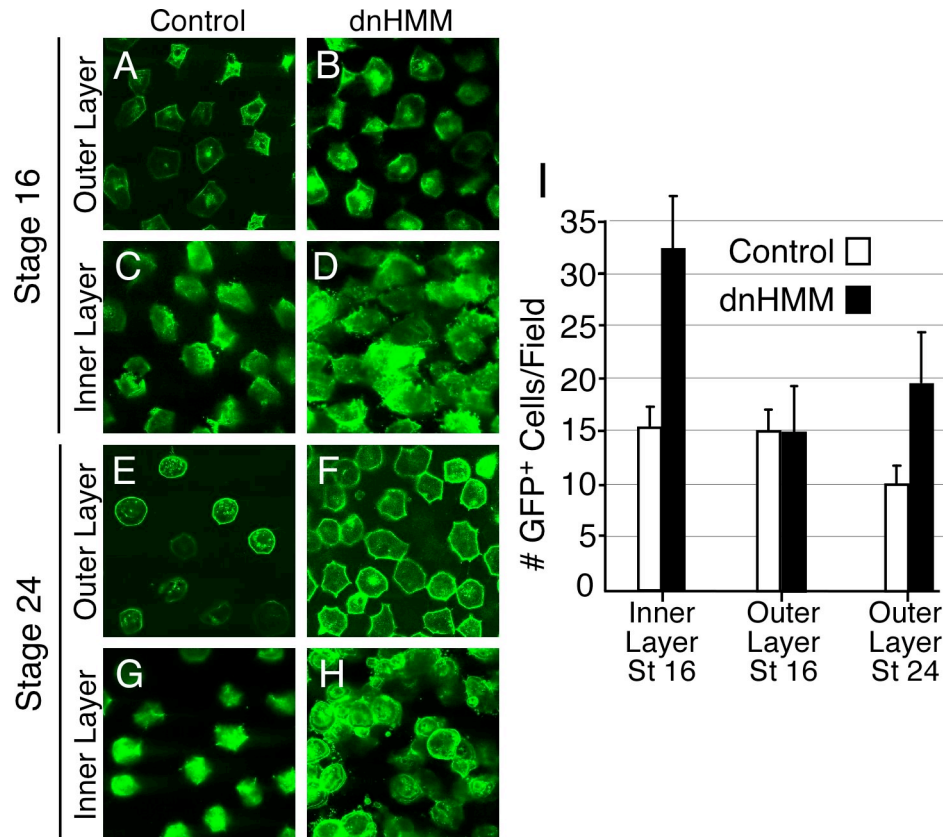
Figure 2.7 Intercalation of excess CCPs: RNA encoding dnHMM was injected into α-tubulin-mGFP transgenics at the two-cell stage along with mRFP RNA to trace the injected side. At early (stage 16) and late (stage 24) neurulae stages, embryos were fixed and image in the confocal microscope. **(A, B, E, F)** Embryos at the designated stages were imaged from the external surface to detect *α-tubulin-mGFP* expressing cells that are embedded in the outer layer. **(C, D, G, H)** When the skin is removed and imaged from the internal surface, the number of mGFP-expressing cells located in the inner layer increases significantly in regions expressing dnHMM (D, H). At stage 18, the mGFP-expressing cells located internally spread out and extend protrusions (D), but at stage 24 have rounded up and appear poorly attached to the surrounding cells (H). **(I)** Number of GFP-expressing cells that could be imaged apically (outer layer) or basally (inner layer) in *α-tubulin-mGFP* transgenic embryos at the indicated stage, either in control regions or regions expressing dnHMM.
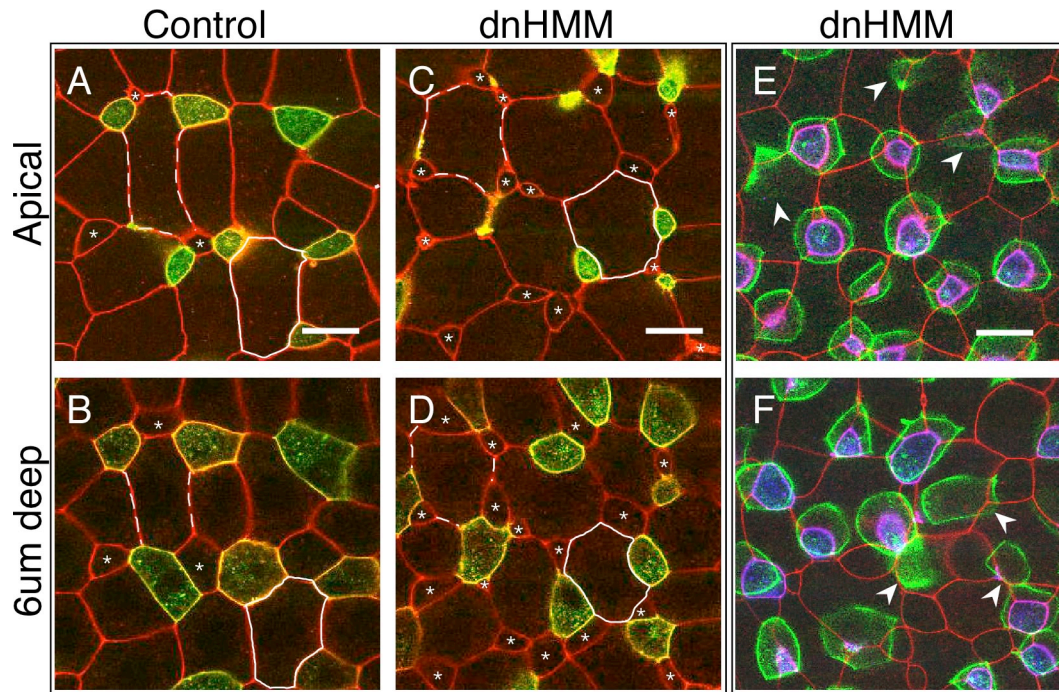
Figure 2.8 Morphology of INCs, CCPs, and OCs during radial intercalation: Albino embryos transgenic for *∝-tubulin-mGFP* were injected at the two-cell stage with mRFP RNA alone (A, B) or a mixture of mRFP and dnHMM RNA (C-F). **(A-D)** Transgenic embryos at an intermediate stage in intercalation (stage ~18) were imaged live in the confocal microscope to score the morphology and number of ciliated cells (mGFP$^+$), outer cells or INCs (asterisks). Panels A and C show a confocal slice apically while B and D show a slice 6 μm below the apical surface. Dotted lines denote cell-cell contacts between outer cells while white lines denote outer cell area. **(E-F)** Confocal images of transgenic embryos at stage 22, showing trapped CCPs (arrowheads) located below the apical surface. Images are a composite of apical mRFP expression, and a 6 μm stack of mGFP expression. Scale bars=10 μm
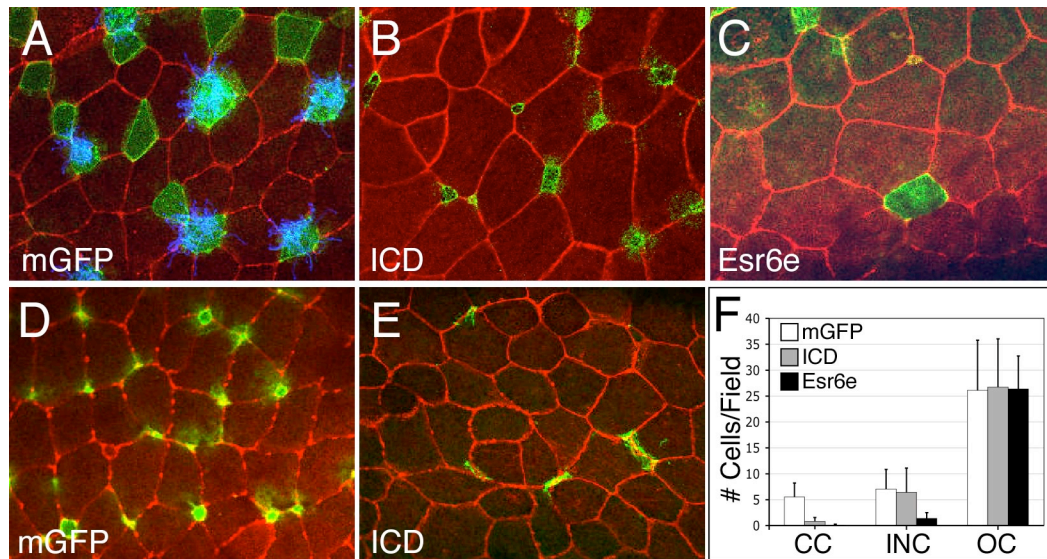
Figure 2.9 ICD and ESR6e repress radial intercalation: mRFP-labeled outer cells were transplanted at stage 10 onto the inner layer of host embryos expressing ICD (B, E), or ESR6e (C) along with mGFP, or with just mGFP (A, D) as a control. At either stage 28 (A-C, tadpole) or stage 20 (D-E, neurula), the embryos were fixed, stained with antibody to ciliated cells (CC, blue) and imaged by confocal microscopy. Note that ESR6e strongly inhibits the formation of ciliated cells, and represses intercalation of INCs (a few remaining INCs are shown in C), as quantified in panel F. Note also that ICD eliminates ciliated cells (B, F), but not INCs at this stage. However, many of the INCs detected at stage 28 in ICD injected embryos have a small apical domain, suggesting that their intercalation was delayed. In line with this idea, ICD strongly inhibits intercalation when scored at stage 20 (compare panel E to D). These data indicate that activation of Notch signaling and, thus ESR6e expression both represses ciliated cell differentiation and delays the intercalation of non-ciliated cells.

Figure 2.10 Notch signaling affects radial intercalation at neurula stages: (A-F) Outer layer ectoderm was transplanted onto control host (A, D, mGFP), onto host embryos expressing an inhibitor of Notch signaling (B, E, dnHMM) or onto host embryos expressing an activator of Notch signaling (C, F, ICD). Transplants were fixed at stage 16 (A-C) or 10 (D-F) and imaged by confocal microscopy. Images through the apical surface, identifying outer cells (red, OC), and intercalating cells (green, IC). **(G-H)** Quantification at stage 16 (G) and 20 (H) of the two different cell types present in ten fields from two transplants for each condition.

CHAPTER III

The Role of Basigin in Intercalation of Specialized Cell Types

in the *Xenopus laevis* External Epithelium

INTRODUCTION

The epidermis of *Xenopus laevis* embryos is a two-layer tissue comprised of several specialized cell types including mucus secreting and ciliated cells (Billett and Gould, 1971; Steinman, 1968). Two populations of cells, ciliated and non-ciliated cells, undergo radial intercalation during neurula stages and join the outer layer of the skin (Deblandre et al., 1999; Drysdale and Elinson, 1993; Stubbs et al., 2006). Once in the outer layer these cells differentiate. Ciliated cells specifically, appear to be constrained by a spacing rule during intercalation, with the result being an evenly spaced final distribution of cells across the epidermis wherein no two ciliated cells touch. Non-ciliated cells, by contrast, do not share these constraints and are often found lying next to other non-ciliated cells in the epithelium (Stubbs et al., 2006). In order to better understand the intercalation process I sought to determine what factors regulate the process of inner cell intercalation, which ultimately results in an even distribution of ciliated cells on the surface of the embryo.

Basigin (Bsg) is a member of the Ig superfamily of proteins, a family of proteins often characterized by their role in intercellular recognition. Basigin is a single pass transmembrane protein with extracellular, type C2, Ig domains (Schlosshauer et al., 1995). The extracellular domain has been shown to be highly glycosylated, a key feature of many cell adhesion and cell-cell recognition molecules. Basigin has been shown to form species-specific homodimers, with dimerization mediated by disulfide bonds in the N-terminal Ig domain (Yoshida et al., 2000). Additionally, Basigin has been shown to form complexes with integrins

(Berditchevski et al., 1997), a class of cell surface receptors that attach to the

extracellular matrix (ECM) but can also be involved in intracellular signaling

(Stupack, 2007).

Basigin was initially identified as glycoprotein 42 (gp42) in a screen looking

for interactors with the fibronectin receptor (Altruda et al., 1989). Shortly thereafter

Bsg was also identified in F9 embryonic carcinoma cells by cDNA screening using an

antibody directed against the receptor of Lotus tetragonolobus agglutinin (LTA) which

has been shown to interact strongly with embryonic cells (Miyauchi et al., 1990). An

additional homolog was identified as neurothelin in chick, and studied quite

extensively due to its unique expression pattern in the endothelial cells of the brain as

well as at the retinal pigment epithelium (RPE) barrier (Schlosshauer and Herzog,

1990). Its unique expression pattern suggested that Bsg might be acting as a

component of the blood-brain barrier. However, gene knockout in mouse embryos did

not lead to any obvious blood-brain barrier defects (Igakura et al., 1998). The

expression pattern of Bsg in tissues that form barriers, and its interactions with cellular

receptors, suggest that Bsg could be involved in cell-cell or cell-matrix recognition

and adhesion.

A second role for Basigin may be as an affector of ECM degradation. Tissue

culture studies have implicated Bsg as potent inducer of matrix metalloproteinase

(MMP) production in fibroblasts and tumor cells (Li et al., 2001). MMPs are zinc-

dependent endopeptidases that are capable of degrading the extracellular matrix

(ECM) and basement membrane (Nagase and Woessner, 1999). MMPs have been

linked to cellular migration events such as leukocyte invasion (Stefanidakis and

Koivunen, 2006), a tightly regulated mechanism, whereby leukocytes pass through the

endothelial wall in response to chemoattractants. In vitro assays have shown that the

invasive capacity of tumor cells was increased upon Bsg transfection, which correlated

with increased MMP production (Caudroy et al., 2002). Additionally, invasive

metastatic tumors express high levels of Bsg. As metastasis is a process which relies

on changes in cell-cell adhesion and loss of adherence to the ECM (Deryugina and

Quigley, 2006), it is reasonable to hypothesize that Bsg expression in tumors results in

MMP production which would result in decreased extracellular matrix adhesion

(Kanekura et al., 2002; Taylor et al., 2002).

Xenopus Basigin (*XBsg*) was identified in the Kintner lab through a microarray

screen of a cDNA library, looking for genes involved in positive and negative

regulation of neuronal differentiation. *XBsg* was selected as an interesting candidate

from this screen due to its frequent upregulation in tissue induced to become

differentiated neurons. However, *in situ* hybridization using an antisense nucleotide

probe revealed that *XBsg* is not expressed in neuronal precursors or primary neurons

but rather in non-neural ectoderm of *Xenopus* embryos in a distinct salt and pepper

pattern reminiscent of α-tubulin, a marker of ciliated cells.

Intercalating cells in the epithelium of *Xenopus* embryos must strictly regulate

cell-cell recognition, adhesion, and motility in order to successfully leave the loosely

packed inner layer of the epithelium and join the outer layer of the epithelium where

they form adherens and tight junctions with cells of the outer layer. This process

occurs during differentiation of the intercalating cells, thus requiring temporal regulation, but must also occur without disrupting the integrity of the epithelium. The expression pattern of Bsg in other systems, as well as its effect the invasive capacity of several cell types suggests that it may be involved as an affector of cell adhesion or migration. Based on these observations I sought to determine if *X*Basigin acts as a regulator of intercalation in *Xenopus* embryos.

RESULTS

Identification of XBasigin and homology to other vertebrate Basigin proteins

Xenopus Basigin (*XBsg*) coding sequence was deduced by identifying numerous EST sequences from PubMed databases. EST sequence analysis revealed two isoforms of Basigin in *Xenopus*, an 813 base pair (bp) sequence referred to as *XBsg* which encodes a putative protein of 271 amino acids (aa) with an approximate molecular weight of 29 kilodaltons (kD). A second, longer isoform of 1164bp, encoding 387aa, with an approximate molecular weight of 43kD was also identified by EST analysis and is referred to as *XBsgL*. The longer isoform of Basigin has been shown in mouse to be generated by alternative splicing wherein there is an addition of exon 1a, a part of intron 1 in the short isoform. This additional N-terminal sequence lies extracellularly and encodes a third, type C2, Ig domain. Both of the predicted isoforms of *Xenopus* Basigin are similar in size to identified homologs in other species.

In order to further ensure that the cDNA clones generated from *Xenopus laevis* were indeed the homologs of Basigin, protein sequences of several vertebrate

homologs were aligned using ClustalW (Figure 3.1). XBsg shares 44%, 43%, and

53% overall homology with human, mouse and chick basigin respectively, and 83%

homology with *Xenopus tropicalis* basigin. XBsgL shares 48%, 58%, and 48%

overall homology with human, chick and zebrafish long isoforms of basigin

respectively. Interestingly, the transmembrane sequence shows almost 100%

homology across species (light gray box Figure 3.1), and all isoforms have a

conserved, positively charged, glutamine residue within the transmembrane domain

(asterisk Figure 3.1). While it is unusual to have positively charged residues in the

transmembrane domain of single pass transmembrane proteins, such residues have

been implicated in intramembrane protein-protein interactions (Muramatsu and

Miyauchi, 2003).

Analysis of XBasigin Expression in the Embryonic Epithelium

In order to determine the expression pattern of *XBsg* embryos at various

developmental stages were probed by in-situ hybridization using an *XBsg* antisense

digoxigenin labeled probe (Figure 3.2A-C). Due to sequence similarities this probe

likely detects both *XBsg* and *XBsgL*. At the neural plate stage (stage 13), when

intercalating cell precursors are selected in the inner layer of the ectoderm, a subset of

cells express high levels of Basigin. This salt and pepper pattern of expression is

maintained through development from neural tube stages (stage 17), when cells are

undergoing intercalation, through tailbud stages (stage 26), when intercalating cell

populations are undergoing differentiation. While it appears that a subset of cells

express a very high level of *XBsg*, there also appears to be as subset of cells at later stages of development that express lower levels of *XBsg* (Figure 3.2C inset).

Both ciliated cell precursors (CCP) and intercalating non-ciliated cells (INC) are negatively regulated by the Notch signaling pathway (Deblandre et al., 1999; Stubbs et al., 2006). Misexpression of the intracellular domain of the Notch receptor (ICD) activates Notch signaling (Chitnis et al., 1995), blocking CCPs and INCs from forming. Conversely misexpression of dominant negative form of human Mastermind (dnHMM) blocks Notch signaling (Fryer et al., 2002) leading to an overproduction of CCPs and INCs. *XBsg* expression was thus analyzed to determine if its expression in the skin was regulated by Notch signaling. *In situ* hybridization analysis shows that *XBsg* expression mimics α-tubulin expression (data not shown) in response to Notch signaling; activation of Notch signaling by ICD RNA injection leads to a downregulation of *XBsg* expression (Figure 3.2E), while blocking Notch signaling by dnHMM RNA injection leads to an upregulation of *XBsg* expression (Figure 3.2F) when compared to control βgal injected embryos (Figure 3.2D). As noted in chapter 2, blocking Notch signaling also leads to increased intercalation (Stubbs et al., 2006). The correlation between increased *XBsg* expression and intercalation, along with increased invasive capacity observed in murine *Bsg* transfected cells (Caudroy et al., 2002) suggests that *XBsg* activity may mediate the increased intercalation observed when Notch signaling is blocked.

Misexpression of XBsg does not affect intercalation

In order to determine if XBsg could lead to an increase in intercalation or invasive capacity of cells in the *Xenopus* epithelium I overexpressed *XBsg* by injecting capped synthetic mRNAs encoding *XBsg* or *XBsgL* along with mRFP mRNA to mark injected regions. To ensure protein synthesis from the synthetic mRNA injections a third construct with 6 myc-tags fused to the C-terminal end of *XBsg* was tested. At stage 26 embryos were fixed and stained with the tight junction marker ZO-1 to mark cell-cell junctions, and a monoclonal acetylated α-tubulin antibody to mark cilia (Figure 3.3A-C). Controls were also stained with a monoclonal anti-Myc antibody (data not shown). Analysis of images obtained using confocal microscopy revealed expression of myc-tagged *XBsg*, and presumably the other *XBsg* constructs. However, no change in the total number of various cell types based on their characteristic morphologies (Stubbs et al., 2006) was observed indicating no change in overall intercalation.

In order to more definitively determine if misexpression of *XBsg* has any effect on intercalation transplant assays were performed as in chapter 2. Donor embryos were injected with mRNA encoding *mRFP* while host embryos were injected with mRNA encoding *mGFP* alone or along with *XBsg* or *XBsgL* as described above. Embryos were then allowed to develop until stage 10, at which time a small piece of the outer layer from the donor embryo was transplanted onto the exposed inner layer of a host embryo. Host embryos were fixed and analyzed at stage 16 (data not shown), when intercalation is just beginning, and at stage 20, a stage at which both CCPs and INCs, (collectively intercalating cell, ICs) are intercalating in earnest into

the outer layer (Figure 3.4A-C). Confocal imaging of the transplanted region, followed by quantification of cell populations, revealed no change in the number of intercalating cells at this stage indicating no overall change in either the timing or amount of intercalation (Figure 3.4D). Additionally, analysis of the intercalating populations revealed no differences in cell morphology or intercalating cell spacing between *XBsg* injected embryos and controls.

The above results suggest that overexpression of *XBsg* does not effect the ability of cells to intercalate or to space themselves evenly in the epithelium. Transmembrane proteins often play a role in cell-cell recognition and adhesion both through interactions in the extracellular domain but also through intracellular signaling mediated by the intracellular domain of the protein. An alternative method to alter the function of *XBsg* in the epithelium I generated expression constructs that could act as potential dominant negatives, to interfere with endogenous *XBsg* activity. In order to attempt to alter intracellular signaling I generated a construct lacking the intracellular domains while retaining the transmembrane and extracellular Ig domains (*XBsgΔC*). By eliminating the intracellular domain this construct could potentially bind to extracellular partners but would be unable to signal intracellular. A second construct was also generated that instead lacks the extracellular domain but retains the transmembrane and intracellular domains (*XBsgΔE*). Expression of this protein on the cell surface could potentially alter intracellular signaling in the absence of extracellular interactions. Misexpression of both isoforms by injection of synthetic capped mRNAs was performed as above, with *mRFP* mRNA as an injection tracer.

Confocal analysis of injected regions showed no overall change in the number of

ciliated cells or INCs as was reported for the full-length constructs (Figure 3.3D-E).

Finally, no ciliated cells were observed contacting each other, indicating that there was

no effect on ciliated cell spacing in the epithelium.

Morpholino Knockdown of XBsg does not Affect Intercalation or Cell Fates

As a final method to determine if *XBsg* is required for cells to intercalate in the

Xenopus epithelium I designed an antisense oligonucleotide morpholino directed

against *XBsg* in an effort to knockdown its expression. As the exon-intron boundaries

are not known for *XBsg*, morpholinos were designed to target the initiation codon in

order to block translation. Additionally, *Xenopus laevis* frogs have an allotetraploid

genome represented by duplicate copies of many genes, referred to as the A and B

form. In order to ensure efficient knockdown it was necessary to determine if *XBsg* is

represented by both an A and B form. BLAST searches of EST databases returned 34

Xenopus laevis sequences with significant similarity to *XBsg*. Comparison of these

sequences determined that there are likely both an A and B form due to the variation

in sequence in the 5' untranslated region (5' UTR) of the *XBsg* ESTs. However, the

sequence directly 5' of the initiation codon is shared such that one morpholino could

likely target both A and B forms. In order to attempt to block translation a morpholino

(XBsgMO1) was designed that matched bases from both the A and B forms, and

which overlapped the initiation codon. Analysis of the ESTs encoding *XBsgL*

determined that the 5' UTR sequence was almost identical to the 5' UTR sequence of

XBsg. However two base pair differences 5' to the XBsgMO1 sequence prompted the

generation of a second morpholino (XBsgMO2) to ensure efficient knockdown of the long isoform as well as the short isoform of *XBsg*.

Antisense morpholino oligonucleotides were injected in all 4 animal quadrants of 2-cell and 4-cell embryos to effectively target injection into all cells of the presumptive epithelium. Tracer mRNA injections were performed following morpholino injections due to their tendency to cause precipitation of the morpholino when mixed together in solution. Embryos were injected with each morpholino separately, or in combination and then allowed to develop until stage 26 at which time they were fixed and stained with ZO-1 and acetylated α-tubulin to mark cell-cell junctions and cilia respectively. Analysis of several areas from a number of embryos revealed no change in the number of outer cells or intercalating cell populations. Additionally, no change in the spacing of ciliated cells was observed. Similarly to the misexpression experiments above, we do not have an antibody that detects *XBsg* so we cannot say with certainty that the level of expression of *XBsg* is affected by morpholino injection.

DISCUSSION

Basigin is expressed at high levels in cells, such as metastatic tumor cells, that are highly invasive (Caudroy et al., 2002). In order for cells to become invasive the ECM surrounding the cells must be broken down, releasing the cells to move from their current location. Indeed MMP production, which can lead to degradation of the ECM has been shown to be stimulated in fibroblasts co-cultured with Bsg expressing cells (Li et al., 2001). Intercalating cell populations of the *Xenopus* larval epithelium

must move from one cell layer to the next. This process may involve delaminating from the fibronectin substrate on the basal surface of the inner layer, which may require the production of MMPs (Kenny et al., 2008). In the developing external epithelium of *Xenopus* embryos a subset of cells, whose distribution resembles that of intercalating populations, express *XBsg*. This observation led to the hypothesis that expression of *XBsg* might facilitate intercalation, possibly through the production of MMPs. However, misexpression of *XBsg*, both ubiquitously in the epithelium, or just in inner cells, failed to increase intercalation or to affect the number or types of cells that intercalate into the outer layer. Alternatively the expression of potential dominant negative constructs to interfere with endogenous signaling, or knockdown by morpholino injection to block expression also failed to affect the ability of cells to intercalate.

Despite failing to affect intercalation, another possible role for *XBsg* could be affecting cell-cell recognition in the developing epithelium. The extracellular domain of *XBsg* and *XBsgL* contains two or three Ig domains, respectively. Ig domains have been shown in many cases to act in intercellular recognition (Williams and Barclay, 1988). One model that could arise from the observed expression pattern, and the unique spacing pattern of ciliated cells in the epithelium, is that *XBsg* is expressed is ciliated cells, allowing ciliated cells to identify, and avoid each other, during intercalation leading to the final observed spacing pattern of ciliated cells in the skin. However, in no instance where potential changes to *XBsg* expression were elicited by misexpression, either in its wildtype form, or as a truncated protein, did I observe

changes consistent with a role for *XBsg* in cell-cell recognition. Additionally, when morpholinos were injected to knockdown the translation of *XBsg* no change was observed in cell-cell recognition.

Taken together these results lead one to conclude that *XBsg* does not play a role in either intercalation or cell-cell recognition. However, given the lack of controls to determine that we are indeed effecting *XBsg* expression, these studies are not conclusive. In order to further these analyses, and definitively rule out a role for *XBsg* in radial intercalation it will likely be necessary to raise an antibody directed against *XBsg*. This would allow us to confirm that misexpression analyses and knockdown techniques are effectively altering the expression of protein. Additionally, a percentage of the murine *Bsg* knockout embryos are early embryonic lethal, suggesting that early development may rely on proper expression of *Bsg*. Thus, *Xenopus* embryos may have a maternal component that we cannot delete by effecting translation. In order to test this possibility, affecting the maternal component of *XBsg* could be accomplished by morpholino injection into oocytes, followed by fertilization (Zhang et al., 1998) or potentially by antibody injection into embryos to bind endogenous *XBsg* potentially blocking its function.

88

Figure 3.1 Protein Alignment of Basigin Homologs: Short and long isoforms of human (Hs), mouse (Mm), chick (Gg), *Xenopus laevis* (Xl), *Xenopus tropicalis* (Xt), and zebrafish (Dr) Basigin. Signal sequence is boxed in dark gray with the likely cleavage site marked by an arrow. The transmembrane domain is boxed in light gray with the conserved glutamine residue in the transmembrane region marked by an asterisk. The Ig domains are underlined in black.
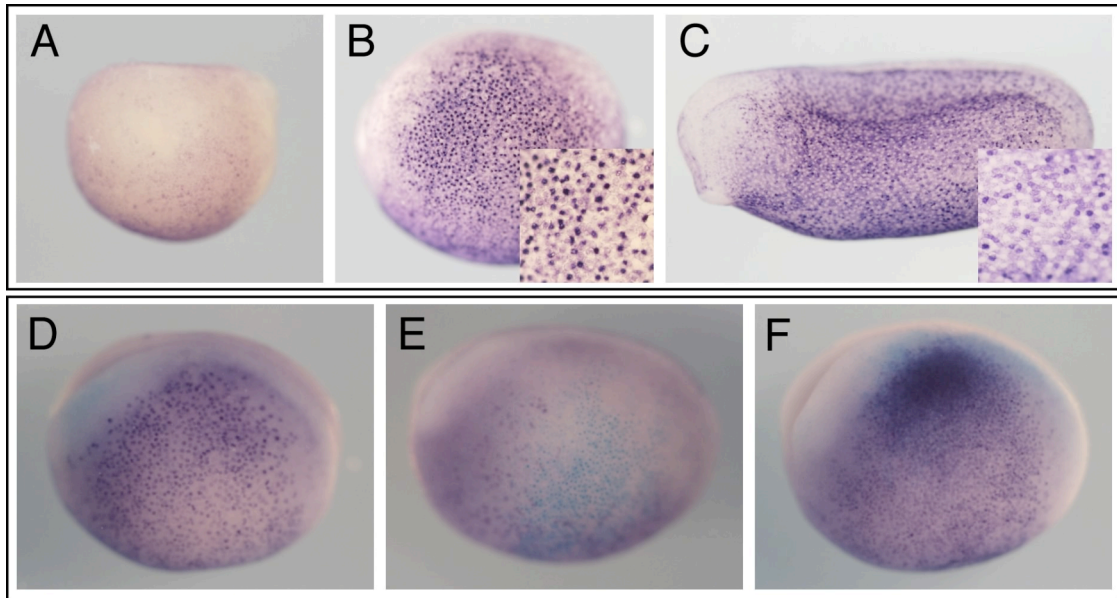
Figure 3.2 Basigin Expression in Embryos: (A-C) Wildtype expression of *XBsg* at stage 13 (A), stage 17 (B) and stage 26 (C), insets in panels B and C show higher magnification views. **(D-F)** *XBsg* expression at stage 17 in response to misexpression of notch reagents. Embryos were all injected with β-gal to mark injected region (blue staining). Control β-gal injection (D), ICD injection to activate Notch signaling (E), dnHMM injection to block Notch signaling (F).
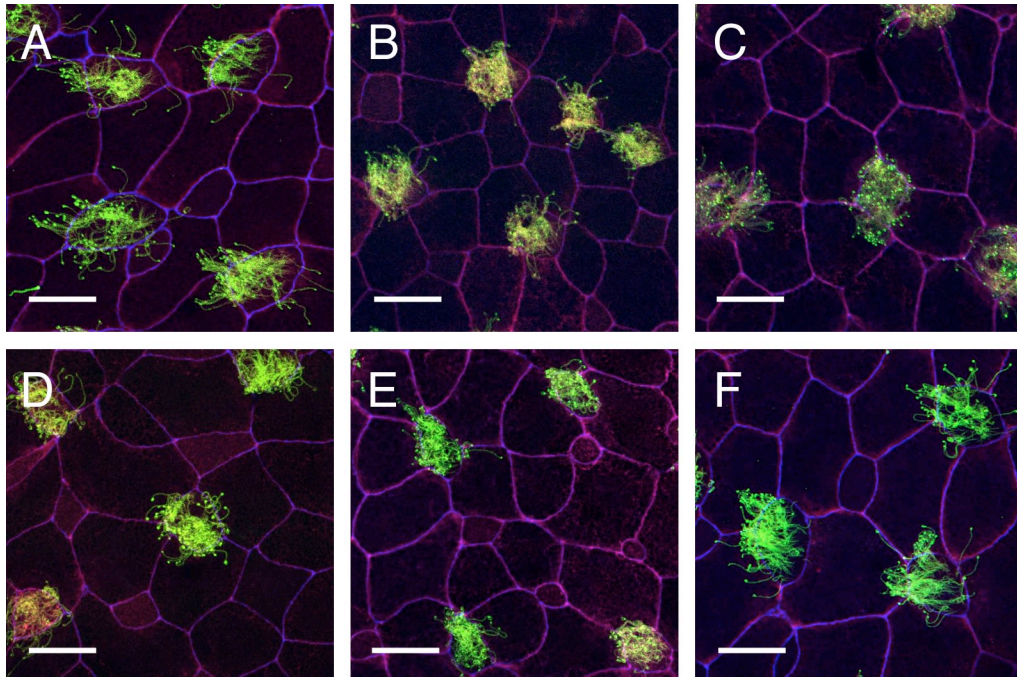
Figure 3.3 XBasigin Misexpression does not affect Intercalation or cell fates: Embryos were injected with XBsg (A), XBsgL (B), myc-tagged XBsg (C), BsgΔC (D), BsgΔE (E) and mRFP (F). **(A-F)** All embryos were injected with mRFP (red) to mark the injected cells then stained with ZO-1 (blue) and acetylated α-tubulin (green) to mark tight junctions and cilia, respectively. Scale bars represent 20μm.
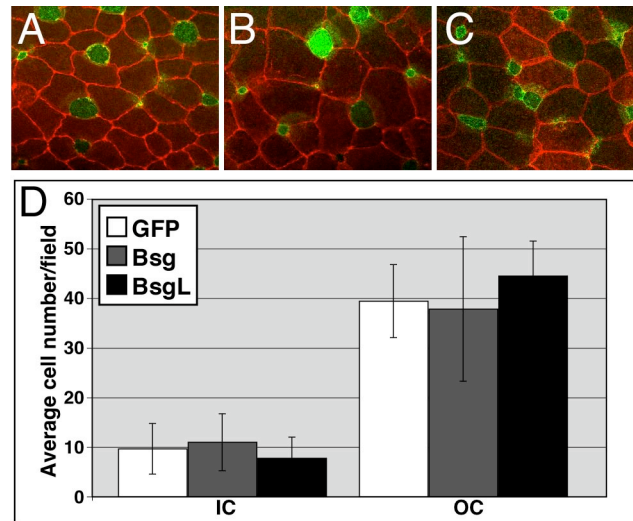
Figure 3.4 XBasigin Misexpression in Transplant: Outer layer ectoderm labeled with mRFP was transplanted onto control host embryos labeled with mGFP (A, E) or host embryos expressing XBsg (B), XBsgL (C) an activator of Notch signaling, ICD (F) or ICD and XBsg (G). Embryos were fixed at stage 20 (A-C) or stage 26 (E-G) and stained with an antibody against acetylated α-tubulin (blue). Images are compressed confocal Z-stacks showing the cells near the apical surface. Outer cells (OC, red), intercalating cells (IC, green, A-C), intercalating non-ciliated cells (INC, green, E-G) or ciliated cells (CC, blue, E-G) were quantified. Quantification of five fields from at least 3 transplants for each condition.
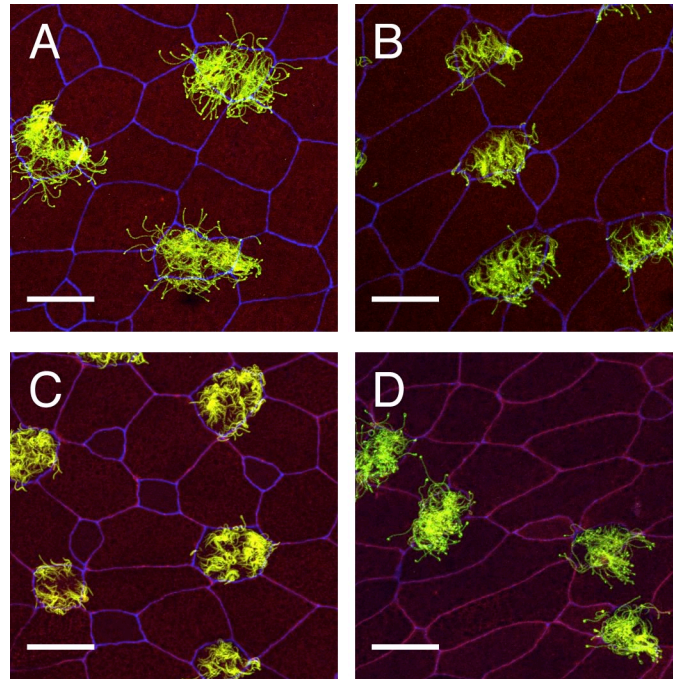
Figure 3.5 XBasigin knockdown: Embryos were injected with XBsg1MO (A), XBsg2MO (B), XBsg1MO + XBsg2MO (C), mRFP (D). **(A-D)** All embryos were injected with mRFP (red) to mark the injected cells then stained with ZO-1 (blue) and acetylated α-tubulin (green) to mark tight junctions and cilia, respectively. Scale bars represent 20μm.

CHAPTER IV

The Forkhead Transcription Factor, FoxJ1, Specifies Node-like Cilia

In *Xenopus* and zebrafish embryos

ABSTRACT

Ciliated cells that produce a leftward fluid flow have been proposed to mediate left-right patterning in mouse, fish and Xenopus embryos. The cilia that produce this flow combine features of primary sensory cilia with those of motile cilia found on highly specialized multi-ciliate cells, but how these cilia are specified is unknown. We address this issue by analyzing the Xenopus and Zebrafish homologs of FoxJ1, a forkhead transcription factor that enables multi-ciliate cells to undergo ciliogenesis in the mouse embryo. We show that the cilia that underlie left-right patterning on the Xenopus gastrocoel roof plate (GRP) and Zebrafish Kupffer's vesicle (KV) are severely shortened or fail to form in embryos injected with morpholinos directed against *FoxJ1*. We also show that misexpressing XFoxJ1 is sufficient to induce ectopic GRP-like cilia in surface epithelial cells of frog embryos. Microarray analysis indicates that XFoxJ1 induces the formation of cilia by upregulating gene expression that encodes the components required for motile cilia. These results indicate that FoxJ1 is a critical determinant in specifying cilia used in left-right patterning, suggesting that this cilia subtype forms in cells using a similar genetic pathway used to generate motile cilia in multi-ciliate cells.

Introduction

Cilia are microtubule-based organelles that project hair-like from the surface of vertebrate cells. Cilia can be generally subdivided into motile and sensory subtypes that differ markedly in structure and function (Satir and Christensen, 2007). Sensory cilia, which can form in many cell types from neurons to fibroblasts (Wheatley et al.,

1996), are typically short in length, lack structural features such as the central pair and dynein arms but play important roles in detecting chemical, or mechanical stimuli as an extension of the cell surface. One hallmark of sensory cilia is that they invariably form as a single cilium on non-dividing cells when the paired centrioles docks at the cell surface, allowing the mother centriole to form a basal body and initiate ciliogenesis, apparently as a default pathway (Spektor et al., 2007). By contrast, motile cilia that form on epithelial cells within such tissues as the oviduct, the ependyma or the respiratory airways are specialized to produce fluid flow (Satir and Christensen, 2007). Cilia of the motile subtype have a 9+2 axonemal structure, use dynein arms to produce a whip-like power stroke and most likely have other structural features required for oriented flow (e.g. structures involved in planar cell polarity). In addition, each flow-producing cell typically projects hundreds of cilia, requiring mechanisms not likely to be initiated in cells with sensory cilia, for example those that mediate acentriolar duplication.

In the mouse, a genetic distinction has been made between cells that form sensory and motile cilia based on the analysis of the forkhead protein, FoxJ1, also known as HFH-4 (Whitsett and Tichelaar, 1999). Mouse FoxJ1, a potent transcriptional activator, is expressed prominently in multi-ciliate cells within the respiratory tract, oviduct and choroid plexus (Hackett et al., 1995; Lim et al., 1997; Pelletier et al., 1998). In mice null for FoxJ1 by targeted deletion, multi-ciliate cells still undergo centriole duplication but these fail to properly target and dock at the apical surface and extend cilia (Gomperts et al., 2004; Huang et al., 2003b; Pan et al.,

2007). By contrast, loss of FoxJ1 does not appear to disrupt the formation of sensory

cilia, such as those present in olfactory epithelium or in the kidney (Brody et al., 2000;

Chen et al., 1998). Thus, FoxJ1 is required for cells to form motile but not sensory

cilia.

A third subtype of cilia found in the mouse is located on cells at the embryonic

node, a structure present in the early embryo that underlies the breaking of left-right

symmetry (Hirokawa et al., 2006). Node cilia beat with a clockwise rotational motion,

thereby creating a linear leftward flow of extracellular fluid over the node surface

(Nonaka et al., 1998). Despite their functional resemblance to the multi-ciliate cells

that produce fluid flow, node cells only form a single cilium, a hallmark of sensory

cilia. Moreover, node cilia at least in the mouse are thought to lack a central pair, thus

resembling both motile and sensory cilia in axonemal structure (Takeda et al., 1999).

Finally, analysis of the FoxJ1 mutant phenotype has not clarified whether node cilia

are more motile-like or sensory-like. FoxJ1 null mice have randomized left-right

asymmetry, indicating a defect in node cilia, but monociliated cells at the embryonic

node are still present (Brody et al., 2000; Chen et al., 1998; Zhang et al., 2004). Thus,

it is not clear whether the formation of node cilia involve pathways used by motile or

sensory cilia and what role FoxJ1 might have in their formation.

In Xenopus (Schweickert et al., 2007) and fish (Essner et al., 2005; Essner et

al., 2002), embryonic structures related to the mouse node have cells with monocilia

that also produce a leftward flow, namely the gastrocoel roof plate (GRP) and

Kupffer's vesicle (KV), respectively. We therefore examined the role of FoxJ1 in the

formation of ciliated cells in these structures, asking whether FoxJ1 function is required for these cells to mediate left-right patterning, and if so how. Our results indicate that FoxJ1 is both necessary and sufficient to drive the formation of node-like cilia in embryonic epithelia, suggesting that this cilia subtype forms in cells using a similar genetic pathway used in multi-ciliate cells.

RESULTS

FoxJ1 in left-right patterning

FoxJ1 null mice have left-right patterning defects but are reported to form node cilia (Brody et al., 2000; Chen et al., 1998; Zhang et al., 2004). To determine whether this is true in other vertebrate species, we initially examined Zebrafish embryos, where monociliated cells within Kupffer's vesicle (KV) produce a directional flow required for the establishment of left-right asymmetry during embryogenesis (Essner et al., 2005). *ZFoxJ1* RNA is first expressed in KV as early as stage 6ss, and then later in the pronephric duct where motile, multi-ciliate cells are known to form (Figure S4.1). To determine the function of ZFoxJ1 in cells of KV, Zebrafish embryos were injected with a morpholino designed to block the translation of *ZFoxJ1* RNA (ZFoxJ1^{MO}). ZFoxJ1 morphants develop with severe defects in left-right heart jogging, consistent with a defect in KV cilia function (Figure 4.1) (Essner et al., 2005; Kramer-Zucker et al., 2005a). When ZFoxJ1 morphants were stained with the acetylated tubulin antibody that stains cilia, KV forms but many of the cells within it lack cilia or have severely shortened cilia (Figure 4.1F,G). Thus, ZFoxJ1 is required for left-right patterning, and moreover is required for cells in the KV to undergo ciliogenesis.

In Xenopus embryos, monociliated cells located on the posterior gastrocoel roof plate (GRP) produce a directional flow, thus acting as the equivalent of KV in left-right patterning (Schweickert et al., 2007). The cells in the GRP express *XFoxJ1* (Figure S4.2). To examine the function of FoxJ1 in these cells, embryos were injected at the two-cell stage with a morpholino (XFoxJ1^{MO}) that was designed to block either the translation or splicing of *XFoxJ1* RNA, and then analyzed at stage 17 by staining the cilia in the GRP using the antibody against acetylated tubulin (Figure 4.1H-K). Injecting embryos with either XFoxJ1 morpholino, but not a control morpholino, resulted in missing or severely shortened node cilia (Figure 4.1I, K). Thus, FoxJ1 is required for cilia formation on the cells that mediate left-right patterning in both Xenopus and Zebrafish embryos.

FoxJ1 is required for ciliogenesis in *Xenopus* multiciliate cells

The role of FoxJ1 in the formation of node-like cilia appears to differ between Zebrafish/Xenopus and the mouse. We therefore extended our analysis of XFoxJ1 to multi-ciliate cells to determine whether in this context, the function of FoxJ1 is conserved. The multi-ciliate cells that form in the Xenopus larval skin after stage 26 closely resemble those found in the mouse respiratory tract and express XFoxJ1 (Figure S4.2), and thus allow one to directly compare FoxJ1 function in the formation of motile cilia in different species.

Injecting either XFoxJ1^{MO}, but not a control morpholino, produced a dose-dependent defect in skin cilia formation: at a lower dose, cilia still formed, but they were reduced in number and often shortened in length while at higher doses, most cilia

were lost in the skin except for an occasional stumpy cilium (data not shown, Figure

4.2B, D). Ciliated cells can be distinguished from other cell types in the skin based on

their characteristic morphology and spacing pattern (Stubbs et al., 2006). Based on

these criteria, ciliated cells were still present at their normal density in embryos

injected with XFoxJ1^{MO} even as cilia were completely lost (data not shown). Thus,

these results indicate that XFoxJ1 plays a conserved role in the ciliogenesis of multi-

ciliate cells.

In the mouse, FoxJ1 has been proposed to activate gene expression required to

dock basal bodies at the apical surface, an obligatory step in the process of ciliogenesis

(Gomperts et al., 2004; Huang et al., 2003b; Pan et al., 2007). To determine whether

this is also true in Xenopus ciliated cells, basal bodies were labeled in the FoxJ1

morphants using a centrin2-GFP fusion protein and visualized using confocal

microscopy (Mitchell et al., 2007) (Figure 4.2E-F). Indeed, the number of basal

bodies localized apically per cell was reduced in FoxJ1 morphants relative to control

by about 30% (167±34 versus 112±28, P<.005). Since this assay may overestimate

the number of basal bodies intimately docked to the apical surface, we examined the

location of basal bodies in ciliated cells in relation to the actin-rich apical cortex that

can be stained with Rhodamine-Phallodin (Mitchell et al., 2007; Park et al., 2006)

(Figure 4.2G-H). In control ciliated cells, this actin-rich network encircles the centrin-

labeled basal bodies, presumably anchoring them apically for ciliogenesis (Figure

4.2G). Strikingly, in FoxJ1 morphants this apical actin staining was lost, while

cortical actin labeling at cell-cell contacts was unaffected (Figure 4.2H). These

observations parallel those in the mouse, suggesting that XFoxJ1 plays a conserved role in ciliogenesis in multi-ciliate cells, presumably by activating genes required for basal body docking and ciliogenesis.

XFoxJ1 expression is sufficient to induce ectopic motile cilia

Previous experiments in which FoxJ1 was mis-expressed in cultured cells or transgenic mice indicated that FoxJ1 is not sufficient to induce multi-ciliate cell differentiation, in line with the idea that FoxJ1 acts relatively late in these cells to promote ciliogenesis (You et al., 2004). By contrast, given the role of FoxJ1 in the formation of node-like cilia shown above, we asked whether FoxJ1 is sufficient to induce the formation of this cilia subtype. FoxJ1 was misexpressed in Xenopus embryos, by injecting two-cell stage embryos with RNA encoding a wildtype form of XFoxJ1. At stage 17 when cilia in the GRP have formed, we scored the presence of ectopic cilia on the superficial layer of epithelium that extends as a continuous sheet from the gastrocoel roof to the outside of the embryo (Shook et al., 2004). In control injected embryos, only the region of this epithelium that lies on the gastrocoel roof forms the node-like cilia that mediate left-right patterning (Figure 4.3A, data not shown). In embryos injected with *FoxJ1* RNA, however, cilia now formed through out this epithelium, including that covering the outside of the embryo (Figure 4.3B). Notably the ectopic cilia induced by XFoxJ1 were identical in morphology to those that form on the GRP and formed on cells that are not normally ciliated. Thus, FoxJ1 can induce ciliogenesis in the embryonic epithelium de novo.

In Xenopus, Notch signaling negatively regulates the differentiation of multi-ciliate cells that form in the skin at later stages but not the formation of cells with node-like cilia. Thus expressing an activated form of the Notch receptor, ICD, in embryos by RNA injection, leads to a complete loss of multi-ciliate cells in the skin (Figure 4.3E) (Deblandre et al., 1999), but not the ciliated cells on the GRP (data not shown). To determine whether cells that respond to FoxJ1 were node-like in this respect, we injected embryos with both FoxJ1 and ICD and examined cilia formation in the skin at stage 26 (Figure 4.3C-F). Even though ICD completely suppresses the formation of multi-ciliate cells (Figure 4.3E), it had no affect on the ability of FoxJ1 to induce the formation of ectopic cilia resembling those on the GRP (Figure 4.3F). Thus, FoxJ1 is sufficient to induce ectopic cilia independently of its role in the differentiation of multi-ciliate cells.

FoxJ1 induced cilia are node-like

We next asked whether the cilia induced by FoxJ1 resemble node-like cilia by characterizing their axonemal structure using transmission electron microscopy (TEM). The motile cilia involved in left-right patterning invariably have dynein arms emanating from each of the nine outer microtubule doublets. In addition, the axoneme of cilia in the KV contains a central microtubule doublet (9+2) much like those in multi-ciliate cells. In the mouse, the node cilia have been reported to be 9+0 but a recent report suggests that they are 9+2 and that the central pair is labile during fixation (Caspary et al., 2007; Takeda et al., 1999). When cilia induced by FoxJ1 were analyzed by TEM, they contained a central doublet (9+2), and dynein arms

(Figure 4.3F), indicating that these cilia are of the motile subtype and virtually identical in structure to the cilia formed by multi-ciliate cells in the skin (Figure 4.3G). Consistent with this conclusion, when the ectopic cilia induced by FoxJ1 were visualized in live tissue using confocal microscopy, they were motile (Figure S4.4).

High levels of FoxJ1 misexpression induces bi-ciliated cells

In embryos injected with higher levels of *XFoxJ1* RNA, many of the cells responded by forming two ectopic cilia rather than a monocilium normally associated with node-like cilia (14.62% +/- 6.96 s.d.) (Figure 4.4B, E). To induce two cilia, XFoxJ1 must either promote a round of centriole duplication, or else split the centriole pair so that both the mother and daughter centrioles can mature as basal bodies and initiate ciliogenesis. To examine this phenotype further, we visualized centrioles in *XFoxJ1* RNA injected embryos using an antibody directed against γ-tubulin. In an uninjected epithelial cell, centriole-pairs labeled with the γ-tubulin antibody tend to be located not apically but in a basolateral position (Figure 4.4A). By contrast, in *XFoxJ1* RNA injected embryos, these structures relocalized to a central apical position where one or two ectopic cilium formed (Figure 4.4B). In some cases, these structures remained paired and the cell formed only one cilia. In about 50% of the cells, however, the centrioles were split, resulting in some cases in two cilia per cell. Together these results indicate that ectopic expression of *XFoxJ1* not only induces apically docking of centrioles as basal bodies, but also has a profound effect on basal body formation in ways that allow a cell to form two cilia.

We next asked whether the bi-ciliated cells induced by XFoxJ1 also appear when cilia form on the GRP. Indeed, in wildtype embryos that were stained with the acetylated tubulin antibody, a significant fraction of the cells on the GRP project two cilia (Figure 4.4E, 13.61% +/- 4.87 s.d.) When cells in the GRP were stained with the γ-tubulin antibody, approximately 40% of cells contained two well-separated centrioles (Figure 4.4F). Thus, bi-ciliate cells normally arise within the GRP presumably in response to higher levels of *FoxJ1* expression.

FoxJ1 activates gene expression encoding components of motile cilia

Based on the proposed function of FoxJ1 in multi-ciliate cells in the mouse, one model is that FoxJ1 induces node-like cilia by simply promoting the docking of centrioles to the apical surface where they form basal bodies and initiate ciliogenesis. An alternative model, however, is that FoxJ1 upregulates genes that are not only required for basal body docking, but also those required for cilia motility. To distinguish between these two models, we used Affymetrix microarrays to survey the genes that are induced ectopically by XFoxJ1 when it induces ectopic cilia formation.

To obtain enough material to carry out this analysis, we exploited that fact that XFoxJ1 can still induces the formation of ectopic cilia when the formation of multi-ciliate cells is blocked by expressing an activated form of the Notch receptor (ICD) (Deblandre et al., 1999) (Figure 4.3C). We therefore prepared RNA from cultured ectoderm that expresses both *ICD* and *XFoxJ1*, as well as RNA from ectoderm injected with just *ICD* RNA. The expression levels of RNAs were then compared

between these two samples, initially focusing on those that were elevated by at least 10-fold by XFoxJ1 in an ICD background (Table S4.1).

Of the approximately 100 genes upregulated 10-fold by XFoxJ1, a third encode the Xenopus homologs of proteins found in a ciliome database assembled using a survey of bioinformatics, genomics and proteomics studies (Inglis et al., 2006), including many proteins found in axonemal structures exclusive to motile cilia. For example, XFoxJ1 induced genes whose products comprise the dynein arms, including heavy chain subunits (DNAH9 and DNAH8), an intermediate chain subunit (DNAI1) a WD40 repeat protein potentially involved in dynein arm assembly, isoforms of adenylate kinase, (AK5 and AK7), a dynein light chain (Tctex-1), and a dynein associated protein (roadblock) related to LC7 in Chlamydomonas. XFoxJ1 also induced at least one component of the central pair complex, Spag6, and various radial spoke proteins, including RSHL2, RSHL3, and radial spoke protein 44. XFoxJ1 induced the expression of four tektin isoforms, including one that is required for the function of motile cilia in the mouse. Thus, when FoxJ1 induces the formation of node-like cilia, it apparently does so by inducing the expression of genes required for cilia motility

Validation of FoxJ1 induced gene expression

To validate the results from the microarray analysis, we examined the expression of several genes on the FoxJ1 upregulated list, focusing on three that are likely to be critical for cilia motility based on mouse mutants, namely *PF16, Tektin-t* and *LR-dynein* (Sapiro et al., 2002; Supp et al., 2000; Tanaka et al., 2004). When

examined by whole mount, in situ hybridization, all three genes are expressed in the multi-ciliate cells in the skin, are lost when ciliated cells are eliminated from the skin by expressing ICD, or when ciliogenesis is blocked in the multi-ciliate cells by injecting the XFoxJ1^{MO} (Data not shown, Figure S4.3). Thus, all three genes are expressed in multi-ciliate cells in a FoxJ1-dependent manner. All three genes are expressed in the GRP and markedly upregulated ectopically in embryos misexpressing FoxJ1 (Figure 4.5A-C). To confirm these observations using a more quantitative assay, real-time PCR was used to measure RNA levels of *PF16*, *Tektin-t* and *LR-dynein* when the embryonic epithelium is explanted on fibronectin-coated glass (Figure 4.5D). In explants injected with *ICD* RNA alone, the expression levels of these three cilia genes dropped approximately 8-fold relative to control, inline with the idea that these genes are expressed in multi-ciliate cells. Moreover, in explants that express both FoxJ1 and ICD, the levels of RNA encoding these three cilia proteins approximately 5-10 fold over the levels found in control larval skin and 50 fold or more relative to ICD injected samples. Thus, these results indicate that when *XFoxJ1* induces node-like cilia in the embryonic epithelium, it upregulates the expression of genes involved in cilia motility.

DISCUSSION

Specification of cilia subtype is a critical aspect of cell type differentiation but the developmental mechanisms involved remain poorly understood. Many cell types form primary sensory cilia, and the formation of this cilia subtype appears to occur as a default pathway that is triggered when certain centriole-associated proteins are

downregulated (Spektor et al., 2007). The implication is that most cells constitutively produce the proteins required for sensory cilia formation, and will do so once centriole function is no longer required during the cell cycle. Conversely, the formation of motile cilia during the differentiation of multi-ciliate cells is likely to involve a more elaborate genetic program, part of which has been shown in the mouse to involve FoxJ1. Here we provide evidence that the differentiation of node-like ciliated cells not only require FoxJ1 but that FoxJ1 is sufficient to induce this pathway of cilia subtype differentiation. Our results reveal an unexpected central role of FoxJ1 in activating gene expression required for the formation of motile node-like cilia, a role that is likely to be relevant to its function in the differentiation of multi-ciliate cells.

In the mouse, a null mutation in FoxJ1 clearly establishes its role in the differentiation of multi-ciliate cells, such as those in the lung (Whitsett and Tichelaar, 1999). The ciliated cells still form, undergo centriole duplication, however docking of these centrioles as basal bodies at the apical surface where ciliogenesis occurs, fails. Further analysis of this phenotype indicates that FoxJ1 mutant ciliated cells fail to properly organize the apical actin network that is presumed required for basal body docking (Pan et al., 2007). The multi-ciliate cells in the Xenopus skin are indistinguishable from those in other ciliated epithelia that are lost in the FoxJ1 mutant mouse. Indeed, when XFoxJ1 activity is inhibited in Xenopus using morpholinos, the ciliated cells in the skin are still present, centriole duplication still occurs, but ciliogenesis is blocked and the apical actin cap disrupted. FoxJ1, therefore, plays a

conserved role in the differentiation of multi-ciliate cells, by promoting a relatively late step in ciliogenesis.

The left-right axis is randomized in FoxJ1 mouse mutants, suggesting defects in node cilia, but the monociliated cells at the node are still present. This observation raises a paradox given the proposed role of FoxJ1 in multi-ciliate cells, since one would expect that FoxJ1 would be required for basal body docking and ciliogenesis in node cells. By contrast, the results obtained with FoxJ1 morpholinos indicate that cilia formation in both Zebrafish KV and Xenopus GRP is severely compromised in the absence of FoxJ1. In addition, ectopic expression of XFoxJ1 is sufficient to induce epithelial cells, which are not ciliated, to form ectopic cilia that are remarkably similar to those found on the GRP. Finally, XFoxJ1 induces the formation of node-like cilia, apparently by activating, either directly or indirectly, a large number of genes that are associated with motile cilia, including those expressed in multi-ciliate cells. These results strongly indicate that FoxJ1 specifies the formation of node-like cilia, and in turn suggest that node-like cilia share a similar genetic program as those multi-ciliate cells and are unlikely to be a modified form of primary sensory cilia.

What might account for the fact that cilia are lost in the Xenopus GRP and Zebrafish KV in FoxJ1 morphants while cells at the embryonic node in FoxJ1 null mice are still ciliated even though their left-right axis is randomized (Zhang et al., 2004)? One explanation is that in Xenopus/Zebrafish the formation of node-like cilia is more dependent on FoxJ1 than in the mouse, where other redundant factors come into play. However, another explanation is based on the observation that mouse node

contains two populations of monociliated cells (McGrath et al., 2003), one of which is centrally located, expresses lrd, and extends a motile cilium while the other is more peripheral, does not express lrd, and extends a sensory cilium. Thus, node cells in the FoxJ1 mutant mouse conceivably form sensory cilia, thus masking the loss of the motile cilia subtype. By contrast, sensory cilia have not been observed in either the Zebrafish KV or the frog GRP. Why sensory cilia are less prevalent in these species is unclear but one consequence is that it makes the loss of the motile node-like cilia more obvious. In this view, FoxJ1 plays a conserved role in specifying the motile, node-like cilia in vertebrates, while the prevalence of sensory cilia among cells that mediate left-right patterning is more variable.

How might FoxJ1 specify node-cilia differentiation? As predicted by the null-phenotype in multi-ciliate cells, one downstream consequence of FoxJ1 misexpression is the apical docking of centrioles/basal bodies, an obligatory step in ciliogenesis. In addition, FoxJ1 also promotes the formation of bi-ciliate cells, suggesting that it activates genes whose products split the centriole pair and promote the maturation of the daughter centriole into a basal body. Finally, FoxJ1 activates the expression of a relatively large panel of genes that encode components exclusive to motile cilia, including those involved in the formation of the dynein arms, central pair, and radial spokes. Thus, FoxJ1 appears to be sufficient to activate the gene expression required to convert a non-ciliated cell into one with the flow producing properties required for left-right patterning.

The ability of FoxJ1 to induce ectopic cilia in the epithelium in Xenopus

embryos is likely due to the unique relationship of the external epithelium with the

presumptive gastrocoel roofplate, wherein these two tissues are contiguous (Shook et

al., 2004). Presumably, any cell in the developing Xenopus epithelium is competent to

generate the GRP when exposed to the proper signals. However, despite the striking

ability of FoxJ1 to induce ectopic cilia, their formation is not universal. Even though

greater than 90% of the cells in the posterior GRP are ciliated, only about 15-35% of

the superficial epithelial cells are ciliated at any given time in *FoxJ1* injected embryos.

In addition, FoxJ1 does not appear to efficiently induce ectopic cilia to form on a

population of skin cells that intercalate from the inner layer along with multi-ciliate

cells. Thus, it is likely that other factors will determine whether or not cells respond to

FoxJ1 to form node-like cilia. One potential regulatory factor is the centriole-

associated protein CP110, which has been proposed to regulate the formation of

primary sensory cilia (Spektor et al., 2007). Indeed, when XCP110 is overexpressed

in Xenopus embryos, it inhibits both ciliogenesis in multi-ciliate cells as well as those

promoted by ectopic FoxJ1, suggesting that it may also be a regulator of motile cilia

formation (J. Stubbs, unpublished observation).

Based on these results, we propose a model for how the different cilia subtypes

are specified in development. In this model, FoxJ1 is sufficient to activate gene

expression required for the formation of node-like cilia, which are genetically distinct

from primary cilia. FoxJ1 can also specify a distinct bi-ciliate cell whose function and

prevalence warrants further investigation. Finally, we propose that FoxJ1 is also

required to activate the motile cilia pathway in multi-ciliate cells, where additional, currently unknown, factors are required to promote the early steps of their differentiation, including the ones that drive the process of centriole duplication. In sum, while sensory cilia have been proposed to form via a default pathway, those used to produce fluid flow during left-right patterning and in multi-ciliate cells require a genetic program driven by FoxJ1. It will be of interest to determine whether the cilia that form using a FoxJ1-dependent pathway share other properties, including how their orientation is determined for directed flow (Marshall and Kintner, 2008).

Chapter Four, in full, consists of the following manuscript submitted for publication in the journal *Nature Genetics.*

Stubbs JL, Oishi I, Izpisúa Belmonte JC, Kintner C. "FoxJ1 specifies node-like cilia in Xenopus and zebrafish embryos".

Figure 4.1 Knock down of FoxJ1 activity inhibits ciliogenesis in the Zebrafish KV and Xenopus GRP. **(A-G)** Analysis of KV cilia in Zebrafish injected with a *ZFoxJ1* morpholino. Left-right organ orientation was measured using a transgenic line where GFP is expressed in the looping heart primordium under the control of myosin light chain 2A promoter (A, B). Even though the KV is clearly apparent in embryos injected with control (D) or *ZFoxJ1* (E) morpholinos, the former has normal left-right asymmetry while the latter is randomized (C). Staining of embryos with an acetylated a-tubulin antibody indicates that cilia are reduced in number and length in KV in *ZFoxJ1* morphants (G) relative to control morphants (F). **(H-K)** Analysis of GRP cilia in Xenopus embryos injected with XFoxJ1 morpholinos (H, J) control morpholino (I, K) and with *mRFP* RNA (J, K). Staining with the acetylated a-tubulin antibody shows a reduction in cilia number and length in morphants (I,K) when compared to control morphants (H, J). Scale bars=20μm in all panels.
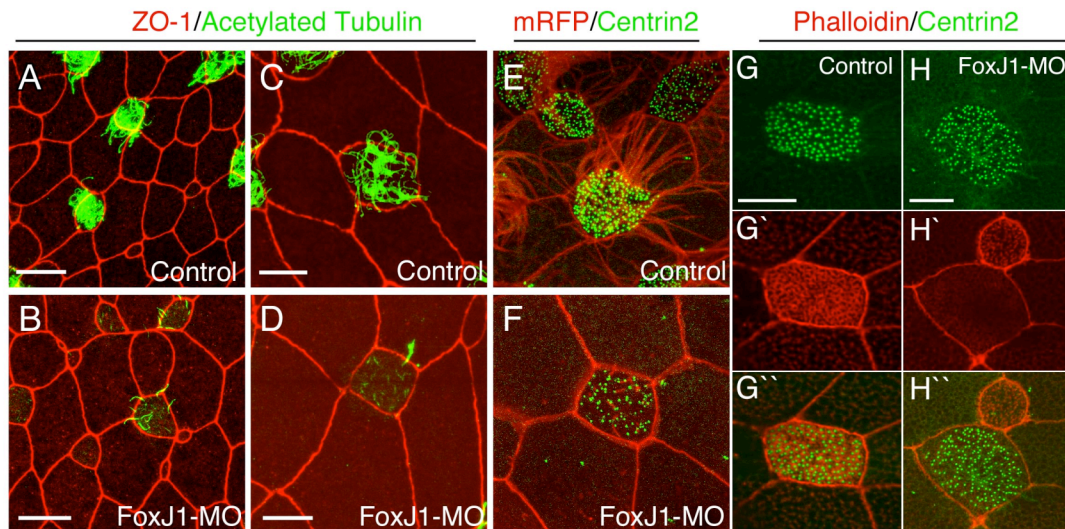
Figure 4.2 FoxJ1^{MO} inhibits ciliogenesis in Xenopus skin cells. (A-D) Embryos were uninjected (Control) or injected with morpholinos directed against FoxJ1 (FoxJ1^{MO}), and stained at stage 26 with ZO-1 (red) and acetylated a-tubulin (green) to label cell borders and cilia, respectively. **(E, F)** Control or FoxJ1 morphants were injected with RNA encoding a membrane-localized RFP (red) and a GFP-centrin2 fusion protein (green), to label cell membranes and basal bodies, respectively. **(G-H)** Control or FoxJ1 morphants were injected with RNA encoding a GFP-centrin2 fusion protein (green), fixed at stage 26 and stained with rhodamine-phalloidin (red) to label the apical actin network. Scale bars represent 20μm in A-B and, 10μm in C-G.
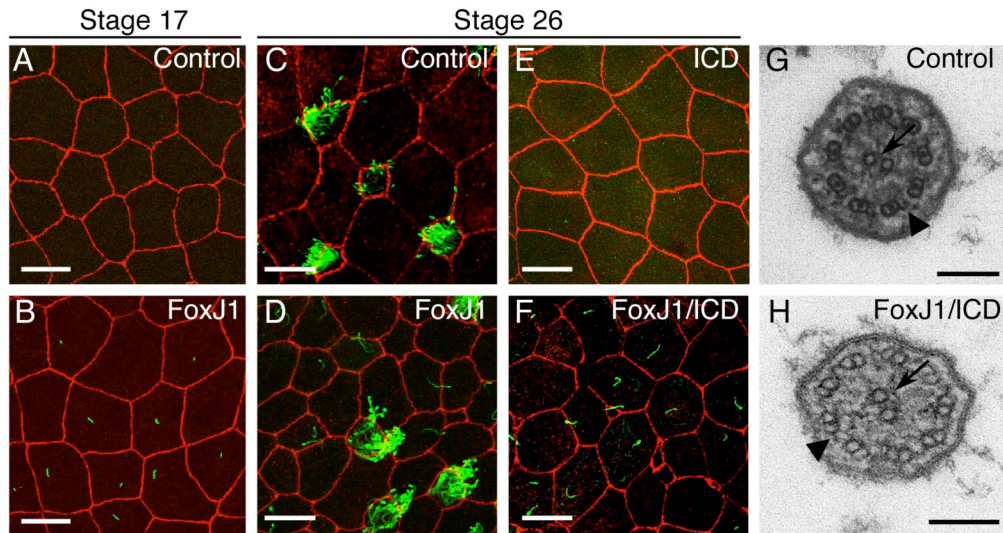
Figure 4.3 *XFoxJ1* RNA misexpression in surface epithelial cells induces ectopic cilia formation. **(A-F)** Shown is a confocal image of the superficial epithelium in *Xenopus* embryos at the indicated stage, stained with antibodies to ZO-1 (Red) and acetylated a-tubulin (green) to label cell borders and cilia, respectively. Embryos were injected at the two-cell stage with *RFP* RNA alone (A,C) with *FoxJ1* and *RFP* RNA (B,D), with *ICD* and *RFP* RNA (E) or with *FoxJ1, ICD* and *RFP* RNA (F). Scale bars are 20μm. **(G,H)** Transmission electron micrographs of cilia in a multiciliate cell (G) or of an ectopic cilium (H) induced by *FoxJ1* RNA in an ICD background (as in panel F). Arrows indicate the central pair and arrowheads indicate outer dynein arms. Scale bars are 100nm
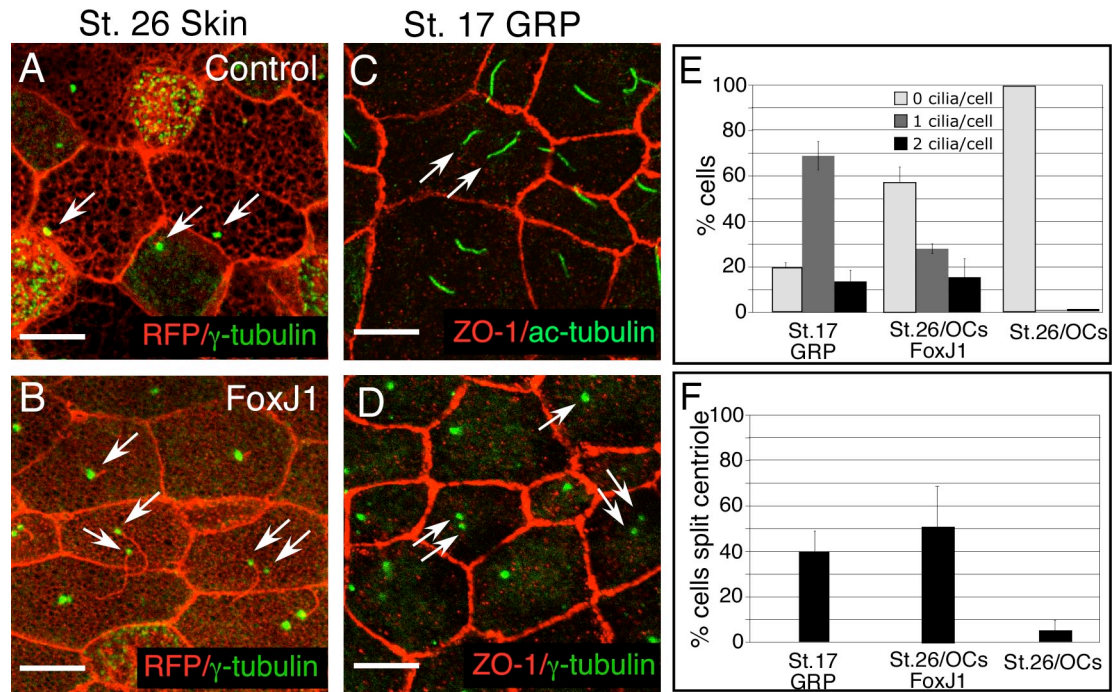
Figure 4.4 Bi-ciliate cells on the GRP and induced ectopically by XFoxj1.
(A-B) Shown is a confocal image of the skin at stage 26 of embryos injected with *RFP* RNA (a) or with both *FoxJ1* and *RFP* RNA (B), and stained with an antibody to γ-tubulin (green). Arrows denote centriole number and position. **(C-D)** Confocal image of the posterior GRP at stage 17, either (C) stained with antibodies to ZO-1 (Red) and acetylated-tubulin (green) or (D) with antibodies to ZO-1 (Red) and γ-tubulin (green). Arrows indicate cilia number (c) or centriole position **(E-F)** Quantification of cilia number (E) and split centrioles (F) in the GRP at stage 17, or in the outer epithelial cells (OCs) of stage 26 embryos injected with *FoxJ1* RNA or with just *RFP* RNA as a control. Scale bars in all panels represent 10μm.
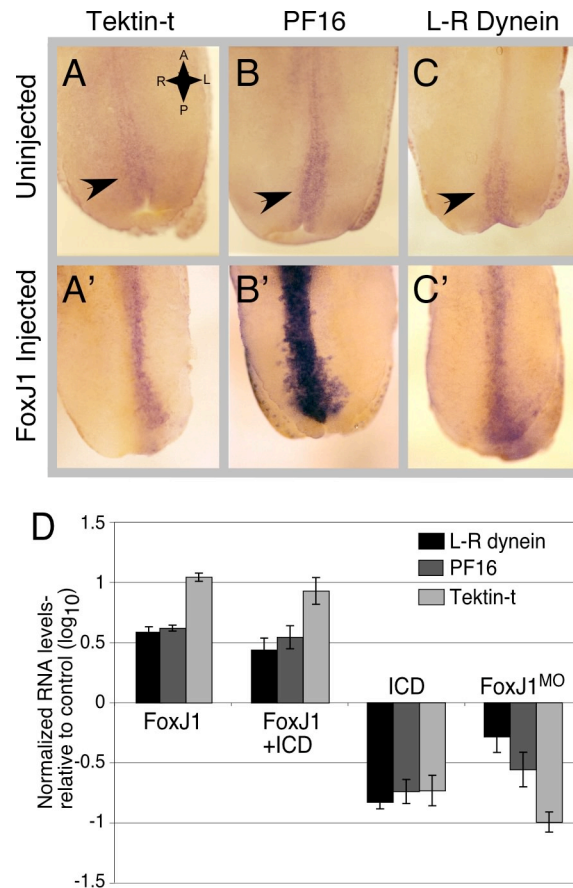
Figure 4.5 Validation of gene expression regulated by *XFoxJ1*. (A-C) Shown is the roof of the gastrocoel in stage 17 embryos after staining for the expression of *Tektin-t* (A,A'), *PF16* (B,B') and *L-R dynein* (C,C') RNA using whole-mount, in situ hybridization. Expression (Red-Blue stain) in the posterior GRP is marked with an arrow. Top panels show staining in uninjected embryos while lower panels shows that in embryos injected once at the two-cell stage with *XFoxJ1* RNA. **(D)** Embryos were injected at the two-cell stage with the indicated RNAs or with *XFoxJ1* or control morpholinos. At stage 10, the ectoderm was isolated, cultured on fibronectin-coated glass to stage 22, and then extracted for total RNA. The levels of *Tektin-t, PF16 (Spag6),* or *L-R dynein* RNA was measured in each sample using quantitative PCR, and normalized relative to a ubiquitously expressed control RNA, *ODC*. Values for each experimental condition is an average of three measurements, and are expressed on a logarithmic plot as a ratio to the average value obtained with a control. Uninjected controls were used for the RNA injected samples and a control morpholino sample was used as a control for FoxJ1 morpholino injection.
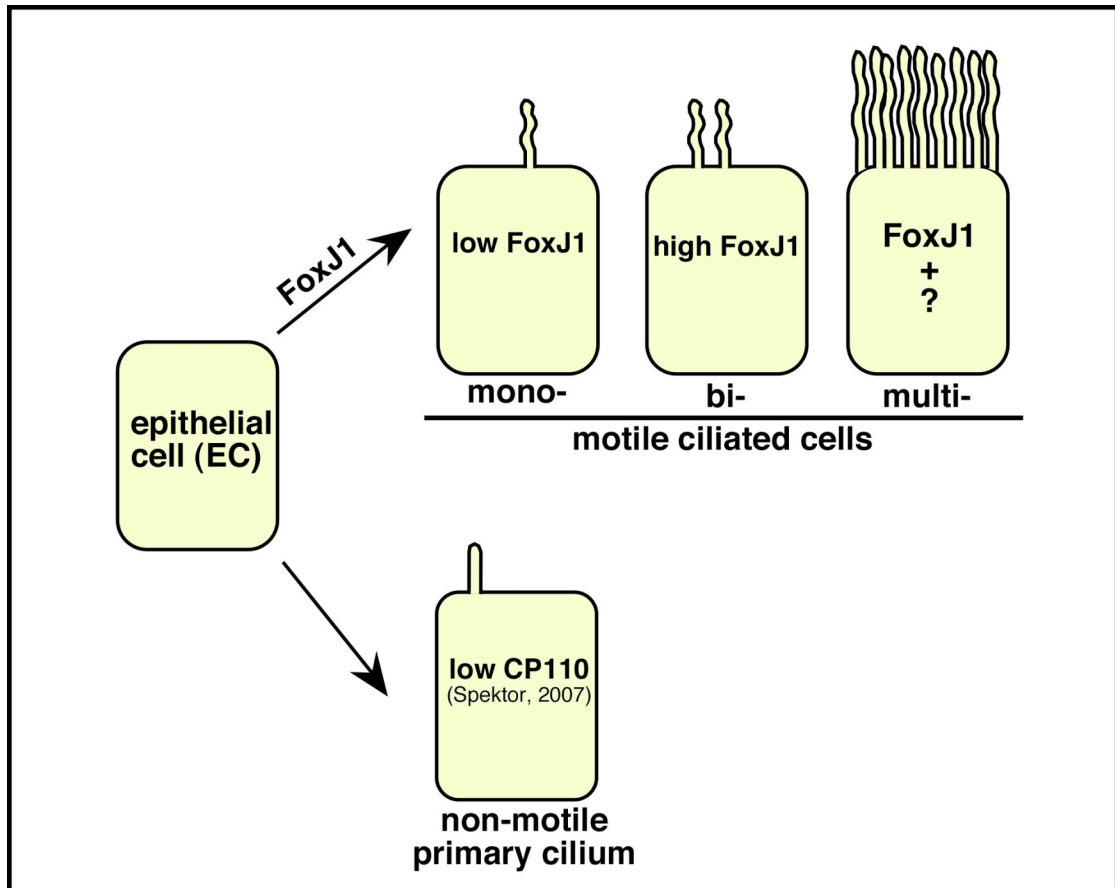
Figure 4.6 Model for cilia subtype specification. Epithelial cells (EC) extend non-motile primary cilia via a default pathway (Spektor, 2007). In response to low levels of FoxJ1 epithelial cells extend a motile monocilia that can mediate flow required for left-right patterning. With increased levels of FoxJ1, ECs can be induced to form bi-ciliate cells. FoxJ1 also regulates the expression of genes required for the formation of motile cilia in multiciliate cells, whose differentiation requires additional unknown factor(s).
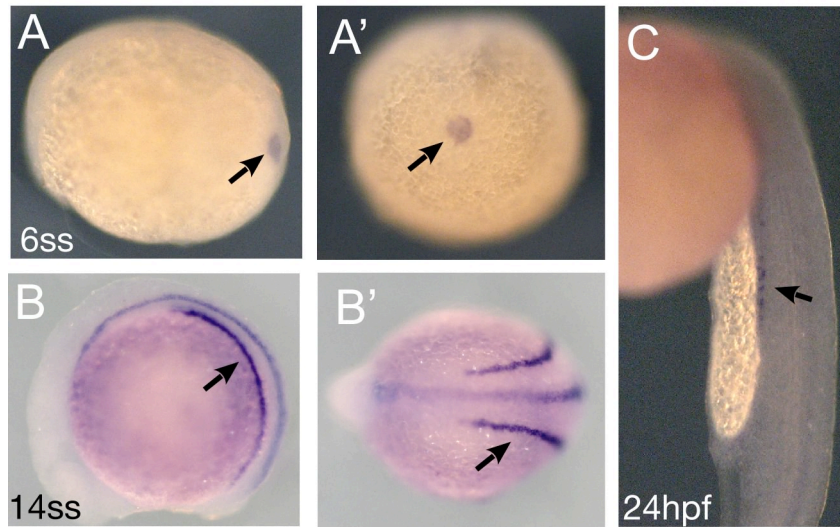
Figure S4.1 Expression of *ZFoxJ1* in ciliated cells of Zebrafish Embryos.
(A-C) At the 6ss stage (A, a'), *ZFoxJ1* RNA is expressed prominently in Kupffer's vesicle (arrow). Shown are side (A) and posterior (A') views.   At the 14ss stage (B, B'), *ZFoxJ1* is expressed prominently in the developing pronephros. Shown is a side (B) and dorsal view (B'). (C) At 24hpf, *ZFoxJ1* continues to be expressed prominently (arrow) in the anterior pronephros where multiciliate cells reside, but is absent from the posterior regions that only contain sensory cilia.
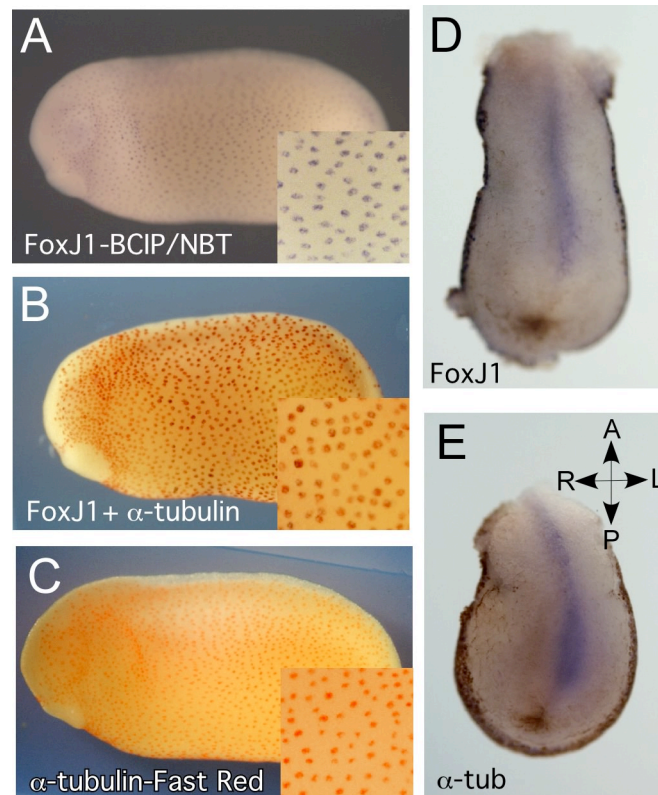
Figure S4.2 Expression of XFoxJ1 in Ciliated Cells of Xenopus Embryos.
(A-C) *Xenopus* embryos at stage 26 were stained with a *XFoxJ1* probe using
BCIP/NBT (A), with an *a-tubulin* probe using fast read (C), or with both probes
together. **(D-E)** Expression of *XFoxJ1* (D) and *a-tubulin* (E) RNA in the GRP
of *Xenopus* embryos at stage 17 revealed by whole mount *in situ*
hybridization.
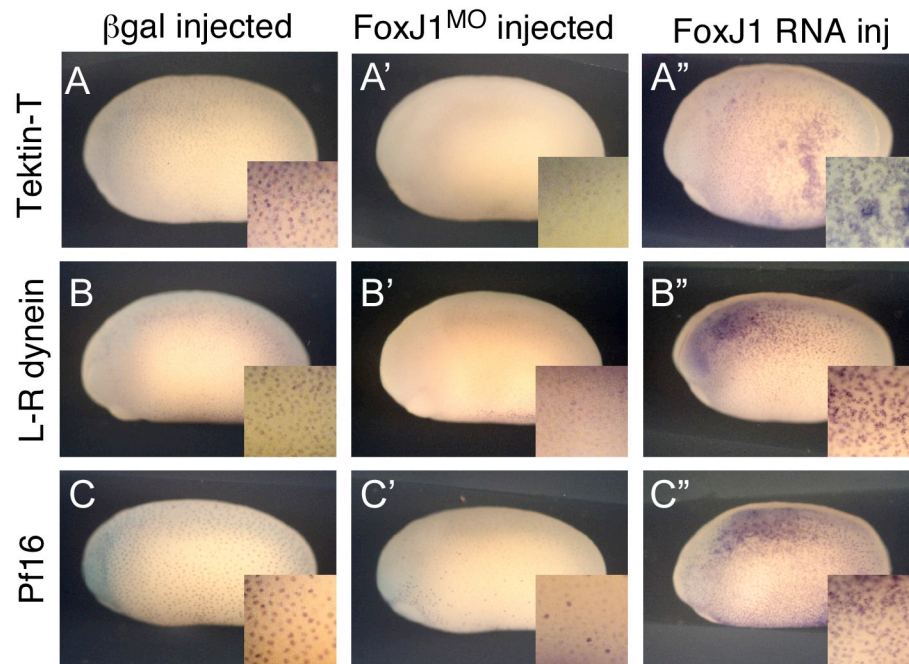
Figure S4.3 Validation of gene expression regulated by *XFoxJ1*. (A-C) Expression of *a-tubulin,* L-R dynein and Pf16 (Spag6) was determined using whole-mount, *in situ* hybridization in β̃gal injected control embryos or in embryos injected with *XFoxJ1* RNA or XFoxJ1 morpholinos.
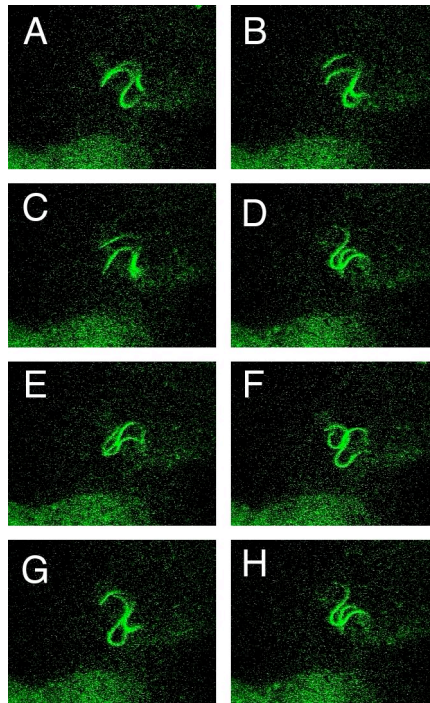
Figure S4.4 FoxJ1 induced ectopic cilia are motile. (A-H) *Xenopus* embryos injected with *XFoxJ1*, *ICD* and *mGFP* RNA were allowed to develop to stage 26 then transferred to a glass coverslip for imaging. Ectopic cilia were imaged on a confocal microscope using Lasersharp 2000 software for data acquisition. Scans to capture motility were performed at 1800 lines per second. Shown are 8 still shots from the movie of one cell with two cilia extending from its surface.

Table S4.1 Genes upregulated in response to *XFoxJ1* Misexpression.
Total RNA from explanted ectoderm was used to generate labeled
complimentary RNA (cRNA) that was hybridized to *Xenopus laevis* Genome
Array chips (Affymetrix #900491). Three data sets were generated using
ectoderm injected with *ICD* RNA and two from ectoderm injected with both
XFoxJ1 and *ICD* RNA. Shown are the genes whose RNA levels changed
greater than 10-fold on average (Avg FC ratio) in a pairwise comparison of
FoxJ1/ICD data sets to the ICD data sets. Structural motifs and human
homologs were identified based on assignment of Unigene identifiers to
Homologene.

Genbank	Unigene	Avg FC Ratio	Cili-ome	Structural Motifs	Human	Description
BC043831.1	Xl.58964	119.43	No	Coiled-Coiled	C14orf45	Coiled-coiled protein of unknown function with SMC2/SMC4 Homology
BJ045367	Xl.14154	84.45	No	None	LOC342346	Conserved protein of unknown function
BJ056774	Xl.14621	53.2	No	Coiled-Coiled	CCDC105	Coiled-coiled protein of unknown function
BJ087835	Xl.4890	48.5	No	Coiled-Coiled/SMC	CCDC78	Coiled-coiled protein of unknown function with SMC domain
BJ092720	Xl.13719	44.74	No	None	None	ESTs and homolog to Trop but no clear coding sequence
AW782665	Xl.12692	42.71	No	DCX	DCDC2B	Doublecortin related
BJ091326	Xl.15506	40.79	No	None	None	Genebank retired
BJ053550	Xl.15358	40.32	Yes	IQ calmodulin, AAA Atpase	IQCA	Tropicalis 155843, AAA Atpase, and IQ calmodulin
BM180891	Xl.14916	38.05	Yes	TPR	TTC12	Trop 175168, Conserved TPR domain protein of unknown function
BQ736249	Xl.15616	37.62	Yes	Tektin	TEKT3	Xenopus homolog of Tektin 3
BC043740.1	Xl.20447	37.62	Yes	Tektin	TEKT2	Xenopus homolog of Tektin 2
BC044268.1	Xl.23534	33.9	No	HLH-PAS	ARNT2	Xenopus homolog of ARNT2
BC049290.1	Xl.3026	33.13	Yes	Dpy-30 ADK	AK7	Xenopus homolog of adenylate kinase 7
BG346046	Xl.9077	30.55	No	WD40 Repeat	WDR16	WD-40 repeat conserved protein of unknown function
BQ398517	Xl.13942	30.2	Yes	Dynein	DNAH9	Dynein Arm Heavy Chain Axonemal
CD361045	Xl.26415	29.86	No	None	TEPP	testis/prostate/placenta-expressed protein, unknown function
BJ085862	Xl.2458	29.51	No	None	C15orf26	Conserved protein with no known function
BJ087968	Xl.34024	29.18	No	None	None	ESTs and homolog to Trop but no clear coding sequence
BG346004	Xl.1504	27.86	Yes	Radial Spoke Protein	RSHL2	Xenopus homolog of Radial spokehead-like 2
BJ076039	Xl.52119	27.86	No	None	MGC33657	Little sequence
BJ085557	Xl.13305	27.22	No	None	C9orf116	Similar to C9orf116, little sequence
BJ054388	Xl.15406	26.91	No	None	None	ESTs and homolog to Trop but no clear coding sequence
AW767950	Xl.11087	26.91	Yes	DM10	EFHC1	Etiology JME
BJ082172	Xl.15603	26.6	Yes	WD40 Repeat	WDR66	Trop 456177, WD-40 repeat conserved protein of unknown function
AF032383.1	Xl.401	26.6	No	reprolyin ACR DISIN	ADAM22	metalloprotease-disintegrin
BG020671	Xl.22343	25.11	No	Coiled-Coiled	Hypothetical C	Trop 03155
BG020534	Xl.3108	24.53	No	L6 membrane protein	TM4SF18	transmembrane 4 superfamily member 18
BG020958	Xl.34888	24.53	No	MAP65 ASE1	CCDC87	Trop 172009: microtubule associated protein.
BM192326	Xl.25877	24.53	Yes	ADK	AK5	Xenopus homolog of adenylate kinase 1
BJ050954	Xl.13352	23.97	Yes	Morn Domains	TSGA2	Testis specific A2 homolog
BI444329	Xl.18717	23.7	No	L6 membrane protein	TM4SF1	tetraspanin-1
BJ051776	Xl.16114	23.7	No	Glycoprotein hormone beta ch	LHB	Trop 377323 Leutinizing hormone Beta
BG021827	Xl.53283	23.7	Yes	None	C13orf26	Conserved protein with no known function

Table S4.1 continued

Genbank	Unigene	Avg FC Ratio	Cili-ome	Structural Motifs	Human	Description
BJ048155	Xl.12380	22.89	Yes	Coiled-Coiled	CCDC19	Similar to nasopharyngeal epithelium specific protein 1
BC041210.1	Xl.7299	22.63	Yes	DUF1309	ODF3	Xenopus homolog of Shippo1, outer dense fiber
BJ091158	Xl.15380	22.37	Yes	IQ calmodulin, AAA Atpase	IQCA	Tropicalis 155843, AAA Atpase, and IQ calmodulin
BG345897	Xl.30012	21.36	Yes	Tektin	TEKT1	Xenopus homolog of Tektin 1
BJ067692	Xl.12380	21.36	Yes	Coiled-Coiled	CCDC19	Similar to nasopharyngeal epithelium specific protein 1
BJ090821	Xl.16464	20.16	Yes	Armadillo repeats	Spag6	Xenopus homolog of Spag6
BF232441	Xl.25839	19.93	No	RCC1 repeats	RCC1	Xenopus homolog of regulator of chromosome condensation 1
BJ050529	Xl.13324	19.93	No	7tm 3	GPR156	Trop 205043, G-coupled receptor of unknown function
BI313854	Xl.24195	19.93	Yes	ADK	AK5	Xenopus homolog of adenylate kinase 1
BJ090136	Xl.7994	19.7	Yes	Dynein Heavy Chain	DNAH8	Inner Dynein Arm Heavy Chain 1-alpha
BJ075928	Xl.13831	19.7	No	None	C6orf97	Little sequence
BJ056722	Xl.12819	19.25	No	IMP dehydrogenase / GMP re	GMPR2	GMP reductase
BJ078477	Xl.16776	19.03	No	Coiled-Coiled/SMC	CCDC63	Conserved Coiled-Coiled domain protein
BC042360.1	Xl.23564	19.03	Yes	Armadillo repeats	Armc4	Conserved protein with no known function
BG816831	Xl.17997	18.81	Yes	NDK Domain, Dyp-30	NME5	Xenopus homolog Nucleoside diphosphate kinase homolog 5
AW643289	Xl.16654	18.81	No	DUF667	C16orf80	Highly conserved protein of unknown function
BJ078979	Xl.16545	18.59	Yes	Tektin	TEKT4	Xenopus homolog of Tektin 4
BJ088741	Xl.16441	17.75	No	WD40 Repeat	WDR16	WD-40 repeat conserved protein of unknown function
BJ085065	Xl.16226	17.75	No	IQ-Calmodulin	None	trop 407388
BJ080667	Xl.13986	17.75	No	IQ-Calmodulin	IQCH	Trop268243, NYD-SP5
BJ089527	Xl.16412	17.55	No	WD40 Repeat	WDR49	WD-40 repeat conserved protein of unknown function
BJ043529	Xl.16202	17.35	No	None	None	trop 165923, Protein not conserved, no motifs
BI446883	Xl.18853	17.35	No	DPY-30	DYDC1	Conserved protein of unknown function
BC046664.1	Xl.15047	17.15	Yes	DUF1309	ODF3	Xenopus homolog of Shippo1, outer dense fiber
AB085631.1	Xl.21383	17.15	Yes	Ank Calcium Transporter	None, related to	Xenopus calcium transporter 2
BJ078884	Xl.16772	17.15	Yes	Dynein	DNALI1	dynein, axonemal, light intermediate chain
BJ087186	Xl.13831	16.95	No	None	C6orf97	Little sequence
BJ086673	Xl.15012	16.76	No	None	LOC463933	Tropicalis Coding, related to human hypothetical LOC463933
BF072033	Xl.6973	16.56	No	Robl LC7	DYNLRB2	Dynein-associated protein Roadblock
CD326460	Xl.26316	16.56	No	DUF1042	C20orf28	Xenopus homolog of sperm flagellar one
BG159877	Xl.11546	16.37	No	WD40 Repeat	None	Trop 156021
BI315451	Xl.18412	16.19	Yes	IQ-Calmodulin, RIIa	SPA17	Trop 183347 PKCRegulatory subunit portion of type II PKA R-subunit
BJ055178	Xl.16599	16	Yes	WD40 Repeat	DNAI1	Homolog of dynein, axonemal, intermediate chain 1

Table S4.1 continued

Genbank	Unigene	Avg FC Ratio	Cili-ome	Structural Motifs	Human	Description
BJ089387	XI.12681	15.82	No	WD40 Repeat	WDR69	WD-40 repeat conserved protein of unknown function
BC049289.1	XI.14119	15.82	Yes	Spectrin repeats	SYNE1	Trop 349414
BJ079557	XI.14126	15.82	No	None	None	Repetitive sequences
BI446799	XI.15888	15.82	No	Leucine-Rich Repeats	LRRC34	Trop 448354
CB592209	XI.15380	15.82	Yes	IQ calmodulin, AAA Atpase	IQCA	Tropicalis 155843, AAA Atpase, and IQ calmodulin
BI447010	XI.18865	15.28	No	Ankyrin Repeats	ANKRD45	Conserved ankyrin repeat protein
CD325641	XI.8555	14.93	No	Reticulon	RTN1	reticulon 1-C.2
BJ079815	XI.15440	14.76	No	C2H2 Zinc Finger gene model	C8orf70	Trop 171270
BG017455	XI.9808	14.76	No	None	C14orf50	Conserved protein with no known function
BJ086368	XI.13468	14.59	No	None	None	ESTs and homolog to Trop but no clear coding sequence
AW766365	XI.15197	14.42	No	WD40 Repeat	P11-175D17.5	WD-40 repeat conserved protein of unknown function
BC044984.1	XI.23512	14.42	No	Homeodomain	HOXA1	HoxA1
BJ098965	XI.15885	14.25	Yes	Leucine-Rich repeats	LRRC51	No known function
BI443114	XI.16654	14.25	No	DUF667	C16orf80	Highly conserved protein of unknown function
BI348453	XI.16544	13.93	Yes	Ropporin-like	ROPN1L	Fibrous sheath of Sperm
BJ091895	XI.12567	13.93	No	DUF1208	FAM92B	Little sequence no tropicalis, although conserved protein
BF071920	XI.10706	13.77	No	Tctex-1	TCTEX1D1	Dynein light chain
BJ046781	XI.51228	13.3	No	F-Box	FBXO31	Trop 169553
BJ054660	XI.16566	13.3	No	ADK, Adenylate Kinase	C9orf98	Unknown function
BJ055241	XI.15554	13.15	Yes	Armadillo, SRP1	RTDR1	Rhap Tumor deleted
BJ092557	XI.16412	13	No	WD40 Repeat	WDR49	WD-40 repeat conserved protein of unknown function
AB022088.1	XI.1220	13	No	P450	CYP1A1	cytochrome P450
BJ043754	XI.15191	12.7	No	S-TKc	NEK5	Trop 467014, NIMA related kinase
BJ048763	XI.15384	12.7	No	None	C6orf206	Conserved protein with no known function
AW643289	XI.16654	12.55	No	DUF667	C16orf80	Highly conserved protein of unknown function
CB756314	XI.5789	12.27	Yes	PDEase I,	PDE4D	3,5-cyclic phosphodiesterase type 9
BJ083558	XI.56924	12.27	No	None	KIAA1370	Conserved protein of unknown function
BQ399047	XI.3112	12.27	No	B41, SH2, TyrKc	JAK2	JAK2, Tyrosine-protein kinase
BJ082817	XI.14402	12.27	No	Calponin, Filamin, IG-Filamin	FLNC	Actin Binding, Filamin related
BJ039543	XI.15384	12.27	No	None	C6orf206	Some similarity to Chamy Radial Spoke protein 9
BJ081503	XI.10830	12.13	No	None	C9orf68	Conserved protein with no known function
AW767983	XI.11177	11.99	No	WD40 Repeat	WDR63	Trop 304328 NYD-SP29 Conserved WD40 protein of unknown function
CD325641	XI.8555	11.85	No	Reticulon	RTN2	reticulon 1-C.2

Table S4.1 continued

Genbank	Unigene	Avg FC Ratio	Cili-ome	Structural Motifs	Human	Description
BJ075955	Xl.13768	11.85	No	None	None	Little sequence no tropicalis
CB562163	Not found	11.71	No	None	None	Genebank retired
BF232515	Xl.46978	11.71	No	C2H2 Zinc Finger gene model	C8orf70	Trop 171270
BJ076059	Xl.15389	11.58	No	None	None	Coding sequence, homolog to Trop sequence and to hypothetical genes
BG017110	Xl.11474	11.58	No	Coiled-Coiled	CCDC96	Tr 468393
BJ083290	Xl.17968	11.31	No	None	SPAG8	Similar to Spag8
BG019848	Xl.9878	11.18	No	None	None	Coding sequence, homolog to Trop sequence and to hypothetical genes
BC046665.1	Xl.23526	11.18	No	DCX	DCDC2	RU2S double cortin domains
BJ043994	Xl.13320	11.06	Yes	Radial Spoke Protein	RSHL3	Radial Spoke related
BJ045936	Xl.18686	11.06	No	None	None	Repetitive sequences
BJ049223	Xl.15761	10.8	No	None	None	ESTs and homolog to Trop but no clear coding sequence
BJ048577	Xl.22500	10.8	No	Leucine-rich repeat	LRRC27	LRR protein of unknown function
BF072242	Xl.10381	10.56	No	Tyrosine Kinase Domain	RAGE	Related to Long flagellar protein 4
BC041731.1	Xl.9439	10.56	No	Homeodomain	HOXA3	Xenopus homolog of homeo box A3
BJ084139	Xl.15806	10.43	Yes	KIF9 Kinesin	KIF9	Trop 401497 Kinesin
BJ058680	Xl.13265	10.2	No	None	None	ESTs and homolog to Trop but no clear coding sequence
BJ090065	Xl.51280	9.85	No	None	None	Ca2+/calmodulin-dependent protein kinase similiarity
BJ099506	Xl.13179	9.85	No	UPF0193	C22orf23	Conserved protein with no known function
AW767983	Xl.11177	9.74	No	WD40 Repeat	WDR63	Trop 304328 NYD-SP29 Conserved WD40 protein of unknown function
BJ075990	Xl.14644	9.74	No	None	LOC728690	Trop 373228 Conserved protein of unknown function
BG555229	Xl.13251	9.62	No	None	None	ESTs and homolog to Trop but no clear coding sequence
BJ048989	Xl.15133	9.4	Yes	WD40 Repeat	WDR78	WD-40 repeat conserved protein of unknown function
BJ081581	Xl.45476	9.4	No	None	LOC641808	Small protein no domains or known functions
BQ386813	Xl.2815	9.4	No	WD40 Repeat	KATNB1	P80 Katanin
BC046836.1	Xl.5161	9.4	No	D-hydantoinases	DPYSL3	dihydropyrimidinase-like 3
BJ092913	Xl.52831	9.3	No	Filamin, Calponin	FLNC	gamma filamin; filamin C, gamma (actin-binding protein-280)
AF343894.1	Xl.2549	9.19	No	None	SMPX	Chisel small muscle protein
BG346059	Xl.11915	9.08	No	WD40 Repeat	IFT122	related to IFT122
AW766968	Xl.55019	8.98	No	Ly-6 antigen / uPA receptor -l	LYPD2	Trop 423284, conserved protein of unknown function
AF467986.1	Xl.17388	8.98	Yes	ARL3	ARL3	ADP-ribosylation factor
BF427142	Xl.2815	8.88	No	WD40 Repeat	KATNB1	P80 Katanin
BC041195.1	Xl.33489	8.67	No	Tubulin	TUBA3	alphatub84b
BG348981	Xl.2428	8.57	No	p450	CYP27A1	Cytochrome P450 27

Table S4.1 continued

Genbank	Unigene	Avg FC Ratio	Cili-ome	Structural Motifs	Human	Description
BE026933	Xl.5614	8.48	No	None	MEIG1	Conserved protein of unknown function
BJ088899	Xl.283	8.48	No	Homeodomain	HOXA1	HoxA1
AW766291	Xl.50997	8.28	No	WD40 Repeat	WDR5B	WD-40 repeat conserved protein of unknown function
U76636.1	Xl.459	8.09	No	EF-Hand	CALB1	Xenopus calbindin D28k
BJ092409	Xl.12902	8	No	Ring Zn Finger, B-Box	TRIM13	Trop 200697
AF146087.1	Xl.585	8	No	bHLH-WRPW	Hes	ESR6e
BJ076814	Xl.21391	7.91	No	Calponin domain	CXorf22	Trop 451268 Conserved protein unknown function, hydrocephaly related
AW766813	Xl.41899	7.91	No	Aminotransferase	None	Trop 458857 Potential Aminotransferase, class-II
AW764843	Xl.13993	7.82	No	None	XRRA1	No trop
BE491113	Xl.10621	7.82	No	None	MGC72075	Trop 450778 Conserved protein of unknown function
BJ048788	Xl.10313	7.73	No	TPR	TTC26	Trop 452453, TPR domain protein of unknown function
BI446980	Xl.15925	7.73	Yes	TPR	DYX1C1	TPR containing, unknown function, associated with dyslexia
BG161130	Xl.4468	7.73	No	None	C21orf59	Conserved protein of unknown function
BM179052	Xl.14712	7.64	No	Ankyrin, Calcium Transport	Trp channel	None, related to trp channels
BF232479	Xl.50855	7.64	No	None	None	Repetitive sequence
AW642521	Xl.48238	7.64	No	EF Hand	KIAA1799	Conserved protein of unknown function
BJ090704	Xl.13737	7.55	No	None	None	Little sequence no tropicalis
BJ087349	Xl.13378	7.55	Yes	TPR	IFT88	Trop 456435, IFT88, polaris
BJ085819	Xl.26220	7.46	Yes	COG1422	CCDC19	nasopharyngeal epithelium specific protein 1
BG234449	Xl.11326	7.38	No	None	None	Little sequence no tropicalis
CA789341	Xl.21493	7.29	No	HSP70	HSPA1L	heat shock protein (hsp70)
BG020413	Xl.3618	7.29	No	BRLZ	CEBPB	C/EBP beta
BE678770	Xl.8047	7.29	No	None	C4orf28	Trop 171546, Conserved protein of unknown function
BJ056076	Xl.58540	7.21	No	None	None	Little sequence no tropicalis
BJ056351	Xl.14396	7.21	No	Coiled-Coiled	CCDC17	Trop 183798, coiled-coiled protein with unknown function
BE026433	Xl.25375	7.13	Yes	RabL4	RABL4	Trop 451804, RAYL, Ras GTPase
BG346469	Xl.2908	7.13	No	None	None	repetitive sequences
BG810779	Xl.34008	7.13	Yes	FAIM	FAIM	Fas apoptotic inhibitory molecule
BJ079438	Xl.17321	6.96	Yes	PCSR	PKHD1L1	Fibrocystin L
BJ081350	Xl.16035	6.96	No	EF-Hand	None	Trop 163299 Conserved EF-hand protein with unknown function
CB562118	Xl.9719	6.88	No	Ig Cam	TTN	Trop 149372
BF071993	Xl.24758	6.88	Yes	DUF1448, DM16	BBS5	Xenopus BBS5
BJ043701	Xl.53590	6.88	No	Ankyrin repeats	ANKRD42	Trop 460707 Ankyrin repeat protein of unknown function

Table S4.1 continued

Genbank	Unigene	Avg FC Ratio	Cili-ome	Structural Motifs	Human	Description
BC045012.1	Xl.15357	6.81	No	Leucine zipper	LZTFL1	Xenopus leucine zipper transcription factor-like 1
BJ055411	Xl.16419	6.81	yes	BBs	BBS4	Little sequence but similar to BBS4
BJ091643	Xl.15916	6.73	No	None	SPAG17	Similarity to Trop 424999, Projection protein 6 perhaps central pair
BJ077199	Xl.13889	6.73	No	None	None	ESTs and homolog to Trop but no clear coding sequence
BQ385153	Xl.10621	6.73	No	None	MGC72075	Trop 450778 Conserved protein of unknown function
BG816583	Xl.46798	6.73	No	None	C9orf9	spermatid specific protein
BI449400	Xl.16400	6.65	No	WD40 Repeat	LOC116143	Conserved protein of unknown function
BI446201	Xl.14868	6.65	No	HDAC interacting	C11orf60	Trop 334909, conserved protein of unknown function
BJ054527	Xl.56724	6.57	No	PDZ, PH syntrophin	SNTA1	basic beta 1 syntrophin
BC041222.1	Xl.4936	6.57	Yes	Carp	RP2	retinitis pigmentosa 2 (X-linked recessive)
BJ077408	Xl.25447	6.57	No	None	None	Little sequence no tropicalis
BJ092352	Xl.24161	6.5	No	DUF714	TMEM38B	Conserved transmembrane protein of unknown function
BJ092913	Xl.52831	6.35	No	Calponin, Filamin, IG-Filamir	FLNC	Trop 48741, gamma filamin; filamin C, gamma
BQ386483	Xl.15070	6.35	No	Trx	TXN	Thioredoxin (ATL-derived factor) (ADF)
AF549903.1	Xl.3939	6.28	No	WD40 Repeat	IFT80	IFT80
BI085168	Xl.15188	6.28	No	Ig Domains	CHL1	Trop 415083, similar to Neural cell adhesion molecule L1
BJ083806	Xl.13251	6.2	No	None	None	ESTs and homolog to Trop but no clear coding sequence
BJ085233	Xl.12333	6.06	No	WD40 Repeat	PQWD	Trop 343201, Conserved WD40 repeat protein of unknown function
CD329661	Xl.26325	6.06	No	None	None	Little sequence no tropicalis
BJ086636	Xl.12454	6.06	No	None	None	Little sequence no tropicalis
BC041183.1	Xl.541	6.06	No	Jun, bZIP	JUN	Xenopus cJUN
BI447405	Xl.19005	5.79	No	None	None	Little sequence no tropicalis
BJ062907	Xl.21648	5.79	No	Ig Domain, TyrKC	KIT	Kit receptor tyrosine kinase homolog (KI-1)
BE678026	Xl.6893	5.79	No	DUF541	IRAK1BP1	Trop 200026. Interleukin-1 receptor-associated kinase 1 binding protein 1
BJ048006	Xl.14992	5.66	No	7tm 1,	ADRB1	Beta-1 adrenergic receptor
BG162597	Xl.8292	5.59	Yes	RdR	RP11-529I10.4	Trop 299052 DPCD, deleted in primary ciliary dyskinesia
BJ077247	Xl.24238	5.46	No	None	None	Little sequence no tropicalis
BJ089886	Xl.58250	5.46	No	None	None	Little sequence no tropicalis
BC043772.1	Xl.5573	5.46	No	WD40 Repeat	KATNB1	katanin p80 subunit B 1
BC044052.1	Xl.6990	5.4	No	Adaptin, Alpha adaptinC2	AP1G2	adaptor-related protein complex 1, gamma 1 subunit
BQ398722	Xl.19973	5.34	No	None	None	Little sequence no tropicalis
BJ055108	Xl.16634	5.34	No	RasGEF, KIND	KNDC1	Cerebral protein-9
BJ047451	Xl.4128	5.28	No	Tryp_SPc	PRSS8	Mast cell protease 7 precursor

Table S4.1 continued

Genbank	Unigene	Avg FC Ratio	Cili-ome	Structural Motifs	Human	Description
BM192289	Xl.14339	5.16	Yes	Coiled-Coiled	BBS2	Trop 278465, Xenopus homolog of BBS-2
BG555802	Xl.4120	5.1	Yes	Dynein light chain	DNAL4	Dynein light chain 4
BJ097317	Xl.1507	5.04	No	TPR	TTC25	TPR containing protein of unknown functon
D87687.1	Xl.160	5.04	No	proteasome beta type 6	PSMB9	Xenopus LMP2
BC045222.1	Xl.3138	5.04	No	Thiolase	HADHB	hydroxyacyl-Coenzyme A dehydrogenase
AJ555191.1	Xl.20476	5.04	No	Coiled-Coiled	CCDC89	Trop 295131 Some similarity to Myosin, rootelin
BQ393344	Xl.19695	4.98	No	None	None	Little sequence no tropicalis
BJ097674	Xl.15231	4.98	No	Coiled-Coiled	CCDC104	Coiled-coiled protein of unknown function
CB561571	Xl.21648	4.76	No	Ig Domain, TyrKC	KIT	Kit receptor tyrosine kinase homolog (KI-1)
BG555802	Xl.4120	4.7	Yes	Dynein light chain	DNAL4	Dynein light chain 4
BI443088	Xl.10608	4.7	No	None	CSPP1	Trop 274241
BG486593	Xl.7550	4.65	No	TPR	TTC30B	TPR containing protein of unknown functon
BJ089334	Xl.8939	4.49	Yes	vATP-synt AC39	ATP6V0D1	H+-transporting two-sector ATPase, C (AC39) subunit
CB562582	Xl.24665	4.39	No	None	C14orf24	Conserved protein of unknown function
CA981857	Xl.24812	4.39	Yes	Arl6	ARL6	ADP-ribosylation factor-like 6
AF218071.1	Xl.23698	4.34	Yes	Tip49	RUVBL2	reptin
AB025414.1	Xl.925	4.34	No	Coiled-Coiled	PCM1	Centriole assembly, implicated in ciliogenesis
BI445755	Xl.14895	4.29	No	EF Hand	CAPS2	Trop 181709 EF-hand containing protein- Calcyphosine 2
BJ079435	Xl.14114	4.24	No	None	None	Repetitive sequences
BC043898.1	Xl.21986	4.24	No	None	C16orf69	Conserved protein of unknown function
BJ044097	Xl.15806	4.19	Yes	Kinesin	KIF9	Trop 401497 KIF9, Kinesin Superfamily Protein 9
AW632862	Xl.11732	4.19	No	K tetra	KCTD14	Conserved protein of unknown function
BG023471	Xl.2433	4.14	Yes	HisRS-like core	HARS	Trop 344463, Histidyl-tRNA synthetase
CD361341	Xl.23672	4.09	No	ZnF C3H1	MBNL1	unknown
BJ056356	Xl.15778	4.05	No	None	None	Repetitive sequences
BJ052593	Xl.16229	4	No	UDPGP	UAP1L1	UTP-glucose-1-phosphate uridylyltransferase, Sperm-associated antigen 2
CB565859	Xl.1549	4	No	None	None	Repetitive sequences
BC043783.1	Xl.18207	3.91	No	SH2, SH3, TyK	FYN	Fyn proto-oncogene
BF072153	Xl.9998	3.73	No	NmrA	NMRAL1	NmrA domain containing protein of unknown function
BC044107.1	Xl.2422	3.69	Yes	ARA1	GCLM	Aldo/keto reductases, glutamate-cysteine ligase
CD362669	Xl.57214	3.65	Yes	Peptidase C13	LGMN	Legumain, peptidase domain
BF047464	Xl.10462	3.65	No	Pecanex	C14orf135	Conserved protein of unknown function
BC043754.1	Xl.14456	3.52	No	COG2872	AARSD1	alanyl tRNA sythase, classII tRNA transferase

CHAPTER V

Conclusions and Future Directions

CONCLUSIONS AND FUTURE DIRECTIONS

Epithelial Morphogenesis

Cell movements underlie many developmental processes and are required in order to convert the developing hollow ball of cells (blastocyst) observed in early development into the embryonic forms observed at later stages of development and in the adult form. During radial intercalation in *Xenopus* cells in the inner layer of the external larval epithelium intercalate, likely through detachment from the fibronectin matrix below the inner layer, followed by migration, and establishment of apical junctional boundaries. The final result of radial intercalation is an even spacing of ciliated cells (CCs) in the epithelium. CCs appear to be spatially regulated, when compared to the other population of intercalating cells, as they are rarely observed sharing cell-boundaries in the epithelium, while it is not uncommon to see intercalating non-ciliated (INCs) sharing boundaries with other INCs. Thus understanding the mechanisms that control these types of cell movements are of particular interest in understanding tissue morphogenesis, as well as how cell movements can contribute to overall tissue architecture.

My studies on epithelial morphogenesis in the external epithelium of *Xenopus* embryos include physical descriptions of the cellular players, for the first time quantifying differences in the sizes and shapes of these distinct populations. In addition to quantification of the physical characteristics, much of my analysis focused on the consequences of overproducing intercalating cell populations, and went on to show that while the number of intercalating cells can be changed, their inherent

physical characteristics remain constant. One interesting observation from these studies is that INCs are not limited by a spacing rule, and in fact when overproduced, are often present at all the available vertices in the outer layer. One consequence of the ability of INCs to freely intercalate is that they may out compete CCPs for space in the outer epithelium.

Using a transgenic promoter to drive mGFP expression in CCPs I have also shown that INCs and CCs are distinct population prior to intercalation. Additionally, I showed that Notch signaling negatively regulates the formation of INCs, in addition to CCs (Deblandre) in the developing epithelium. Initially, we pondered whether the intercalation of INCs was a non-cell autonomous effect; as more ciliated cells were produced, more factors to stimulate intercalation would be produced, thus allowing more INCs to intercalate. Two lines of evidence suggest that this is not the case. First, embryos injected with ICD do not form ciliated cell precursors, neither are INCs observed. This suggests that either INCs are a population that are also regulated by the Notch signaling pathway, or a population of cells that cannot intercalate in the absence of other intercalating cells. However, results from a second line of study (see below) suggests that INCs are indeed a specialized cell type, ionocytes, and as such, likely need to intercalate as part of their differentiation process.

We have performed an additional microarray analysis to identify genes involved in cell specification and intercalation by comparing dnHMM injected explants (overproduced CCPs and INCs) to ICD injected explants (no CCPs or INCs). Many of the genes most highly upregulated in response to dnHMM are components of

proton ATPases and ion channels/pumps, both classes of genes that are expressed in ionocytes. Interestingly, the most highly upregulated gene was *FoxI1*, a transcription factor of the FoxI subgroup, members of which have been shown to control ionocyte differentiation (Hsiao 2007, Janicke 2007). Analysis of the expression pattern of many of these genes, including *FoxI1*, shows that they are expressed in a punctate pattern in the skin, but unlike ciliated cells, these genes are not expressed in regions of the head and tail. Additionally, antibody staining of the ciliated cell population, using an anti-acetylated α-tubulin antibody, following *in situ* hybridization shows that these genes are expressed in a population distinct from ciliated cells. Further, in a preliminary experiment, the function of ionocytes was blocked by drug treatments, resulting in embryo lethality at pH 4 and pH 10, both pHs at which untreated embryos survive. These results strongly suggest that INCs are indeed ionocytes and likely undergo intercalation as part of their differentiation program. One question that still remains is how these two populations are initially selected to become ionocytes and ciliated cells and how Notch signaling is involved in the initial selection of these cell types.

With the identification of INCs as ionocytes, it may now be possible to find a transgenic promoter that can drive expression specifically in INCs. Using such a system, it would be interesting to specifically target INCs or CCs for cell death, possibly by driving expression of a pro-apoptotic gene, in that specific population. If we could indeed eliminate one population, for example INCs, this would enable us to determine what happens during intercalation when CCPs are overproduced, but not

competing with INCs for intercalation sites. Such an experiment may allow us to determine whether morphological constraints, cell-cell recognition or both are modulating the pattern of ciliated cells in the epithelium.

Basigin in the Developing Epithelium

Based on the experiments that I performed I did not identify a role for *XBsg* in cell-cell recognition or intercalation during the formation of the *Xenopus* epithelium. However, there are a few caveats to these observations. First, we do not have antibody to detect *XBsg*, thus in knockdown assays we cannot determine if we are indeed knocking down expression of Basigin. Similarly, while the myc-tagged *XBsg* was expressed and appeared to localize to the membrane, as assessed by anti-myc antibody staining, I could not control for expression, or proper cellular localization of the other *XBsg* constructs. One explanation for the lack of changes in cell-cell recognition or intercalation could be a third, unexplored, role for *XBsg* in cellular metabolism in the developing epithelium.

In mouse muscle GP70, a glycoprotein closely related to Basigin, was shown to closely associate with monocarboxylate transporter 1 (MCT1) (Poole and Halestrap, 1997). Immunolocalization experiments in mouse muscle show MCTs also co-localize with murine Basigin. MCTs are 12 pass transmembrane proteins that move metabolically important molecules such as lactate and pyruvate across the cell membrane (Halestrap and Price, 1999). Lactate is the byproduct of anaerobic metabolism, but buildup in the cell can decrease cellular pH effecting cellular homeostasis, requiring its transport out of the cell by MCTs. However, cells that are

very metabolically active, such as the neurons, cardiac and skeletal muscle, often oxidize lactate for energy, and require MCTs to bring lactate into the cell (for review see Halestrap and Price, 1999). Furthermore, in transfection assays, murine MCTs failed to localize to the membrane unless murine *Bsg* was co-expressed in the same cells (Kirk et al., 2000) suggesting that MCTs may require *Bsg* in order to function at the membrane.

In a survey of *in situ* hybridization probes the Wallingford group identified a number of molecular markers that distinguish the three cell types (OC, INC, CC) in the developing *Xenopus* epithelium (Hayes et al., 2007). INCs, which we have determined are likely ionocytes, were shown to express *MCT3* in the characteristic salt and pepper pattern that is excluded from the head and tail regions (Hayes et al., 2007). While our analysis of microarray results comparing dnHMM and ICD injected explants shows that *MCT4* was upregulated in response to overproduction of INCs and CCs by dnHMM injection.

Re-examination of the wildtype expression pattern of *XBsg* at stage 26 (Figure 3.2 C) shows that expression is somewhat excluded from the head and tail regions of the embryo, similar to the expression pattern of INC markers. In addition to the darkly staining cells, there appear to be a large number of cells that express a lower level of *XBsg* at stages 17 and 26 (Figure 3.2B, C). High magnification views of the cells show that low level expressing cells lie next to each other and often surround non-stained cells. Based on the characteristic morphology of cells observed in the epithelium (Stubbs et al., 2006) the non-staining cells at stage 26 are most likely

ciliated cells, and the light staining cells are likely outer cells (OC). This suggests that either ciliated cells transiently express *XBsg* early with INCs and OCs upregulating expression at later stages, or that ciliated cells do not express *XBsg*.

Ionocytes, act by constantly pumping ions against a concentration gradient. While mucus secreting cells also pump ions against a concentration gradient in order to acidify the mucus containing cellular vesicles, keeping mucus inert prior to release by exocytosis (Williams et al., 2006). Thus both cell types are metabolically active and may utilize monocarboxylates as a cellular fuel. Taken together, these recent findings suggest that *XBsg* may play a role in cellular metabolism, rather than in morphogenesis. It would be of interest to perform further expression analysis to determine if and when *XBsg* is expressed in the three cell types of the Xenopus epithelium. Two methods could achieve this aim; first performing double *in situ* hybridizations using *XBsg* probes, and the newly identified molecular markers for outer cells and INCs; secondly, marking ciliated cells by anti-GFP antibody staining in *α-tubulin-mGFP* transgenics, following *in situ* hybridizations using any of the above mentioned molecular markers of INCs or OCs, and *XBsg*, to determine if signals are overlapping. Functional studies, determining if *XBsg* is required for proper ionocyte function prove to be slightly more challenging as currently our only assay to determine if ionocytes are functioning is based on embryo survival, and cannot measure slight changes in cellular function.

Cilia Specification

FoxJ1 has been recognized as a transcription factor required for ciliogenesis in multiciliate cells for almost a decade. Based on phenotypes in knockout mice, where basal bodies are formed but fail to dock at the apical surface, *Foxj1* was ascribed a late role in ciliated cell differentiation, modulating basal body anchoring in multiciliate cells, but having no role in monociliate cells. Typically monocilia are non-motile, thus most of the literature has further expanded the role of *Foxj1* to basal body docking of motile cilia (Brody et al., 2000). However, the *foxj1* null mouse itself contradicts this model. Nodal cilia have been shown to be composed of a mixed population of both motile and non-motile monocilia (McGrath et al., 2003), and *foxj1* null mice do not have any apparent basal body defect at the node, as these cells are still able to generate monocilia (Brody et al., 2000; Chen et al., 1998; Zhang et al., 2004). While the morphology of the node appears normal in *foxj1* null mice, functionality is not normal, as null embryos develop left-right asymmetry defects.

The studies I present in this dissertation provide evidence that FoxJ1 has a conserved role in multiciliate cells in *Xenopus* embryos, such that knockdown of *XFoxJ1* results in basal body docking defects. However, in contrast to the mouse, the monocilia in the node-like structures in *Xenopus* and zebrafish fail to form when FoxJ1 expression is knocked down. TEM studies of zebrafish KV cilia show that they are 9 + 2 in structure, while in the mouse node it has been reported that cilia are 9 + 0 (Kramer-Zucker et al., 2005b; Takeda et al., 1999). One explanation of the disparity between the role of FoxJ1 in the node of mouse and KV and GRP of zebrafish and Xenopus, respectively is that FoxJ1 is responsible for specifying 9 + 2 type cilia.

However, one group recently reported that they observed 9 + 2 cilia, and suggested that the inner pair was labile during fixation (Caspary et al., 2007). Thus, it is not likely that FoxJ1 specifies 9 +2 cilia, as *foxj1* null mice have an apparently normal structure at the node, but still exhibit L-R asymmetry defects.

A second possibility is that FoxJ1 is specifying the motile cilia subtype. Our results are in support of this possibility as the misexpression of *XFoxJ1* in Xenopus embryos can lead to the formation of motile ectopic cilia on cells of the embryonic epithelium (see Figure S4.1). Both microarray analysis and semi-quantitative RT-PCR show that *XFoxJ1* can turn on genes required for cilia motility (see Figure 4.5, S4.2) in addition to cilia structure genes (see Table 1). However, when we misexpressed *ZFoxJ1* in zebrafish embryos we failed to induce the formation of ectopic cilia in the epithelium or any other examined structures. However, knocking down *ZFoxJ1* resulted in the loss of cilia in the KV node (see Figure 4.1). These results led us to a third possibility, that FoxJ1 specifies node-like cilia in *Xenopus* and zebrafish.

In support of this role for node-like cilia are two main observations. First, the *Xenopus* external epithelium is contiguous with the GRP, where node-like cilia form. In animal cap assays cells can be induced to form a variety of tissues, such as mesoderm or neurons, upon treatment or injection of the appropriate factors. Thus, it is reasonable to surmise that any cell in the developing animal cap that receives the correct signals, could give rise to the GRP or GRP-like cells. Thus, we suggest that due to this unique cellular plasticity in *Xenopus* embryos that we can induce the

formation of ectopic cilia, whereas assays in mouse embryos or tissue culture have failed to form such cilia (You et al., 2004). Secondly, the ectopic cilia formed in response to misexpression of *XFoxJ1* share characteristics with cilia on the GRP. Up to 15% of the cells on the GRP are bi-ciliated. While, in embryos in which *XFoxJ1* is expressed at high levels anywhere from 15-35% of affected cells are bi-ciliate (see Figure 4.4). In addition in cells where *XFoxJ1* is misexpressed the centrioles are often found located apically and centrally, in contrast to control cells where they are normally located basolaterally, suggesting that FoxJ1 is acting to prime the cell to extend a cilium by facilitating localization of the centrioles to a central apical position.

Taken together these results suggest that motile cilia found at the node are more similar to motile cilia found on multiciliate cells than to non-motile sensory cilia. Thus, in addition to the roles in basal body docking in multiciliate cells we have shown that FoxJ1 can turn on genes required for motility, and can specify the formation of node-like cilia in tissues that are receptive to such induction. While these findings do not explain the morphology of the mouse node in *foxj1* null mice, one possibility is that cells at the node are still able to undergo a default ciliogenesis pathway, by down regulation of CP110 and form a non-motile sensory cilium (Spektor et al., 2007) in the absence of FoxJ1. No analysis of fluid flow has been performed in the node of *foxj1* mutant mice to suggest that this is the case, but based on the L-R asymmetry defects it is likely that nodal flow is disturbed.

Additional Transcriptional Regulation

FoxJ1 alone is unable to specify the formation of multiciliate cells, indeed it fails to effect several aspects of multiciliate cell differentiation including basal body duplication, and intercalation, thus during the course of my studies I have performed several experiments to determine if a second transcription factor plays a role in specifying multiciliate cells (see Appendix 1). Misexpression of XRFX2 from the post-gastrulation stages can induce the formation of small ectopic cilia, but based on preliminary findings they are likely non-motile. Co-expression of XFoxJ1 and XRFX2 led to the formation of cilia that most closely resembled FoxJ1 induced cilia, but did not lead to the formation of multiciliate cells. Additionally, knockdown of XRFX2 with a potential translation blocking morpholino, or misexpression of a constitutive repressor fused to XRFX2 failed to effect the formation of multiciliate cells in the epithelium. Misexpression, at stages post gastrulation, also resulted in changes to the morphology of the external epithelium, making further analysis of roles in ciliogenesis challenging. Taken together these results suggest that RFX2 is not required for the generation of multiciliate cells in *Xenopus* embryos.

One aspect of XRFX2 function that I did not explore is a possible role the formation of cilia on the GRP. Thus far RFX factors have only been shown to have functional roles in monocilia, thus looking at the effects of XRFX2 misexpression or knockdown on cilia on the GRP may identify role for XRFX2 in ciliogenesis in *Xenopus*. Additionally, there are four other RFX family members in vertebrates and any of those factors could potentially play a role in ciliogenesis. It would be interesting to isolate these family members either from *Xenopus tropicalis*, a closely

related species, or by degenerate PCR and determine if misexpression either alone or

in combination with FoxJ1 can affect multiciliate cell formation.

Direct Regulation of Cilia Genes

One question that remains unanswered is whether XFoxJ1 can directly regulate

the expression of cilia genes, or if it acting through some downstream partner.   In

order to explore this I determined that a bioinformatics approach looking for

conserved FoxJ1 binding sites in the promoters of cilia genes would be a first step to

answering this question. I sought the assistance of the Manning lab at the Salk

Institute to perform a series of bioinformatics analyses. I provided their lab with a list

of the 49 identified cilia genes from the FoxJ1 versus ICD microarray analysis (see

Table 4.1). Unigene identifiers for the *Xenopus* genes were then used to identify the

corresponding human gene. At the onset of these analyses I was also considering a

role for XRFX2 in the specification of multiciliate cells. Given the high rate of RFX

binding sites (X-box sites) in the promoters of cilia genes in *C. elegans* I reasoned that

in addition to FoxJ1 sites there might also be RFX binding sites in these promoters.

The consensus DNA binding sites for FoxJ1 and RFX2 were obtained from

TRANSFAC and used to search the 3kb region upstream of each gene.

The initial analysis showed no FoxJ1 binding sites in the upstream promoters,

however the consensus sequence is quite stringent. Upon moderate relaxation of the

parameters 15 genes were shown to have FoxJ1 binding sites. However, when the

promoter regions of 49 random genes were assayed using this less stringent parameter,

17 promoters were found to have a FoxJ1 binding site. When RFX binding sites were

analyzed in the cilia subset, 29 promoters were found to have RFX binding sites, while the random set had 28 promoters with RFX binding sites. Thus the initial analysis suggested that there was no enrichment of either binding site.

As a caveat to this, during the analysis our collaborator noted that many of the regions upstream of cilia genes were quite short in the human genome, with 11 of 49 being less than 1kb and 5 of those under 250bp in length. When compared to a random set of genes only 2 promoters were less than 1kb in length. Thus, in an additional analysis the Manning lab determined the number of FoxJ1 or RFX sites per kb of promoter sequence analyzed. Again, FoxJ1 binding sites showed no enrichment when compared to a random set of promoters, however RFX binding sites showed a slight enrichment when compared to random promoters (0.71 sites/kb versus 0.6 sites/kb). These results are far from conclusive, indeed the X-box has been shown to be the most highly represented DNA binding domain in the human genome (Xie et al., 2007). However, this analysis does suggest that the RFX family of transcription factors may indeed play a role in controlling ciliogenesis in *Xenopus* and likely warrant further studies.

One possibility is that FoxJ1 functions by regulating the transcription of other transcription factors, such as members of the RFX family, which then affect cilia gene expression. Preliminary experiments showed that *RFX2-hGR* misexpression could induce upregulation of *XFoxJ1*, indeed misexpression of *XFoxJ1* appears to upregulate *XRFX2* expression as well (data not shown), suggesting that there may exist positive feedback loops between several transcription factors that contribute to multiciliate cell

formation. Additionally, based on searches of *in situ* expression databases there are several other transcription factors that are expressed in a salt and pepper pattern in the epithelium. None of these transcription factors, or their homologs has been implicated in ciliogenesis, so I have not yet done a full analysis to determine if they are involved in ciliated cell formation in *Xenopus*, but such an analysis could identify co-factors that could work together with FoxJ1 to specify multiciliate cells.

Cilia Polarity

As a final note, recent studies have indicated that there is a positive feedback mechanism that drives the polarity of cilia in the external epithelium, where an initial bias, likely set up by global cues identifying the embryonic axes, is then refined through ciliary flow, which requires functional beating cilia (Mitchell et al., 2007). Components of the planar cell polarity pathway have been recently shown to localize asymmetrically at the basal bodies in multiciliate cells and their functionality is required for cells to refine their polarity (Park, 2008 accepted for publication). However, the mechanisms that control how cells in any node-like structure are polarized such that they generate a leftward fluid flow is still unknown. It has been shown that node cilia are localized to the posterior edge of the cell (Marshall and Kintner, 2008; Schweickert et al., 2007), which coupled to angle of the cilia and its vortical beating lead to the leftward flow (Marshall and Kintner, 2008). However, the signals that direct node cilia to their proper location are unknown.

The monocilia on the *Xenopus* GRP, and node-like cilia induced by *XFoxJ1*, are both excellent candidates to begin to explore these issues. First it would be of

interest to determine if GRP cilia have a basal foot or rootlet, and if such structures indicate polarity of the cilia as they do in multiciliate cells. Second, would be to determine if the node-like cilia produced when *XFoxJ1* is misexpressed also contain such structures. Of additional interest will be to determine if these XFoxJ1 induced, motile ectopic, cilia can become polarized, either with relation to global cues, such as anterior-posterior position, or in response to the vigorous fluid flow generated by the external epithelium. Based on the outcome of these initial studies one can expand on possible courses of action, including affecting the PCP pathway to determine if cilia polarity is altered, or if blocking motility of these monocilia affects their ability to polarize, as in the multiciliate cells of the external epithelium (Mitchell et al., 2007).

Final Comments

As a whole, my dissertation has shed light on how the external epithelium in the Xenopus embryo is generated, both in terms of morphology and specification of the cell types found decorating its surface. I have shown that the outer layer of the epithelium, imposes restrictions on intercalating populations, and that the morphologies of intercalating cells also likely contribute to their ability to intercalate. Additionally, my studies on FoxJ1 have shown a conserved role in basal body docking in multiciliate cells. I have also identified a novel role for FoxJ1, in part due to continuity of the GRP with the external epithelium, in the specification of a cilia subtype, the node-like cilia in Xenopus and zebrafish.

APPENDIX I

RFX2 in Epithelial Development

INTRODUCTION

Cilia are microtubule-based organelles that form hair-like structures on the surface of many vertebrate cells (Wheatley et al., 1996). In cells such as in the neurons or kidney, cells project a single cilium as a sensory apparatus to mediate the detection of chemical or mechanical stimuli (Pazour and Witman, 2003; Singla and Reiter, 2006). Sensory cilia are non-motile, generally short in length, and lack structural features such as the central pair or dynein arms (9+0) (Salisbury, 2004). At the other end of the spectrum are the specialized multiciliate cells that produce a vigorous fluid flow in such epithelia as the oviduct, the ependyma or the respiratory airways (Afzelius, 1995). The motile cilia in these cells are typically long (5-10 μM), present in multiple copies per cell, and are specialized for motility and the production of ciliary flow (9+2) (Satir and Christensen, 2007). The formation of these different cilia subtypes is likely to involve similar processes that are common to all forms of ciliogenesis, such as intraflagellar transport. However, the factors that drive ciliogenesis to specify different types of cilia are still poorly understood.

In the studies presented in chapter four of this dissertation I showed that FoxJ1 is necessary for the formation of node-like cilia in *Xenopus* and zebrafish embryos. Node cilia are a subtype of motile monocilia that are found in the organs of L-R asymmetry in many vertebrates. The leftward fluid flow produced by these cilia is responsible for the breaking of early embryonic symmetry, and are thus critical for normal development. The expression of *XFoxJ1* is also required for the formation of the multiciliate cells that decorate the external epithelium of *Xenopus* embryos.

However, despite the ability of FoxJ1 to induce node-like cilia in the external epithelium of Xenopus embryos, FoxJ1 alone is not sufficient to drive the early steps of multiciliate cell differentiation and ciliogenesis, such as radial intercalation and basal body duplication. Thus, it is likely that other factors, along with FoxJ1 are necessary to drive differentiation of multiciliate cells. In an effort to find other factors required for multiciliate cell formation I looked for transcription factors implicated in ciliogenesis in other systems.

The family of X-box binding (RFX) transcription factors has been shown to be important for ciliogenesis in a variety of ciliated cell types across several species, suggesting that they may have a conserved role in ciliogenesis. In *C.elegans* and *Drosophila*, DAF-19 and dRFX, respectively, have been shown to be necessary for sensory cilia formation in neurons (Dubruille et al., 2002; Swoboda et al., 2000). While, in mouse, targeted deletion of RFX3 results in malformation of motile monocilia at the embryonic node, and is associated with L-R asymmetry defects (Bonnafe et al., 2004). In the zebrafish pronephros there are two populations of ciliated cells, mono- and multi-ciliate. Early in development *rfx2* is expressed throughout the kidney and then becomes restricted to the multiciliate cells (Liu et al., 2007), suggesting that in zebrafish *rfx2* may be necessary for specification of both cell types, but may play an additional role in multiciliate cells. The RFX family of transcription factors are therefore involved in the formation of a variety of different cilia subtypes, making them good candidates as co-factors that may act in concert with FoxJ1 in multiciliate cell formation. In the following appendix I describe several

experiments I performed to determine if RFX2 is acting as such a co-factor in the external epithelium in *Xenopus* embryos.

RESULTS

In order to identify if any RFX factors are expressed in *Xenopus* embryos I began by searching the NIBB Xenopus EST database for RFX family members. This database contains sequences from several *Xenopus* cDNA libraries that have been annotated both by BLAST against nr-aa and *X. laevis* Unigene (NCBI) sequences. My search revealed two clones; one that is associated with *Xenopus RFX2* Unigene (XL013j21) and a second that shares sequence homology with *RFX3* by BLAST search (XL056e04). The clones were ordered from NIBB and used to make antisense probes for *in situ* hybridization. Embryos begin expressing *RFX2* RNA at neural plate stages (stage 14) in a punctate pattern in the skin, and expression is maintained through tailbud stages (stage 24) (Figure A1.1A-C). By contrast, no clear expression pattern was observed for *RFX3* RNA (Figure A1.1D-F). Based on the relative expression patterns, and the potential role of RFX2 in multiciliate cells in the zebrafish pronephros, I chose to focus on the first clone, and will refer to it as XRFX2 for my remaining experiments.

XRFX2 misexpression affects ciliated cell formation

In order to determine if XRFX2 can induce the formation of ciliated cells I injected embryos at the 2-cell stage with *XRFX2* mRNA. Embryos analyzed at stage 26 had a phenotype resembling that of XFoxJ1^{MO} injected embryos, ciliated cells were present but cilia were reduced in number and length (data not shown). This result was

somewhat surprising, given the necessity for RFX factors in the formation of cilia in other developmental contexts. In order to determine if the cilia defects I observed could be due to non-specific effects on early development or ciliated cell specification I generated a human glucocorticoid receptor (hGR) XRFX2 chimera to allow temporal control of *XRFX2* function in the developing embryo.

Chimera proteins between the hGR ligand binding domain and transcription factors have been shown useful in a variety of systems to enable ligand-dependent induction of transcription (Becker et al., 1989; Webster et al., 1988). Non-ligand bound hGR resides in the cytoplasm, and upon ligand binding hGR translocates to the nucleus (Picard and Yamamoto, 1987; Qi et al., 1989) where can affect transcriptional activity. Thus, a transcription factor can be sequestered to the cytoplasm by fusion of the hGR ligand-binding domain and then induced to translocate to the nucleus by treatment with the hormone agonist dexamethasone (Dex). Thus, chimeric *XRFX2-hGR* RNA was injected into embryos at the two-cell stage. Dexamethasone treatment at gastrulation stages (stages 11-13) would likely result in *XRFX2-hGR* translocation to the nucleus, thus affecting transcription at gastrulation stages, allowing me to determine if the ciliogenesis defects caused by *XRFX2* are specific for ciliated cells, or potentially a non-specific development defect.

Indeed, injection of *XRFX2-hGR* RNA at the two-cell stage followed by addition of dexamethasone (induction) to the growth media at stage 12, resulted in the formation of small ectopic cilia on outer cells, with no effect on ciliogenesis in multiciliate cells, while not ectopic cilia were observed in controls treated with

DMSO. Concomitant with the induction of ectopic cilia in outer cells was a

morphological change in cells, such that cells were much smaller, and often took on a

triangular, rather than hexagonal appearance. Additionally, in areas where this

morphological change was most pronounced multiciliate cells appeared to be excluded

(Figure A1.2A-D). While, waiting to induce until stage 17 resulted in the generation

of very few ectopic cilia formation and a decrease in morphological changes that did

not include the exclusion of ciliated cells (Figure A1.2E-H). Taken together, the

above results suggest that misexpression of *XRFX2* throughout early developmental

may lead to non-specific effects that ultimately lead to ciliogenesis defects in

multiciliate cells. While *XRFX2-hGR* expression from gastrulation stages appears to

be able to induce ectopic cilia formation, in a manner similar to *XFoxJ1*. However

XRFX2-hGR also affects the morphology of epithelial cells, and appears to affect

either the specification of multiciliate cells or their ability to intercalate.

XRFX2 misexpression in the inner layer does not affect intercalation

In order to address the effects of *XRFX2-hGR* on multiciliate cells I performed

transplant assays as in chapter two. Host embryos were injected with *mRFP* mRNA

alone or in combination with *XRFX2-hGR* RNA. At stage 10 the outer layer from

donors expressing mGFP was transplanted onto host embryos. Embryos were treated

with Dex at stage 12, allowed to develop to stage 26, when they were fixed and

stained with an acetylated α-tubulin antibody to mark ciliated cells, and imaged by

confocal microscopy (Figure A1.3A-B). Cell counts show no change in the number of

intercalating cells from the *XRFX2-hGR* expressing inner layer into the wildtype outer

layer (Figure A1.3C). These results suggest that the morphological changes observed may be specific to the outer layer. Due to the restrictions imposed on intercalating cells by the outer layer (Stubbs et al., 2006) the morphological changes caused by induction of *XRFX2-hGR* may limit the ability of intercalating populations to join the outer layer. In order to more definitively test this hypothesis we will need to perform transplants where the cells in the outer layer are expressing *XRFX2-hGR* in addition to mGFP to determine if there are changes in outer layer morphology, and if such changes can affect intercalation.

XFoxJ1 and XRFX2 co-expression does not affect multiciliate cell formation

Misexpression of XFoxJ1 can induce the formation of node-like cilia in the *Xenopus* epithelium, but alone cannot generate multiciliate cells. XRFX2, when induced at gastrulation stages, can also lead to the formation of ectopic cilia. In order to determine if these two factors can act synergistically to generate multiciliate cells I co-injected *XFoxJ1* and *XRFX2-hGR* RNA into two-cell embryos, then induced *XRFX2-hGR* at approximately stage 12. Injection of either RNA alone induces ectopic cilia as expected (Figure A1.4B, C), however while ectopic cilia were observed when both RNAs were present, no additive effect was observed (Figure A1.4D). Indeed, ectopic cilia induced by both RNAs most closely resemble those formed by misexpression of XFoxJ1 alone, based on their length. Thus, XFoxJ1 does not appear to be working together with XRFX2 to specify multiciliate cells.

Loss of RFX2 function does not affect ciliogenesis in multiciliate cells

Misexpressing RFX2 alone or along with FoxJ1 does not specify the formation of multiciliate cells, however its ability to induce the formation of ectopic cilia suggest that *XRFX2* may be an important factor in ciliogenesis. In order to determine if *XRFX2* is required for the differentiation of multiciliate cells in the developing *Xenopus* epithelium I injected embryos at the two-cell stage with a morpholino to *XRFX2* (XRFX2[MO]) designed to block translation. Fixed embryos were then analyzed after ciliated cell differentiation by staining with antibody directed against acetylated α-tubulin (Figure A1.5B). Injection of XRFX2[MO] failed to alter ciliated cell number or ciliogenesis when compared to control embryos (Figure A1.5A). We do not have an antibody directed against *XRFX2* so we have not been able to determine if expression of *XRFX2* is effectively reduced in response to the morpholino. We also have not yet designed a morpholino to block mRNA splicing, whose function can be tested by RT-PCR. Thus, while these results suggest that XRFX2 is not required for ciliated cell formation, they are not conclusive.

As an alternative approach to knocking down expression of XRFX2 using a morpholino I designed a potential dominant negative construct of XRFX*2*. RFX family members have regions rich in proline, glutamine or acidic amino acids, a characteristic of many transcriptional activators (Emery et al., 1996). Indeed two family members have been shown to be transcriptional activators (Durand et al., 1994; Siegrist and Mach, 1993; Steimle et al., 1995). A strategy that has previously been employed to block the function of transcriptional activators is to generate a fusion protein between the transcription factor of interest and the repressor domain of the

Drosophila engrailed protein. Such a fusion protein will presumably bind its native DNA target sequence, but transcription will not be activated due to active repression by the *engrailed* repressor domain (Jaynes and O'Farrell, 1991). I generated such a construct with the EnR domain fused to the C-terminus of XRFX2 (XRFX2-EnR). Embryos were injected with *XRFX2-EnR* mRNA at the two-cell stage and analyzed at stage 26 for ciliogenesis defects. Similar to the results obtained with the XRFX2^{MO} injected embryos, no change in the number of the various skin cell types or in the differentiation of multiciliate cells was observed when compared to controls (Figure A1.5C, D). Taken together, the above results suggest that XRFX2 is not required for multiciliate cell formation in the *Xenopus* epithelium.

RFX2 can induce the expression of FoxJ1

The ectopic cilia observed when both *XRFX2* and *XFoxJ1* RNAs are injected closely resemble the cilia generated when *XFoxJ1* RNA alone is injected. When *XFoxJ1* is misexpressed alone there is a dose dependence on the number of ectopic cilia that form (see Chapter 4 for discussion). Thus, one explanation that could account for the formation of small ectopic cilia in *XRFX2* injected embryos is that XRFX2 is upregulating FoxJ1 expression at low levels, resulting in the formation of small ectopic cilia. While when the two RNAs are co-expressed the effect of XRFX2 is masked by the cilia induced by the high levels of XFoxJ1.

In order to determine if XRFX2 expression can affect the expression of *XFoxJ1* I injected embryos with *XRFX2-hGR* and *nBgal* mRNA, or *nBgal* alone to mark the injected regions. Following induction at stage 12, embryos were fixed at

stage 26 and stained with X-gal to mark the injected region. *In situ* hybridizations were performed using an *XFoxJ1* antisense digoxigenin labeled probe. *In situ* hybridization revealed an increase in expression of *XFoxJ1* in regions injected with *XRFX2-hGR* when compared to control *nBgal* injected regions (Figure A1.6), or to embryos injected with *XRFX2-hGR* but not induced with dexamethasone (data not shown). These results suggest that XRFX2 may be inducing the formation of ectopic cilia through the upregulation of *XFoxJ1* expression.

DISCUSSION

How cells regulate both the number and type of cilia they form during development is still poorly understood. In chapter four of this dissertation I show that in *Xenopus* FoxJ1 is required for the formation of node-like cilia, as well as aspects of multiciliate cell differentiation. However, the additional factors that are required to generate multiciliate cells are unknown. The RFX transcription factor family has been shown to be involved in the formation of a variety of cilia subtypes including modified sensory cilia (Dubruille et al., 2002; Efimenko et al., 2005; Swoboda et al., 2000) and motile monocilia at the node (Bonnafe et al., 2004). Additionally, despite no characterized functional role, zebrafish *RFX2* is expressed in multiciliate cells (Liu et al., 2007) suggesting that the RFX family of transcription factors may be involved in cilia subtype specification. Here I show that misexpression of XRFX2 is sufficient to induce the formation of ectopic cilia when expressed at stages post gastrulation, possibly through the upregulation of XFoxJ1, but that it is not likely to be required for multiciliate cell differentiation in the developing *Xenopus* skin.

In situ hybridization analysis showed that *Xenopus RFX2,* but not *RFX3*, is expressed in the developing external epithelium of embryos from neural plate stages (stage 14) through tailbud stages (stage 24). Misexpression of XRFX2 from the two-cell stage resulted in a defect in ciliogenesis in multiciliate cells. One possible explanation for this phenotype is that early expression of XRFX2 is resulting in early embryonic non-specific effects. XRFX2 could be required for another process in early development and as we did not determine if embryos express *XRFX2* at stages earlier than stage 14, this is a possibility we cannot rule out.

Use of an inducible XRFX2 construct allowed careful timing of XRFX2 function that resulted in the formation of ectopic cilia. The ability of XRFX2-hGR to induce ectopic cilia suggests that XRFX2 may play a role in cilia formation in *Xenopus*. However, the cilia induced by *XRFX2-hGR* were quite short and often appear only as small puncta on the cell surface (see Figure A1.4C). Indeed, when XRFX2-hGR and XFoxJ1 were misexpressed in the same cells the resulting cilia were FoxJ1-like based on their length. Further, XRFX2-hGR misexpression can also induce the expression of *XFoxJ1*, a potent inducer of ectopic cilia. Taken together these results suggest that XRFX2 and XFoxJ1 do not act together to specify multiciliate cells.

In addition to the ectopic cilia formed in response to XRFX2-hGR induction post gastrulation, additional morphological changes were observed. Many of the injected cells had small, triangular apical domains, compared to the large, hexagonal shape normally observed in outer layer cells. Indeed, while differentiation in terms of

forming cilia did not appear to be altered in multiciliate cells, they did appear to be excluded from the injected region. Indeed, in areas with more mild morphological phenotypes ciliated cells were still present and did not appear to have ciliogenesis defects, suggesting that XRFX2 is not affecting specification of ciliated cells. In support of this, in transplant assays, where only the inner layer is expressing XRFX2-hGR ciliated cells appear to form and intercalate normally, suggesting that the defects may be instead due to morphological constraints imposed by the outer layer on intercalating cell populations. These morphological effects, suggest that in addition to a role in ciliogenesis XRFX2 may play a potentially interesting role in tissue morphogenesis as well.

Finally, two assays were performed to determine if XRFX2 expression is necessary for the formation of multiciliate cells, knockdown by morpholino injection and injection of *XRFX2-EnR* to act as a potential dominate negative. Neither of these approaches resulted in a phenotype in multiciliate cell formation suggesting that *XRFX2* may not be required for multiciliate cell formation in Xenopus. As a caveat, at this time I am unable to determine if the morpholino is effectively blocking translation as we do not have an antibody directed against RFX2. Nor do I have any assay to determine if the XRFX2-EnR is indeed acting as a dominant negative.

However, due to the lack of knockdown phenotype and lack of synergistic effect when misexpressed with XFoxJ1, it is unlikely that XRFX2 is the single XFoxJ1 co-factor required to specify multiciliate formation in the *Xenopus* epithelium. Additionally, the morphological effects on outer layer cells suggest that XRFX2 might

also be involved in aspects of morphogenesis in addition to any roles in ciliogenesis. This morphogenetic role may affect aspects of intercalation, as evidenced by the lack of multiciliate cells when high levels of XRFX2-hGR are expressed, confounding our ability to score the formation of multiciliate cells.

Based on their role in cilia formation in other systems it is likely that RFX factors play a role in ciliated cell formation in *Xenopus*. However, based on these preliminary experiments it is not clear that XRFX2 is the relevant RFX factor, or if it plays any essential role in ciliogenesis in *Xenopus*. Thus, identification of the other *Xenopus* RFX family members, and analysis of their function in ciliogenesis will be necessary to determine if RFX transcription factors are necessary for cilia formation in *Xenopus*.
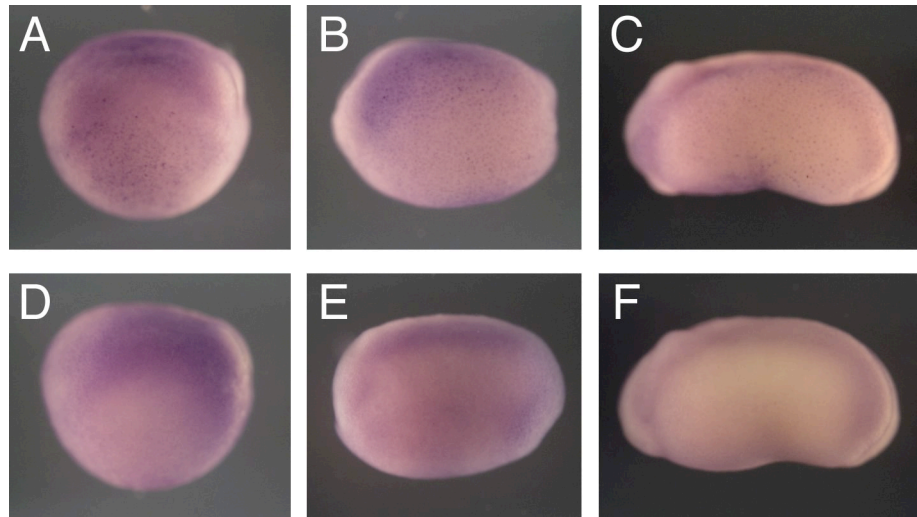
Figure A1.1 Expression pattern of *XRFX2* and *XRFX3* in *Xenopus* embryos. **(A-C)** Embryos stained with a *XRFX2* probe **(D-F)** Embryos stained with a *XRFX3* probe. Expression was analyzed at stage 13/14 (A, D), stage 17 (B, E) and stage 24 (C, F).
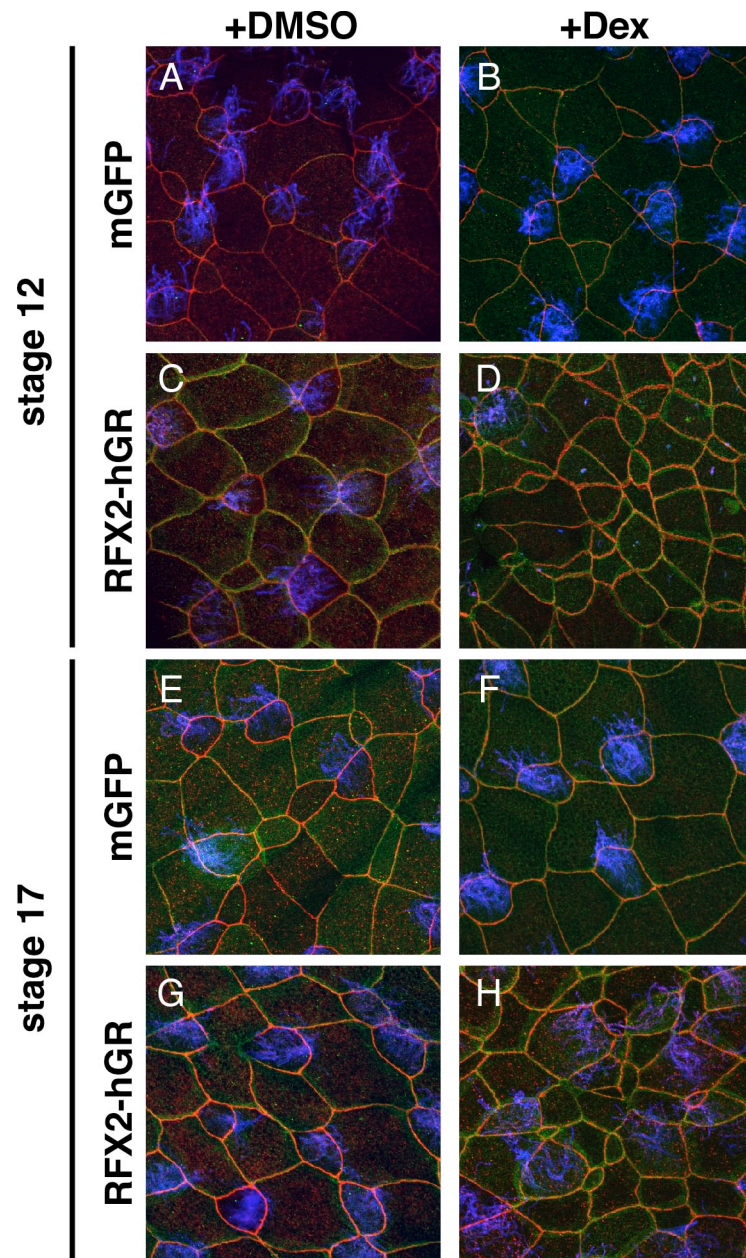
Figure A1.2 Expression of XRFX2 induces ectopic cilia and morphological changes in the external epithelium. Embryos were injected with RNA encoding mGFP (A, B, E, F) or XRFX2-hGR (C, D, G, H) and treated at the indicated stages with Dexamethasone (B, D, F, H) or mock treated with DMSO (A, C, E, G). **(A-D)** Induction of XRFX2-hGR at stage 12 leads to the formation of ectopic cilia, and induces changes in cellular morphology. **(E-H)** Induction of XRFX2-hGR at stage 17 results in less severe morphological changes and formation of fewer ectopic cilia.
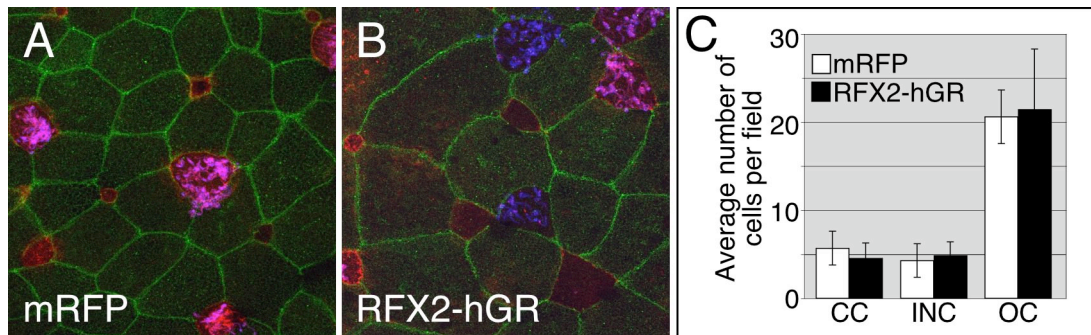
Figure A1.3 Expression of XRFX2 in the inner layer does not affect intercalation. (A-B) Outer layer ectoderm expressing mGFP (green) was transplanted onto control host (mRFP) or onto host embryos expressing XRFX2-hGR. Induction by Dex treatment was performed at stage 12. Transplants were fixed at stage 26 and stained at with an acetylated α-tubulin antibody (blue) to mark ciliated cells, then imaged by confocal microscopy. Images identify outer cells (green), intercalating non-ciliated cells (red, not blue, INC) and ciliated cells (red/blue, CC). **(D)** Quantification of the three different cell types in at least five fields from three transplants for each condition.
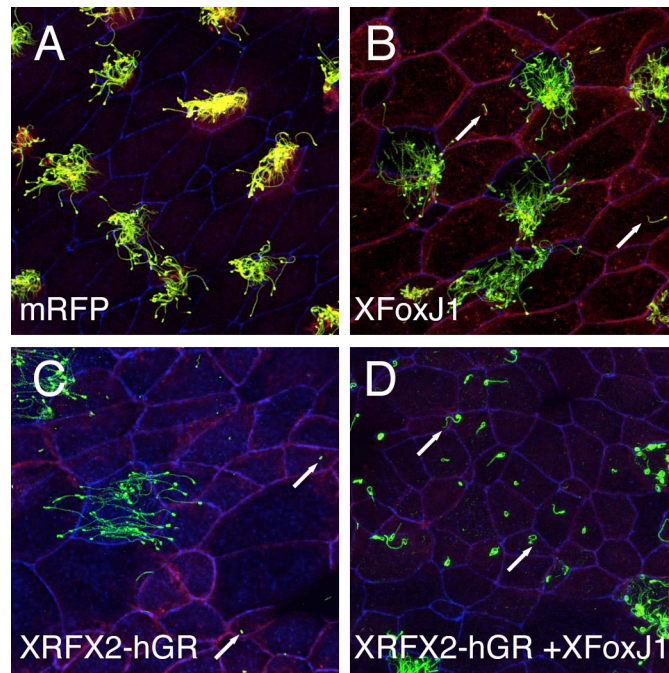
Figure A1.4 XRFX2 and XFoxJ1 coupled misexpression generate FoxJ1-like ectopic cilia. (A-D) Shown are confocal images of stage 26 *Xenopus* embryos stained with antibodies to ZO-1 (blue) and acetylated α-tubulin (green). All embryos were injected with mRFP RNA (red) as an injection tracer alone (A) with *XFoxJ1* (B), *XRFX2-hGR* (C), or *XFoxJ1* and *XRFX2-hGR* together.
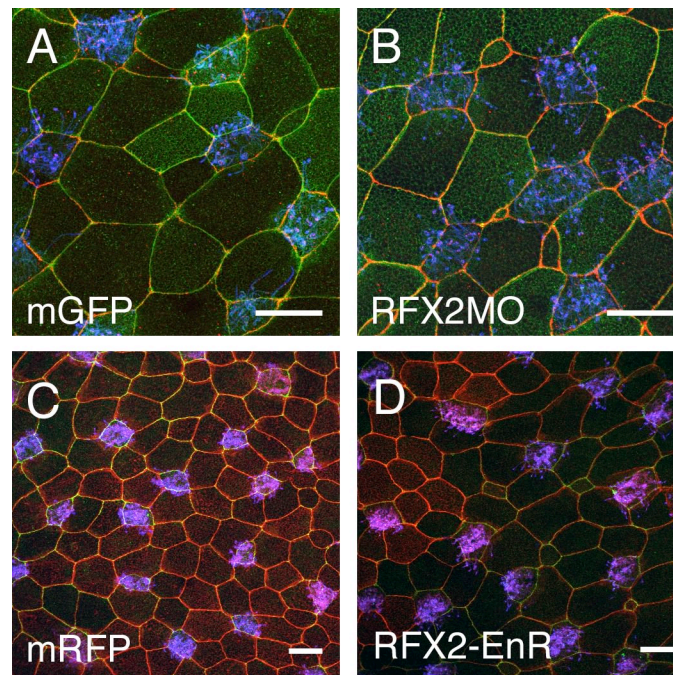
Figure A1.5: RFX2MO and XRFX2-EnR injections do not affect ciliogenesis. Shown are confocal images of the superficial epithelium in *Xenopus* embryos at stage 26 stained with antibodies to ZO-1 (red A, B, green C, D) and acetylated α-tubulin (blue) to mark tight junctions and cilia, respectively. **(A-B)** Embryos were injected at the two-cell stage with mGFP RNA alone (A) or following RFX2MO injections (B) **(C-D)** Embryos were injected at the two-cell stage with mRFP RNA alone (C) or with XRFX2-EnR RNA (D). Scale bars in all images represent 20μm.
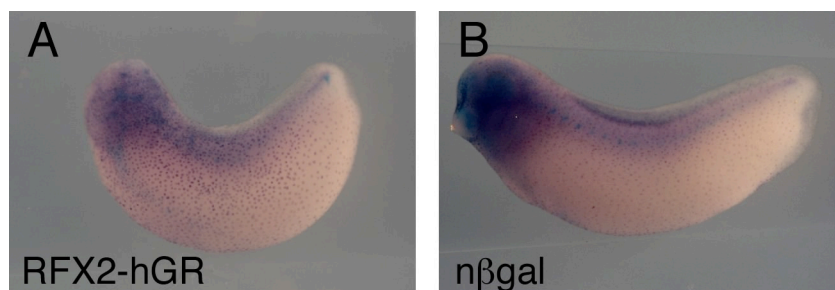
Figure A1.6 XRFX2 misexpression upregulate expression of *XFoxJ11*: *XFoxJ1* expression is increased at stage 28+ in response to misexpression of XRFX2-hGR (A) compared to control (B). All embryos were injected with nβgal (blue staining) to mark the injected side of the embryo.

APPENDIX II

Materials and Methods

MATERIALS AND METHODS

***Xenopus laevis* fertilizations and embryo culture**

Xenopus embryos were obtained by *in vitro* fertilization using standard protocols (Sive et al., 2000). Embryos were maintained in 0.1X Marc's Modified Ringer's (MMR) unless otherwise stated. Embryos were staged according to the normal tables of Nieuwkoop and Faber (Nieuwkoop and Faber, 1967).

RNA and Morpholino Injection

Xenopus embryos were injected at the two-cell or four-cell stage with capped, synthetic mRNAs (1-5 ng) or morpholinos (30-105ng, Genetools) (Heasman, 2002; Nasevicius and Ekker, 2000). Injections were targeted to the presumptive ectoderm, or presumptive gastrocoel roof plate in *Xenopus* embryos based on fate maps (Sive et al., 2000). The following misexpression constructs were generous gifts or previously generated in the Kintner lab; membrane-localized RFP or GFP, which were used as lineage tracers, the intracellular domain of Notch (ICD), dominant-negative form of mastermind (dnHMM; (Fryer et al., 2002)), Enhancer of split-related6e (Esr6e; (Deblandre et al., 1999)), centrin fused to GFP (centrin-GFP;(Mitchell et al., 2007)).

Cloning of misexpression constructs from cDNA

Full-length clones were amplified from a stage 17 cDNA library for generation of misexpression constructs. Primers included restriction sites for incorporation into the pCS2+ expression vector. Primers for each construct are listed below:

Basigin primers: XBsg, XBsg-MT, XBsgΔC, XBsgΔE constructs respectively BsgF1

5'-CGGGATCCGGCAGAACGATGGG-3'

BsgR1 5'-GCTCTAGAGCTCAGTTTGAATTCCTCTGGCGCAG-3'

Myc tagged Bsg, use BsgF1 and BsgMTR1 5'-

CGGGATCCGTTTGAATTCCTCTGGCGC -3'

Long isoform BsgLF1 5'- GCAGATCTCGATGGGTCTCGGGTTGCTTAC -3',

BsgLR1 5'- CGGATATCTGGATGGTCAATGACC -3'

BsgΔC, use BsgF1 and BsgΔCR1 5'-

GCTCTAGATCAAGGCTTTCTCCTCTTCTCATA -3' BsgΔE, BsgΔEF1 5'-

GCGGATCCCATTTCCACGTGCGAAGTCGT -3' and BsgR1. The long isoform

was generated by PCR amplification of the 5' end of the long isoform from st17

cDNA library, through an EcoRV site within the second Ig domain. This fragment

was then inserted into the short isoform construct in place of the short isoform start

and signal sequence. Primers were XBsgL-F1 5'-

GCAGATCTCGATGGGTCTCGGGTTGCTTAC-3' and XBsgL-R1 5'-

CGGATATCTGGATGGTCAATGACC-3'. Truncation clones, with the extracellular

domain (XBsgΔE) or the cytoplasmic domain (XBsgΔC) of the short isoform were

generated by restriction digest elimination of unnecessary coding regions from the

pCS2+ XBsg expression construct.

XFoxJ1 was cloned with the listed primers into pGEM T-Easy vector

(Promega A1360) following PCR amplification. XFoxJ1 coding region was then

subcloned into pCS2+ expression vector by ligation following StuI/XbaI digestion.

XFoxJ1-F1 5'-GAAGGCCTATGTTTGACCTGCCCAGGGCGGC-3' and XFoxJ1-R1 5'-GCTCTAGATTATATAGGAACCCAGGACG-3'. FLAG tagged expression construct for rescue experiments was generated by excising XFoxJ1 from pCS2+ with StuI/XbaI, followed by ligation into pCS2+Flag cut with the same enzymes. Resulting construct puts FLAG tag in frame, on the N-terminus of XFoxJ1.

XRFX2 with the 3' and 5' UTRs was generated by subcloning from NIBB clone XL013j21. Insert was digested with XbaI, blunted by Klenow digestion, digested with XhoI, then ligated into pCS2+ digested with StuI/XbaI. XRFX2 lacking the 3' and 5' UTRs was PCR amplified from the above vector using the following primers: XRFX2-F1 5'-CCATCGATAGAAACCAGTATGCAGAATTC-3' and XRFX2-R1 5'-CCGCTCGAGCTACATTTCTTGCATTGAG-3' followed by digestion with ClaI/XhoI and ligation into pCS2+ digested with the same enzymes. The hGR fusion construct was generated by amplification from XL013j21 with XRFX2-F1, and XRFX2-R2 5'-CCGCTCGAGGCATTTCTTGCATTGAGTGG-3', followed by digestion with ClaI/XhoI and ligation into pCS2+-hGR vector, resulting in RFX2 in frame with hGR on its C-terminal end. RFX2-EnR construct was generated by excising RFX2 coding sequence from RFX2-hGR construct by digestion with ClaI/XhoI and blunting with Klenow. The insert was then ligated into pCS2+EnR, generated by D. Wettstein in the lab, digested with StuI, resulting in a C-terminal fusion of the EnR domain to RFX2 coding sequence.

Morpholino Sequences:

NTL1MO: 5'-AGCGTAAGCAACCCGAGACCCATCG-3'

NTL2MO: 5'-AGCGTAAGCAGCCCGAGACCCAT-3'

XFoxJ1MO^{AUG}: 5'-GCAGGTCAAACATTAATAAAGCCCT-3'

XFoxJ1MO^{Spl}: 5'-TGCTCCTACAATGCAA-GCAGAGAAT-3'

zfFoxJ1MO: 5'-CATGGAGAGCATGGTCCTGACAAAT-3'

RFX2MO: 5'-CCACTGTCTGAATTCTGCATACTGG-3'

Control zebrafish MO: 5'-CCTCTTACCTCAGTTACAATTTATA-3'

Transplant assays and explant cultures

To introduce lineage tracers, embryos were injected four times at the 2-4 cell stages with capped, synthetic mRNA encoding membrane-localized forms of GFP or RFP. At stage 10, a fine needle or hair was used to peel off the outer layer from a region of the ectoderm from a donor embryo, which was transferred onto the host embryos after removing a similar patch of outer cells. While the transplanted tissue healed onto the host embryo, it was kept in place by pressing down with a small piece of a glass coverslip, held in place with silicone grease. In some transplants, host embryos were not only injected with RNA encoding a tracer but also with RNA that either activate (ICD) or inhibit the Notch pathway (dnHMM), misexpress Esr6e, or XRFX2. Transplants were performed in Danilchik's buffer + 0.1% BSA (DFA) (Davidson et al., 2002). After healing of the transplanted tissue, embryos were returned to 0.1X Marc's Modified Ringers (MMR). Ectoderm was also explanted in DFA onto coverslips coated with fibronectin as described (Davidson et al., 2002).

Transgenic construct generation

The promoter region of ∝-*tubulin* was isolated by screening a *Xenopus laevis* genomic library (Stratagene) with ^{32}P radiolabelled DNA fragment from the ∝-*tubulin* cDNA (Deblandre et al., 1999) followed by plaque purification of positive clones. Templates for anchored PCR were generated by digesting purified phage DNA with either EcoR1, Xho1, HindIII or BamHI, followed by ligation to pBluescript digested with the same enzyme. DNA sequences lying upstream of the ∝-*tubulin* gene were then amplified by PCR, using one primer corresponding to cDNA sequences around the start of translation of the ∝-tubulin protein and the other corresponding to the T3 polymerase recognition sequence in pBluescript. The largest PCR fragment generated was cloned into the CS2 vector (Turner and Weintraub, 1994) replacing the CMV promoter upstream of the membrane-localized form of GFP. Clones containing the correct region of the ∝-*tubulin* gene were verified by sequencing.

Transgenic embryo generation

In order to generate transgenic embryos, ∝-*tubulin-mGFP* DNA was isolated away from vector sequences by digestion with Sal1 and Acc651, mixed with sperm nuclei and injected into unfertilized eggs, as described by Amaya and Kroll (Amaya and Kroll, 1999) with modifications (Lamar and Kintner, 2005; Sparrow et al., 2000). Routinely 50-70% of the embryos were transgenic.

Whole mount *in situ* hybridization in *Xenopus* and zebrafish embryos

Whole mount *in situ* hybridization of *Xenopus* embryos were performed according to Harland with modifications described by Knect et al. (Harland, 1991;

Knecht et al., 1995) using digoxigenin-labeled antisense RNA probes for *Xenopus α-tubulin*, *XBsg*, *XFoxJ1* and *XRFX2*. Whole mount in situ hybridizations were performed as described (Thisse et al., 1994) using a digoxigenin-labeled antisense RNA probe for *ZFoxJ1*.

Cloning of *In Situ* Probes

XFoxJ1 cloned from cDNA into pGEM (see above) was linearized and used as a template to generate antisense digoxigenin probes. XBsg, XRFX2, tektin, Pf16 and L-R dynein cDNA clones were obtained from the NIBB database, clones number XL007a01, XL013j21, XL008o07, Xl110d06 and XL100m24, respectively. Amplicons from PCR using T7 and T3 primers were used as templates for T7 RNA Polymerase reactions to generate antisense digoxigenin probes. zFoxJ1 was amplified from 2dpf zebrafish cDNA using the following primers: zFoxJ1 F1 5'-CGGGATCCATGGGCTCAGACGCGCCCTC-3', zFoxJ1 R1 5'-CGGAATTCCTTCAGAGAACTAAATTTGCACC-3' and inserted into the pGEM vector. zFoxJ1 in pGEM was then linearized and used as a template for antisense digoxigenin probe synthesis.

Zebrafish strains and scoring of L-R asymmetry

Transgenic *mlc2a-eGFP* (Huang et al., 2003a; Raya et al., 2003) zebrafish strains were used for all zebrafish experiments. Embryos were injected with 2-5ng of ZFoxJ1MO into the yolk at the one-cell stage. Embryos were staged according to standard staging tables (Kimmel et al., 1995). In order to score L-R asymmetry embryos were allowed to develop until 30hpf when they were imaged live under

epifluorescence using a dissecting microscope. Heart jogging based on GFP expression was scored as left jog, right jog or no jog if the heart tube remained in the center of the embryo.

RNA Isolation from explants and whole embryo

Whole embryos or ectoderm explants, which were lifted off fibronectin coverslips, were transferred to eppendorf tubes. Excess media was removed and 10 volumes of homogenization buffer (50mM NaCl, 50mM Tris-Cl (pH7.5), 5mM EDTA (ph8.0), 0.5% SDS, 200μg/ml Proteinase K) was added to each tube, followed by incubation for 1hr at 37°C. Nucleic acids were then extracted by Phenol-chloroform extraction and ethanol precipitation. Further extraction by addition of 4M Lick followed by centrifugation. DNA was removed from samples by treating for 2hrs at 37°C in DNase (Promega M6101). RNA was resuspended in a small volume of DEPC H$_2$0. For long-term storage add 1/10th volume of DEPC treated 3M NaOAc and 3 volumes of 100% ethanol, store at -80°C.

cDNA Synthesis

cDNA was synthesized from total RNA using the Superscript III kit (Invitrogen 18080-044). In short 3μg RNA was mixed with 100ng of random hexamer oligonucleotides and 0.5mM dNTPs (final). The reaction was incubated at 65°C for 5', then quenched on ice. First strand buffer, 5mM DTT (final) and 1μl RNasin (Promega N2511) and 1μl SuperScript III to +RT reactions or 1μl DEPC H$_2$0 to –RT reactions then incubated 1hr at 50°C. Reactions were stopped by incubating at 70°C for 15'.

Genomic DNA Isolation and Cloning of FoxJ1 Exon Intron Boundaries

Ten stage 30 embryos were used to generate genomic DNA using Qiagen QIAamp Tissue Kit (Qiagen #51304). Primers were designed approximately 50bp in either direction from exon/intron boundaries based on *Xenopus tropicalis* exon/intron boundary predictions. PCR amplification from genomic DNA using the primers listed below amplified introns 1 and 2, splicing sequences were then determined and used to generate a splice blocking morpholino. Primers: XLIntron1-F1 5'-GCTGTTGCTGCTGCTTCCAGAACC-3', XLIntron1-R1 5'-GGACTCTTGCCCCTGCTCTTCCTC-3', XLIntron2-F1 5'-GCAAGCAAGAAGACCAAGATCACAC-3'. XLIntron2-R1 5'-CTTCCAGAAACCTCCTTTGCC-3'

Immunofluorescence and confocal microscopy

Fixation of embryos for confocal microscopy was performed in 4% paraformaldehyde in Phosphate Buffered Saline (PBS) for 1 hour on ice (*Xenopus*) or overnight at 4°C (Zebrafish), followed by dehydration in 100% ethanol *Xenopus* embryos were rehydrated, washed with PBS/0.1% TritonX-100 (PBT), and blocked with PBT containing 10% heat-inactivated normal goat serum (PBT/HIGS) for at least one hour. Zebrafish embryos were rehydrated in PBS/0.1% Tween-20 (PTW), and blocked in PTW + 5% HIGS + 2% Bovine Serum Albumin (BSA). Embryos were incubated with primary antibody in PBT/HIGS overnight as follows: Rabbit anti-ZO-1 (Zymed 1:200), mouse monoclonal anti-acetylated α-tubulin (Sigma, 1:200-1:1000), mouse monoclonal anti-*Xenopus* E-cadherin (5D3, Developmental

Studies Hybridoma Bank, 1:500), rabbit anti-GFP (Molecular Probes, 1:1000) or

monoclonal anti-gamma tubulin (Sigma, 1:1000). After washing, embryos were

incubated overnight in Cy2, Cy3, or Cy5 labeled Goat anti-IgG of the appropriate

species (all used at 1:500, Jackson ImmunoResearch), washed in PBT or PTW and

then mounted in PVA/DABCO. Mounted embryos were imaged on a BioRad

Radiance 2100 confocal mounted to a Zeiss inverted microscope using a 40X or 63X

objective.

Timelapse

Imaging of outer cells was performed using low light epifluorescence time-

lapse sequences at two wavelengths with collection at multiple positions from a

cooled CCD camera (Hamamatsu; Bridgewater, NJ) mounted on an inverted

compound microscope (Olympus; Melville NY). Camera settings, XYZ-position,

shutter, and filters were computer controlled by image acquisition software

(Metamorph; Molecular Devices Corp., Downington PA).

Timelapse imaging of intercalating cell populations was performed using a

BioRad Radiance 2100 confocal mounted to a Zeiss inverted microscope using a 63X

objective. Embryos were taken from several areas or a single area once an hour

depending on the assay.

Microarray Analysis

Total RNA from explanted ectoderm was used to generate labeled

complimentary RNA (cRNA) that was hybridized to *Xenopus laevis* Genome Array

chips (Affymetrix #900491). Microarray data were obtained from three independent

experiments in which embryos were injected with *ICD* RNA alone, and two

independent experiments in which embryos were injected with both *ICD* and *FoxJ1*

RNA. These data sets were analyzed using Bullfrog analysis software (Zapala et al.,

2002) using a pair-wise comparison, with the minimum fold change set at 3. Data

presented in supplemental Table 1 show all genes with an average change of 10-fold

or greater. Annotation of the dataset was then performed using Unigene identifiers.

Quantitative RT-PCR

Animal caps were isolated and explanted on fibronectin-coated coverslips as

above. Total RNA was isolated at stage 22-24. cDNA templates were generated

from 3μg of RNA using SuperScript III Reverse Transcriptase (Invitrogen 18080-

093). Quantitative RT-PCR reactions were performed using the ABI Prism 7900HT

Thermal Cycler using the following primers:

ODC-F 5'-CTG-CCGCCTCAGTGTGAA,

ODC-R 5'-TGCCCGCTCCAGAAGC,

DHC9-F 5'-CA-GAATCCAGCCATCCGTG,

DHC9-R 5'-TTGTGAACCGAACACCAGTTG,

Pf16-F 5'-AAGAAAGCAGCAGCCTTTGTG,

Pf16-R 5'-CCCCAGAGTCCACTATTGACTGA,

Tektin-F 5'-CGCAATGAGACAAGCAACCA,

Tektin-R 5'-CACGTCATCTATGCGTTCATCA.

Data was analyzed using Applied Biosystems Sequence Detection System

(SDS) software. Samples were normalized to ornithine decarboxylase to account for

differences in cDNA synthesis efficiency. mRNA injected samples were compared to uninjected controls, and XFoxJ1^{MO} injected samples were compared to control morpholino injected embryos.

Transmission Electron Microscopy

Embryos were fixed overnight at 4ºC in 2% Glutaraldehyde, post fixed in OsO4, stained with uranyl acetate, then embedded in EPON epoxy resin. Thin sections (60nm) were cut and mounted on copper slot grids coated with parlodion, stained with uranyl acetate /lead citrate and imaged on a Philips CM100 electron microscope. Extensive use was made of the goniometer in conjunction with the rotation-tilt specimen holder and the orientation of the grids was adjusted up to $\pm$ 60 degree tilt to optimize as far as possible the cross sectional profile of the cilia. Images were documented using Kodak SO163 EM film that were scanned at 600 lpi using a Fuji FineScan 2750xl and converted to tif format.

REFERENCES

Adams, C. L., Chen, Y. T., Smith, S. J. and Nelson, W. J. (1998). Mechanisms of epithelial cell-cell adhesion and cell compaction revealed by high-resolution tracking of E-cadherin-green fluorescent protein. *J Cell Biol* **142**, 1105-19.

Adams, C. L., Nelson, W. J. and Smith, S. J. (1996). Quantitative analysis of cadherin-catenin-actin reorganization during development of cell-cell adhesion. *J Cell Biol* **135**, 1899-911.

Adams, G. M., Huang, B., Piperno, G. and Luck, D. J. (1981). Central-pair microtubular complex of Chlamydomonas flagella: polypeptide composition as revealed by analysis of mutants. *J Cell Biol* **91**, 69-76.

Afzelius, B. (1959). Electron microscopy of the sperm tail; results obtained with a new fixative. *J Biophys Biochem Cytol* **5**, 269-78.

Afzelius, B. A. (1976). A human syndrome caused by immotile cilia. *Science* **193**, 317-9.

Afzelius, B. A. (1979). The immotile-cilia syndrome and other ciliary diseases. *Int Rev Exp Pathol* **19**, 1-43.

Afzelius, B. A. (1995). Role of cilia in human health. *Cell Motil Cytoskeleton* **32**, 95-7.

Afzelius, B. A. (2004). Cilia-related diseases. *J Pathol* **204**, 470-7.

al-Shroof, M., Karnik, A. M., Karnik, A. A., Longshore, J., Sliman, N. A. and Khan, F. A. (2001). Ciliary dyskinesia associated with hydrocephalus and mental retardation in a Jordanian family. *Mayo Clin Proc* **76**, 1219-24.

Altruda, F., Cervella, P., Gaeta, M. L., Daniele, A., Giancotti, F., Tarone, G., Stefanuto, G. and Silengo, L. (1989). Cloning of cDNA for a novel mouse membrane glycoprotein (gp42): shared identity to histocompatibility antigens, immunoglobulins and neural-cell adhesion molecules. *Gene* **85**, 445-51.

Amaya, E. and Kroll, K. L. (1999). A method for generating transgenic frog embryos. *Methods Mol Biol* **97**, 393-414.

Anderson, R. G. and Brenner, R. M. (1971). The formation of basal bodies (centrioles) in the Rhesus monkey oviduct. *J Cell Biol* **50**, 10-34.

Assheton, R. (1896). Notes on the ciliation of the ectoderm of amphibian embryos. *Q. J. Microscope Sci* **38**, 465-484.

Avidor-Reiss, T., Maer, A. M., Koundakjian, E., Polyanovsky, A., Keil, T., Subramaniam, S. and Zuker, C. S. (2004). Decoding cilia function: defining specialized genes required for compartmentalized cilia biogenesis. *Cell* **117**, 527-39.

Baas, D., Meiniel, A., Benadiba, C., Bonnafe, E., Meiniel, O., Reith, W. and Durand, B. (2006). A deficiency in RFX3 causes hydrocephalus associated with abnormal differentiation of ependymal cells. *Eur J Neurosci* **24**, 1020-30.

Banizs, B., Pike, M. M., Millican, C. L., Ferguson, W. B., Komlosi, P., Sheetz, J., Bell, P. D., Schwiebert, E. M. and Yoder, B. K. (2005). Dysfunctional cilia lead to altered ependyma and choroid plexus function, and result in the formation of hydrocephalus. *Development* **132**, 5329-39.

Barnes, S. N. (1971). Fine structure of the photoreceptor and cerebral ganglion of the tadpole larva of Amaroucium constellatum (Verril) (subphylum: Urochordata; class: Ascidiacea). *Z Zellforsch Mikrosk Anat* **117**, 1-16.

Becker, D. M., Hollenberg, S. M. and Ricciardi, R. P. (1989). Fusion of adenovirus E1A to the glucocorticoid receptor by high-resolution deletion cloning creates a hormonally inducible viral transactivator. *Mol Cell Biol* **9**, 3878-87.

Berditchevski, F., Chang, S., Bodorova, J. and Hemler, M. E. (1997). Generation of monoclonal antibodies to integrin-associated proteins. Evidence that alpha3beta1 complexes with EMMPRIN/basigin/OX47/M6. *J Biol Chem* **272**, 29174-80.

Beyer, L. A., Odeh, H., Probst, F. J., Lambert, E. H., Dolan, D. F., Camper, S. A., Kohrman, D. C. and Raphael, Y. (2000). Hair cells in the inner ear of the pirouette and shaker 2 mutant mice. *J Neurocytol* **29**, 227-40.

Billett, F. S. and Gould, R. P. (1971). Fine structural changes in the differentiating epidermis of Xenopus laevis embryos. *J Anat* **108**, 465-80.

Bisgrove, B. W. and Yost, H. J. (2006). The roles of cilia in developmental disorders and disease. *Development* **133**, 4131-43.

Blacque, O. E., Perens, E. A., Boroevich, K. A., Inglis, P. N., Li, C., Warner, A., Khattra, J., Holt, R. A., Ou, G., Mah, A. K. et al. (2005). Functional genomics of the cilium, a sensory organelle. *Curr Biol* **15**, 935-41.

Blouin, J. L., Meeks, M., Radhakrishna, U., Sainsbury, A., Gehring, C., Sail, G. D., Bartoloni, L., Dombi, V., O'Rawe, A., Walne, A. et al. (2000). Primary ciliary dyskinesia: a genome-wide linkage analysis reveals extensive locus heterogeneity. *Eur J Hum Genet* **8**, 109-18.

Boisvieux-Ulrich, E., Laine, M. C. and Sandoz, D. (1990). Cytochalasin D inhibits basal body migration and ciliary elongation in quail oviduct epithelium. *Cell Tissue Res* **259**, 443-54.

Boisvieux-Ulrich, E. and Sandoz, D. (1991). Determination of ciliary polarity precedes differentiation in the epithelial cells of quail oviduct. *Biol Cell* **72**, 3-14.

Bonnafe, E., Touka, M., AitLounis, A., Baas, D., Barras, E., Ucla, C., Moreau, A., Flamant, F., Dubruille, R., Couble, P. et al. (2004). The transcription factor RFX3 directs nodal cilium development and left-right asymmetry specification. *Mol Cell Biol* **24**, 4417-27.

Bozkurt, H. H. and Woolley, D. M. (1993). Morphology of nexin links in relation to interdoublet sliding in the sperm flagellum. *Cell Motil Cytoskeleton* **24**, 109-18.

Bray, S. (1998). Notch signalling in Drosophila: three ways to use a pathway. *Semin Cell Dev Biol* **9**, 591-7.

Brody, S. L., Yan, X. H., Wuerffel, M. K., Song, S. K. and Shapiro, S. D. (2000). Ciliogenesis and left-right axis defects in forkhead factor HFH-4-null mice. *Am J Respir Cell Mol Biol* **23**, 45-51.

Brokaw, C. J. and Kamiya, R. (1987). Bending patterns of Chlamydomonas flagella: IV. Mutants with defects in inner and outer dynein arms indicate differences in dynein arm function. *Cell Motil Cytoskeleton* **8**, 68-75.

Brueckner, M., D'Eustachio, P. and Horwich, A. L. (1989). Linkage mapping of a mouse gene, iv, that controls left-right asymmetry of the heart and viscera. *Proc Natl Acad Sci U S A* **86**, 5035-8.

Carlen, B. and Stenram, U. (2005). Primary ciliary dyskinesia: a review. *Ultrastruct Pathol* **29**, 217-20.

Carlsson, P. and Mahlapuu, M. (2002). Forkhead transcription factors: key players in development and metabolism. *Dev Biol* **250**, 1-23.

Carthew, R. W. (2005). Adhesion proteins and the control of cell shape. *Curr Opin Genet Dev* **15**, 358-63.

Caspary, T., Larkins, C. E. and Anderson, K. V. (2007). The graded response to Sonic Hedgehog depends on cilia architecture. *Dev Cell* **12**, 767-78.

Caudroy, S., Polette, M., Nawrocki-Raby, B., Cao, J., Toole, B. P., Zucker, S. and Birembaut, P. (2002). EMMPRIN-mediated MMP regulation in tumor and endothelial cells. *Clin Exp Metastasis* **19**, 697-702.

Chen, J., Knowles, H. J., Hebert, J. L. and Hackett, B. P. (1998). Mutation of the mouse hepatocyte nuclear factor/forkhead homologue 4 gene results in an absence of cilia and random left-right asymmetry. *J Clin Invest* **102**, 1077-82.

Chitnis, A., Henrique, D., Lewis, J., Ish-Horowicz, D. and Kintner, C. (1995). Primary neurogenesis in Xenopus embryos regulated by a homologue of the Drosophila neurogenic gene Delta. *Nature* **375**, 761-6.

Choi, Y. S. and Gumbiner, B. (1989). Expression of cell adhesion molecule E-cadherin in Xenopus embryos begins at gastrulation and predominates in the ectoderm. *J Cell Biol* **108**, 2449-58.

Clausen, B. E., Waldburger, J. M., Schwenk, F., Barras, E., Mach, B., Rajewsky, K., Forster, I. and Reith, W. (1998). Residual MHC class II expression on mature dendritic cells and activated B cells in RFX5-deficient mice. *Immunity* **8**, 143-55.

Cohen, E., Binet, S. and Meininger, V. (1987). In situ appearance of the cold-stable microtubules in the growing axons of the tectal plate of mouse investigated immunocytochemically after polyethyleneglycol (PEG) embedding. *Brain Res* **433**, 171-80.

Cole, D. G., Chinn, S. W., Wedaman, K. P., Hall, K., Vuong, T. and Scholey, J. M. (1993). Novel heterotrimeric kinesin-related protein purified from sea urchin eggs. *Nature* **366**, 268-70.

Corbit, K. C., Aanstad, P., Singla, V., Norman, A. R., Stainier, D. Y. and Reiter, J. F. (2005). Vertebrate Smoothened functions at the primary cilium. *Nature* **437**, 1018-21.

Crowe, R., Henrique, D., Ish-Horowicz, D. and Niswander, L. (1998). A new role for Notch and Delta in cell fate decisions: patterning the feather array. *Development* **125**, 767-75.

Davidson, L. A., Hoffstrom, B. G., Keller, R. and DeSimone, D. W. (2002). Mesendoderm extension and mantle closure in Xenopus laevis gastrulation: combined roles for integrin alpha(5)beta(1), fibronectin, and tissue geometry. *Dev Biol* **242**, 109-29.

Dawe, H. R., Farr, H. and Gull, K. (2007). Centriole/basal body morphogenesis and migration during ciliogenesis in animal cells. *J Cell Sci* **120**, 7-15.

Deblandre, G. A., Wettstein, D. A., Koyano-Nakagawa, N. and Kintner, C. (1999). A two-step mechanism generates the spacing pattern of the ciliated cells in the skin of Xenopus embryos. *Development* **126**, 4715-28.

Delattre, M. and Gonczy, P. (2004). The arithmetic of centrosome biogenesis. *J Cell Sci* **117**, 1619-30.

Deryugina, E. I. and Quigley, J. P. (2006). Matrix metalloproteinases and tumor metastasis. *Cancer Metastasis Rev* **25**, 9-34.

Drysdale, T. A. and Elinson, R. P. (1993). Inductive events in the patterning of the Xenopus laevis hatching and cement glands, two cell types which delimit head boundaries. *Dev Biol* **158**, 245-53.

Dubruille, R., Laurencon, A., Vandaele, C., Shishido, E., Coulon-Bublex, M., Swoboda, P., Couble, P., Kernan, M. and Durand, B. (2002). Drosophila regulatory factor X is necessary for ciliated sensory neuron differentiation. *Development* **129**, 5487-98.

Durand, B., Kobr, M., Reith, W. and Mach, B. (1994). Functional complementation of major histocompatibility complex class II regulatory mutants by the purified X-box-binding protein RFX. *Mol Cell Biol* **14**, 6839-47.

Dutcher, S. K. (1995). Flagellar assembly in two hundred and fifty easy-to-follow steps. *Trends Genet* **11**, 398-404.

Dutcher, S. K., Huang, B. and Luck, D. J. (1984). Genetic dissection of the central pair microtubules of the flagella of Chlamydomonas reinhardtii. *J Cell Biol* **98**, 229-36.

Efimenko, E., Bubb, K., Mak, H. Y., Holzman, T., Leroux, M. R., Ruvkun, G., Thomas, J. H. and Swoboda, P. (2005). Analysis of xbx genes in C. elegans. *Development* **132**, 1923-34.

Eggenschwiler, J. T. and Anderson, K. V. (2007). Cilia and developmental signaling. *Annu Rev Cell Dev Biol* **23**, 345-73.

Eley, L., Yates, L. M. and Goodship, J. A. (2005). Cilia and disease. *Curr Opin Genet Dev* **15**, 308-14.

Emery, P., Strubin, M., Hofmann, K., Bucher, P., Mach, B. and Reith, W. (1996). A consensus motif in the RFX DNA binding domain and binding domain mutants with altered specificity. *Mol Cell Biol* **16**, 4486-94.

Essner, J. J., Amack, J. D., Nyholm, M. K., Harris, E. B. and Yost, H. J. (2005). Kupffer's vesicle is a ciliated organ of asymmetry in the zebrafish embryo that initiates left-right development of the brain, heart and gut. *Development* **132**, 1247-60.

Essner, J. J., Vogan, K. J., Wagner, M. K., Tabin, C. J., Yost, H. J. and Brueckner, M. (2002). Conserved function for embryonic nodal cilia. *Nature* **418**, 37-8.

Fawcett, D. W. and Porter, K. R. (1954). A study of the fine structure of ciliated epithelia. *J. Morphology* **94**, 221-282.

Fiuza, U. M. and Arias, A. M. (2007). Cell and molecular biology of Notch. *J Endocrinol* **194**, 459-74.

Fliegauf, M. and Omran, H. (2006). Novel tools to unravel molecular mechanisms in cilia-related disorders. *Trends Genet* **22**, 241-5.

Fristrom, D. (1988). The cellular basis of epithelial morphogenesis. A review. *Tissue Cell* **20**, 645-90.

Fryer, C. J., Lamar, E., Turbachova, I., Kintner, C. and Jones, K. A. (2002). Mastermind mediates chromatin-specific transcription and turnover of the Notch enhancer complex. *Genes Dev* **16**, 1397-411.

Gibbons, I. R. (1961). The relationship between the fine structure and direction of beat in gill cilia of a lamellibranch mollusk. *J Biophys Biochem Cytol* **11**, 179-205.

Gibbons, I. R. and Grimstone, A. V. (1960). On flagellar structure in certain flagellates. *J Biophys Biochem Cytol* **7**, 697-716.

Gilula, N. B. and Satir, P. (1972). The ciliary necklace. A ciliary membrane specialization. *J Cell Biol* **53**, 494-509.

Gomperts, B. N., Gong-Cooper, X. and Hackett, B. P. (2004). Foxj1 regulates basal body anchoring to the cytoskeleton of ciliated pulmonary epithelial cells. *J Cell Sci* **117**, 1329-37.

Greenstone, M. A., Jones, R. W., Dewar, A., Neville, B. G. and Cole, P. J. (1984). Hydrocephalus and primary ciliary dyskinesia. *Arch Dis Child* **59**, 481-2.

Gumbiner, B. (1987). Structure, biochemistry, and assembly of epithelial tight junctions. *Am J Physiol* **253**, C749-58.

Hackett, B. P., Brody, S. L., Liang, M., Zeitz, I. D., Bruns, L. A. and Gitlin, J. D. (1995). Primary structure of hepatocyte nuclear factor/forkhead homologue 4 and characterization of gene expression in the developing respiratory and reproductive epithelium. *Proc Natl Acad Sci U S A* **92**, 4249-53.

Hagiwara, H., Aoki, T., Ohwada, N. and Fujimoto, T. (1997). Development of striated rootlets during ciliogenesis in the human oviduct epithelium. *Cell Tissue Res* **290**, 39-42.

Halestrap, A. P. and Price, N. T. (1999). The proton-linked monocarboxylate transporter (MCT) family: structure, function and regulation. *Biochem J* **343 Pt 2**, 281-99.

Harland, R. M. (1991). In situ hybridization: an improved whole-mount method for Xenopus embryos. *Methods Cell Biol* **36**, 685-95.

Harrison, A. and King, S. M. (2000). The molecular anatomy of dynein. *Essays Biochem* **35**, 75-87.

Hayes, J. M., Kim, S. K., Abitua, P. B., Park, T. J., Herrington, E. R., Kitayama, A., Grow, M. W., Ueno, N. and Wallingford, J. B. (2007). Identification of novel ciliogenesis factors using a new in vivo model for mucociliary epithelial development. *Dev Biol* **312**, 115-30.

Heasman, J. (2002). Morpholino oligos: making sense of antisense? *Dev Biol* **243**, 209-14.

Hirokawa, N., Tanaka, Y., Okada, Y. and Takeda, S. (2006). Nodal flow and the generation of left-right asymmetry. *Cell* **125**, 33-45.

Holzbaur, E. L. and Vallee, R. B. (1994). DYNEINS: molecular structure and cellular function. *Annu Rev Cell Biol* **10**, 339-72.

Huang, B., Ramanis, Z. and Luck, D. J. (1982). Suppressor mutations in Chlamydomonas reveal a regulatory mechanism for Flagellar function. *Cell* **28**, 115-24.

Huang, C. J., Tu, C. T., Hsiao, C. D., Hsieh, F. J. and Tsai, H. J. (2003a). Germ-line transmission of a myocardium-specific GFP transgene reveals critical regulatory elements in the cardiac myosin light chain 2 promoter of zebrafish. *Dev Dyn* **228**, 30-40.

Huang, T., You, Y., Spoor, M. S., Richer, E. J., Kudva, V. V., Paige, R. C., Seiler, M. P., Liebler, J. M., Zabner, J., Plopper, C. G. et al. (2003b). Foxj1 is required for apical localization of ezrin in airway epithelial cells. *J Cell Sci* **116**, 4935-45.

Igakura, T., Kadomatsu, K., Kaname, T., Muramatsu, H., Fan, Q. W., Miyauchi, T., Toyama, Y., Kuno, N., Yuasa, S., Takahashi, M. et al. (1998). A null mutation in basigin, an immunoglobulin superfamily member, indicates its important roles in peri-implantation development and spermatogenesis. *Dev Biol* **194**, 152-65.

Inglis, P. N., Boroevich, K. A. and Leroux, M. R. (2006). Piecing together a ciliome. *Trends Genet* **22**, 491-500.

Jaynes, J. B. and O'Farrell, P. H. (1991). Active repression of transcription by the engrailed homeodomain protein. *Embo J* **10**, 1427-33.

Jenkins, P. M., Hurd, T. W., Zhang, L., McEwen, D. P., Brown, R. L., Margolis, B., Verhey, K. J. and Martens, J. R. (2006). Ciliary targeting of olfactory CNG channels requires the CNGB1b subunit and the kinesin-2 motor protein, KIF17. *Curr Biol* **16**, 1211-6.

Jorissen, M., Willems, T. and Van der Schueren, B. (2000). Ciliary function analysis for the diagnosis of primary ciliary dyskinesia: advantages of ciliogenesis in culture. *Acta Otolaryngol* **120**, 291-5.

Kamiya, R. (2002). Functional diversity of axonemal dyneins as studied in Chlamydomonas mutants. *Int Rev Cytol* **219**, 115-55.

Kanekura, T., Chen, X. and Kanzaki, T. (2002). Basigin (CD147) is expressed on melanoma cells and induces tumor cell invasion by stimulating production of matrix metalloproteinases by fibroblasts. *Int J Cancer* **99**, 520-8.

Keller, R., Davidson, L. A. and Shook, D. R. (2003). How we are shaped: the biomechanics of gastrulation. *Differentiation* **71**, 171-205.

Keller, R. E. (1980). The cellular basis of epiboly: an SEM study of deep-cell rearrangement during gastrulation in Xenopus laevis. *J Embryol Exp Morphol* **60**, 201-34.

Kenny, H. A., Kaur, S., Coussens, L. M. and Lengyel, E. (2008). The initial steps of ovarian cancer cell metastasis are mediated by MMP-2 cleavage of vitronectin and fibronectin. *J Clin Invest* **118**, 1367-79.

Kimmel, C. B., Ballard, W. W., Kimmel, S. R., Ullmann, B. and Schilling, T. F. (1995). Stages of embryonic development of the zebrafish. *Dev Dyn* **203**, 253-310.

Kintner, C. (2003). Notch signaling in vertebrate development.: Oxford: Academic Press.

Kirk, P., Wilson, M. C., Heddle, C., Brown, M. H., Barclay, A. N. and Halestrap, A. P. (2000). CD147 is tightly associated with lactate transporters MCT1 and MCT4 and facilitates their cell surface expression. *Embo J* **19**, 3896-904.

Knecht, A. K., Good, P. J., Dawid, I. B. and Harland, R. M. (1995). Dorsal-ventral patterning and differentiation of noggin-induced neural tissue in the absence of mesoderm. *Development* **121**, 1927-35.

Konig, G. and Hausen, P. (1993). Planar polarity in the ciliated epidermis of Xenopus embryos. *Dev Biol* **160**, 355-68.

Kozminski, K. G., Beech, P. L. and Rosenbaum, J. L. (1995). The Chlamydomonas kinesin-like protein FLA10 is involved in motility associated with the flagellar membrane. *J Cell Biol* **131**, 1517-27.

Kozminski, K. G., Johnson, K. A., Forscher, P. and Rosenbaum, J. L. (1993). A motility in the eukaryotic flagellum unrelated to flagellar beating. *Proc Natl Acad Sci U S A* **90**, 5519-23.

Kramer-Zucker, A. G., Olale, F., Haycraft, C. J., Yoder, B. K., Schier, A. F. and Drummond, I. A. (2005a). Cilia-driven fluid flow in the zebrafish pronephros, brain and Kupffer's vesicle is required for normal organogenesis. *Development* **132**, 1907-21.

Kramer-Zucker, A. G., Olale, F., Haycraft, C. J., Yoder, B. K., Schier, A. F. and Drummond, I. A. (2005b). Cilia-driven fluid flow in the zebrafish pronephros, brain and Kupffer's vesicle is required for normal organogenesis. *Development* **132**, 1907-1921.

Kunwar, P. S., Starz-Gaiano, M., Bainton, R. J., Heberlein, U. and Lehmann, R. (2003). Tre1, a G protein-coupled receptor, directs transepithelial migration of Drosophila germ cells. *PLoS Biol* **1**, E80.

Lamar, E. and Kintner, C. (2005). The Notch targets Esr1 and Esr10 are differentially regulated in Xenopus neural precursors. *Development* **132**, 3619-30.

Li, J. B., Gerdes, J. M., Haycraft, C. J., Fan, Y., Teslovich, T. M., May-Simera, H., Li, H., Blacque, O. E., Li, L., Leitch, C. C. et al. (2004). Comparative genomics identifies a flagellar and basal body proteome that includes the BBS5 human disease gene. *Cell* **117**, 541-52.

Li, R., Huang, L., Guo, H. and Toole, B. P. (2001). Basigin (murine EMMPRIN) stimulates matrix metalloproteinase production by fibroblasts. *J Cell Physiol* **186**, 371-9.

Lim, L., Zhou, H. and Costa, R. H. (1997). The winged helix transcription factor HFH-4 is expressed during choroid plexus epithelial development in the mouse embryo. *Proc Natl Acad Sci U S A* **94**, 3094-9.

Lin, B., Wang, S. W. and Masland, R. H. (2004). Retinal ganglion cell type, size, and spacing can be specified independent of homotypic dendritic contacts. *Neuron* **43**, 475-85.

Liu, Y., Pathak, N., Kramer-Zucker, A. and Drummond, I. A. (2007). Notch signaling controls the differentiation of transporting epithelia and multiciliated cells in the zebrafish pronephros. *Development* **134**, 1111-22.

Longo, D., Peirce, S. M., Skalak, T. C., Davidson, L., Marsden, M., Dzamba, B. and DeSimone, D. W. (2004). Multicellular computer simulation of morphogenesis: blastocoel roof thinning and matrix assembly in Xenopus laevis. *Dev Biol* **271**, 210-22.

Luck, D., Piperno, G., Ramanis, Z. and Huang, B. (1977). Flagellar mutants of Chlamydomonas: studies of radial spoke-defective strains by dikaryon and revertant analysis. *Proc Natl Acad Sci U S A* **74**, 3456-60.

Luscinskas, F. W., Ma, S., Nusrat, A., Parkos, C. A. and Shaw, S. K. (2002a). Leukocyte transendothelial migration: a junctional affair. *Semin Immunol* **14**, 105-13.

Luscinskas, F. W., Ma, S., Nusrat, A., Parkos, C. A. and Shaw, S. K. (2002b). The role of endothelial cell lateral junctions during leukocyte trafficking. *Immunol Rev* **186**, 57-67.

Lyons, R. A., Saridogan, E. and Djahanbakhch, O. (2006). The reproductive significance of human Fallopian tube cilia. *Hum Reprod Update* **12**, 363-72.

Manton, I. and Clarke, B. (1950). Electron microscope observations on the spermatozoid of Fucus. *Nature* **166**, 973-4.

Marshall, W. F. and Kintner, C. (2008). Cilia orientation and the fluid mechanics of development. *Curr Opin Cell Biol* **20**, 48-52.

Mastronarde, D. N., O'Toole, E. T., McDonald, K. L., McIntosh, J. R. and Porter, M. E. (1992). Arrangement of inner dynein arms in wild-type and mutant flagella of Chlamydomonas. *J Cell Biol* **118**, 1145-62.

McGrath, J., Somlo, S., Makova, S., Tian, X. and Brueckner, M. (2003). Two populations of node monocilia initiate left-right asymmetry in the mouse. *Cell* **114**, 61-73.

Menco, B. P. and Farbman, A. I. (1985). Genesis of cilia and microvilli of rat nasal epithelia during pre-natal development. II. Olfactory epithelium, a morphometric analysis. *J Cell Sci* **78**, 311-36.

Merzdorf, C. S. and Goodenough, D. A. (1997). Localization of a novel 210 kDa protein in Xenopus tight junctions. *J Cell Sci* **110 (Pt 8)**, 1005-12.

Mistretta, C. M. and Liu, H. X. (2006). Development of fungiform papillae: patterned lingual gustatory organs. *Arch Histol Cytol* **69**, 199-208.

Mitchell, B., Jacobs, R., Li, J., Chien, S. and Kintner, C. (2007). A positive feedback mechanism governs the polarity and motion of motile cilia. *Nature* **447**, 97-101.

Miyauchi, T., Kanekura, T., Yamaoka, A., Ozawa, M., Miyazawa, S. and Muramatsu, T. (1990). Basigin, a new, broadly distributed member of the immunoglobulin superfamily, has strong homology with both the immunoglobulin V domain and the beta-chain of major histocompatibility complex class II antigen. *J Biochem* **107**, 316-23.

Montorzi, M., Burgos, M. H. and Falchuk, K. H. (2000). Xenopus laevis embryo development: arrest of epidermal cell differentiation by the chelating agent 1,10-phenanthroline. *Mol Reprod Dev* **55**, 75-82.

Munger, B. L. and Ide, C. (1988). The structure and function of cutaneous sensory receptors. *Arch Histol Cytol* **51**, 1-34.

Muramatsu, T. and Miyauchi, T. (2003). Basigin (CD147): a multifunctional transmembrane protein involved in reproduction, neural function, inflammation and tumor invasion. *Histol Histopathol* **18**, 981-7.

Nagase, H. and Woessner, J. F., Jr. (1999). Matrix metalloproteinases. *J Biol Chem* **274**, 21491-4.

Nasevicius, A. and Ekker, S. C. (2000). Effective targeted gene 'knockdown' in zebrafish. *Nat Genet* **26**, 216-20.

Nieuwkoop, P. D. and Faber, J. (1967). Normal table of *Xenopus laevis*.

Nonaka, S., Tanaka, Y., Okada, Y., Takeda, S., Harada, A., Kanai, Y., Kido, M. and Hirokawa, N. (1998). Randomization of left-right asymmetry due to loss of nodal cilia generating leftward flow of extraembryonic fluid in mice lacking KIF3B motor protein. *Cell* **95**, 829-37.

Obara, T., Mangos, S., Liu, Y., Zhao, J., Wiessner, S., Kramer-Zucker, A. G., Olale, F., Schier, A. F. and Drummond, I. A. (2006). Polycystin-2 immunolocalization and function in zebrafish. *J Am Soc Nephrol* **17**, 2706-18.

Omoto, C. K. and Kung, C. (1980). Rotation and twist of the central-pair microtubules in the cilia of Paramecium. *J Cell Biol* **87**, 33-46.

Ostrowski, L. E., Blackburn, K., Radde, K. M., Moyer, M. B., Schlatzer, D. M., Moseley, A. and Boucher, R. C. (2002). A proteomic analysis of human cilia: identification of novel components. *Mol Cell Proteomics* **1**, 451-65.

Pan, J. and Snell, W. (2007). The primary cilium: keeper of the key to cell division. *Cell* **129**, 1255-7.

Pan, J., You, Y., Huang, T. and Brody, S. L. (2007). RhoA-mediated apical actin enrichment is required for ciliogenesis and promoted by Foxj1. *J Cell Sci* **120**, 1868-76.

Park, T. J., Haigo, S. L. and Wallingford, J. B. (2006). Ciliogenesis defects in embryos lacking inturned or fuzzy function are associated with failure of planar cell polarity and Hedgehog signaling. *Nat Genet* **38**, 303-11.

Pazour, G. J., Agrin, N., Leszyk, J. and Witman, G. B. (2005). Proteomic analysis of a eukaryotic cilium. *J Cell Biol* **170**, 103-13.

Pazour, G. J., Wilkerson, C. G. and Witman, G. B. (1998). A dynein light chain is essential for the retrograde particle movement of intraflagellar transport (IFT). *J Cell Biol* **141**, 979-92.

Pazour, G. J. and Witman, G. B. (2003). The vertebrate primary cilium is a sensory organelle. *Curr Opin Cell Biol* **15**, 105-10.

Pelletier, G. J., Brody, S. L., Liapis, H., White, R. A. and Hackett, B. P. (1998). A human forkhead/winged-helix transcription factor expressed in developing pulmonary and renal epithelium. *Am J Physiol* **274**, L351-9.

Perez-Moreno, M., Jamora, C. and Fuchs, E. (2003). Sticky business: orchestrating cellular signals at adherens junctions. *Cell* **112**, 535-48.

Picard, D. and Yamamoto, K. R. (1987). Two signals mediate hormone-dependent nuclear localization of the glucocorticoid receptor. *Embo J* **6**, 3333-40.

Piperno, G., Huang, B. and Luck, D. J. (1977). Two-dimensional analysis of flagellar proteins from wild-type and paralyzed mutants of Chlamydomonas reinhardtii. *Proc Natl Acad Sci U S A* **74**, 1600-4.

Plattner, H. (2002). My favorite cell--Paramecium. *Bioessays* **24**, 649-58.

Pohl, B. S. and Knochel, W. (2004). Isolation and developmental expression of Xenopus FoxJ1 and FoxK1. *Dev Genes Evol* **214**, 200-5.

Poole, R. C. and Halestrap, A. P. (1997). Interaction of the erythrocyte lactate transporter (monocarboxylate transporter 1) with an integral 70-kDa membrane glycoprotein of the immunoglobulin superfamily. *J Biol Chem* **272**, 14624-8.

Porter, J. C. (2008). Epithelial rho GTPases and the transepithelial migration of lymphocytes. *Methods Enzymol* **439**, 205-17.

Qi, M., Hamilton, B. J. and DeFranco, D. (1989). v-mos oncoproteins affect the nuclear retention and reutilization of glucocorticoid receptors. *Mol Endocrinol* **3**, 1279-88.

Raya, A., Koth, C. M., Buscher, D., Kawakami, Y., Itoh, T., Raya, R. M., Sternik, G., Tsai, H. J., Rodriguez-Esteban, C. and Izpisua-Belmonte, J. C. (2003). Activation of Notch signaling pathway precedes heart regeneration in zebrafish. *Proc Natl Acad Sci U S A* **100 Suppl 1**, 11889-95.

Rice, L. M. and Agard, D. A. (2002). Centriole duplication: centrin in on answers? *Curr Biol* **12**, R618-9.

Rivera, J. (1962). Cilia, Ciliated Epithelia and Ciliary Activity. Oxford, New York: Pergamon Press.

Rosenbaum, J. L. and Witman, G. B. (2002). Intraflagellar transport. *Nat Rev Mol Cell Biol* **3**, 813-25.

Salisbury, J. L. (2004). Primary cilia: putting sensors together. *Curr Biol* **14**, R765-7.

Sapiro, R., Kostetskii, I., Olds-Clarke, P., Gerton, G. L., Radice, G. L. and Strauss, I. J. (2002). Male infertility, impaired sperm motility, and hydrocephalus in mice deficient in sperm-associated antigen 6. *Mol Cell Biol* **22**, 6298-305.

Satir, P. and Christensen, S. T. (2007). Overview of structure and function of mammalian cilia. *Annu Rev Physiol* **69**, 377-400.

Satir, P., Guerra, C. and Bell, A. J. (2007). Evolution and persistence of the cilium. *Cell Motil Cytoskeleton* **64**, 906-13.

Schlosshauer, B., Bauch, H. and Frank, R. (1995). Neurothelin: amino acid sequence, cell surface dynamics and actin colocalization. *Eur J Cell Biol* **68**, 159-66.

Schlosshauer, B. and Herzog, K. H. (1990). Neurothelin: an inducible cell surface glycoprotein of blood-brain barrier-specific endothelial cells and distinct neurons. *J Cell Biol* **110**, 1261-74.

Schock, F. and Perrimon, N. (2002). Molecular mechanisms of epithelial morphogenesis. *Annu Rev Cell Dev Biol* **18**, 463-93.

Scholey, J. M. (2008). Intraflagellar transport motors in cilia: moving along the cell's antenna. *J Cell Biol* **180**, 23-9.

Schweickert, A., Weber, T., Beyer, T., Vick, P., Bogusch, S., Feistel, K. and Blum, M. (2007). Cilia-driven leftward flow determines laterality in Xenopus. *Curr Biol* **17**, 60-6.

Shook, D. R., Majer, C. and Keller, R. (2004). Pattern and morphogenesis of presumptive superficial mesoderm in two closely related species, Xenopus laevis and Xenopus tropicalis. *Dev Biol* **270**, 163-85.

Siegrist, C. A. and Mach, B. (1993). Antisense oligonucleotides specific for regulatory factor RFX-1 inhibit inducible but not constitutive expression of all major histocompatibility complex class II genes. *Eur J Immunol* **23**, 2903-8.

Singla, V. and Reiter, J. F. (2006). The primary cilium as the cell's antenna: signaling at a sensory organelle. *Science* **313**, 629-33.

Sive, H. L., Grainger, R. M. and Harland, R. M. (2000). Early Development of *Xenopus laevis*: A Laboratory Manual: Cold Spring Harbor Laboratory Press.

Smith, E. F. and Lefebvre, P. A. (1997). The role of central apparatus components in flagellar motility and microtubule assembly. *Cell Motil Cytoskeleton* **38**, 1-8.

Smith, E. F. and Sale, W. S. (1992). Regulation of dynein-driven microtubule sliding by the radial spokes in flagella. *Science* **257**, 1557-9.

Smith, J. C., Northey, J. G., Garg, J., Pearlman, R. E. and Siu, K. W. (2005). Robust method for proteome analysis by MS/MS using an entire translated genome: demonstration on the ciliome of Tetrahymena thermophila. *J Proteome Res* **4**, 909-19.

Snow, J. J., Ou, G., Gunnarson, A. L., Walker, M. R., Zhou, H. M., Brust-Mascher, I. and Scholey, J. M. (2004). Two anterograde intraflagellar transport motors cooperate to build sensory cilia on C. elegans neurons. *Nat Cell Biol* **6**, 1109-13.

Sorokin, S. P. (1968). Centriole formation and ciliogenesis. *Aspen Emphysema Conf* **11**, 213-6.

Sparrow, D. B., Latinkic, B. and Mohun, T. J. (2000). A simplified method of generating transgenic Xenopus. *Nucleic Acids Res* **28**, E12.

Spektor, A., Tsang, W. Y., Khoo, D. and Dynlacht, B. D. (2007). Cep97 and CP110 suppress a cilia assembly program. *Cell* **130**, 678-90.

Stannard, W. and O'Callaghan, C. (2006). Ciliary function and the role of cilia in clearance. *J Aerosol Med* **19**, 110-5.

Stefanidakis, M. and Koivunen, E. (2006). Cell-surface association between matrix metalloproteinases and integrins: role of the complexes in leukocyte migration and cancer progression. *Blood* **108**, 1441-50.

Steimle, V., Durand, B., Barras, E., Zufferey, M., Hadam, M. R., Mach, B. and Reith, W. (1995). A novel DNA-binding regulatory factor is mutated in primary MHC class II deficiency (bare lymphocyte syndrome). *Genes Dev* **9**, 1021-32.

Steinman, R. M. (1968). An electron microscopic study of ciliogenesis in developing epidermis and trachea in the embryo of Xenopus laevis. *Am J Anat* **122**, 19-55.

Stolc, V., Samanta, M. P., Tongprasit, W. and Marshall, W. F. (2005). Genome-wide transcriptional analysis of flagellar regeneration in Chlamydomonas reinhardtii identifies orthologs of ciliary disease genes. *Proc Natl Acad Sci U S A* **102**, 3703-7.

Stubbs, J. L., Davidson, L., Keller, R. and Kintner, C. (2006). Radial intercalation of ciliated cells during Xenopus skin development. *Development* **133**, 2507-15.

Stupack, D. G. (2007). The biology of integrins. *Oncology (Williston Park)* **21**, 6-12.

Sui, H. and Downing, K. H. (2006). Molecular architecture of axonemal microtubule doublets revealed by cryo-electron tomography. *Nature* **442**, 475-8.

Supp, D. M., Potter, S. S. and Brueckner, M. (2000). Molecular motors: the driving force behind mammalian left-right development. *Trends Cell Biol* **10**, 41-5.

Supp, D. M., Witte, D. P., Potter, S. S. and Brueckner, M. (1997). Mutation of an axonemal dynein affects left-right asymmetry in inversus viscerum mice. *Nature* **389**, 963-6.

Swoboda, P., Adler, H. T. and Thomas, J. H. (2000). The RFX-type transcription factor DAF-19 regulates sensory neuron cilium formation in C. elegans. *Mol Cell* **5**, 411-21.

Takeda, S., Yonekawa, Y., Tanaka, Y., Okada, Y., Nonaka, S. and Hirokawa, N. (1999). Left-right asymmetry and kinesin superfamily protein KIF3A: new insights in determination of laterality and mesoderm induction by kif3A-/- mice analysis. *J Cell Biol* **145**, 825-36.

Tanaka, H., Iguchi, N., Toyama, Y., Kitamura, K., Takahashi, T., Kaseda, K., Maekawa, M. and Nishimune, Y. (2004). Mice deficient in the axonemal protein Tektin-t exhibit male infertility and immotile-cilium syndrome due to impaired inner arm dynein function. *Mol Cell Biol* **24**, 7958-64.

Tanaka, Y., Okada, Y. and Hirokawa, N. (2005). FGF-induced vesicular release of Sonic hedgehog and retinoic acid in leftward nodal flow is critical for left-right determination. *Nature* **435**, 172-7.

Taylor, P. M., Woodfield, R. J., Hodgkin, M. N., Pettitt, T. R., Martin, A., Kerr, D. J. and Wakelam, M. J. (2002). Breast cancer cell-derived EMMPRIN stimulates fibroblast MMP2 release through a phospholipase A(2) and 5-lipoxygenase catalyzed pathway. *Oncogene* **21**, 5765-72.

Teilmann, S. C. and Christensen, S. T. (2005). Localization of the angiopoietin receptors Tie-1 and Tie-2 on the primary cilia in the female reproductive organs. *Cell Biol Int* **29**, 340-6.

Teilmann, S. C., Clement, C. A., Thorup, J., Byskov, A. G. and Christensen, S. T. (2006). Expression and localization of the progesterone receptor in mouse and human reproductive organs. *J Endocrinol* **191**, 525-35.

Thisse, C., Thisse, B., Halpern, M. E. and Postlethwait, J. H. (1994). Goosecoid expression in neurectoderm and mesendoderm is disrupted in zebrafish cyclops gastrulas. *Dev Biol* **164**, 420-9.

Tichelaar, J. W., Wert, S. E., Costa, R. H., Kimura, S. and Whitsett, J. A. (1999). HNF-3/forkhead homologue-4 (HFH-4) is expressed in ciliated epithelial cells in the developing mouse lung. *J Histochem Cytochem* **47**, 823-32.

Tilney, L. G., Hatano, S., Ishikawa, H. and Mooseker, M. S. (1973). The polymerization of actin: its role in the generation of the acrosomal process of certain echinoderm sperm. *J Cell Biol* **59**, 109-26.

Turner, D. L. and Weintraub, H. (1994). Expression of achaete-scute homolog 3 in Xenopus embryos converts ectodermal cells to a neural fate. *Genes Dev* **8**, 1434-47.

Vasioukhin, V., Bauer, C., Yin, M. and Fuchs, E. (2000). Directed actin polymerization is the driving force for epithelial cell-cell adhesion. *Cell* **100**, 209-19.

Wallingford, J. B., Fraser, S. E. and Harland, R. M. (2002). Convergent extension: the molecular control of polarized cell movement during embryonic development. *Dev Cell* **2**, 695-706.

Wargo, M. J., McPeek, M. A. and Smith, E. F. (2004). Analysis of microtubule sliding patterns in Chlamydomonas flagellar axonemes reveals dynein activity on specific doublet microtubules. *J Cell Sci* **117**, 2533-44.

Warner, F. D. (1976). Ciliary inter-microtubule bridges. *J Cell Sci* **20**, 101-14.

Webster, N. J., Green, S., Jin, J. R. and Chambon, P. (1988). The hormone-binding domains of the estrogen and glucocorticoid receptors contain an inducible transcription activation function. *Cell* **54**, 199-207.

Wedaman, K. P., Meyer, D. W., Rashid, D. J., Cole, D. G. and Scholey, J. M. (1996). Sequence and submolecular localization of the 115-kD accessory subunit of the heterotrimeric kinesin-II (KRP85/95) complex. *J Cell Biol* **132**, 371-80.

Wheatley, D. N., Wang, A. M. and Strugnell, G. E. (1996). Expression of primary cilia in mammalian cells. *Cell Biol Int* **20**, 73-81.

Whitsett, J. A. and Tichelaar, J. W. (1999). Forkhead transcription factor HFH-4 and respiratory epithelial cell differentiation. *Am J Respir Cell Mol Biol* **21**, 153-4.

Williams, A. F. and Barclay, A. N. (1988). The immunoglobulin superfamily--domains for cell surface recognition. *Annu Rev Immunol* **6**, 381-405.

Williams, O. W., Sharafkhaneh, A., Kim, V., Dickey, B. F. and Evans, C. M. (2006). Airway mucus: From production to secretion. *Am J Respir Cell Mol Biol* **34**, 527-36.

Witman, G. B., Plummer, J. and Sander, G. (1978). Chlamydomonas flagellar mutants lacking radial spokes and central tubules. Structure, composition, and function of specific axonemal components. *J Cell Biol* **76**, 729-47.

Xie, X., Mikkelsen, T. S., Gnirke, A., Lindblad-Toh, K., Kellis, M. and Lander, E. S. (2007). Systematic discovery of regulatory motifs in conserved regions of the human genome, including thousands of CTCF insulator sites. *Proc Natl Acad Sci U S A* **104**, 7145-50.

Yoshida, S., Shibata, M., Yamamoto, S., Hagihara, M., Asai, N., Takahashi, M., Mizutani, S., Muramatsu, T. and Kadomatsu, K. (2000). Homo-oligomer formation by basigin, an immunoglobulin superfamily member, via its N-terminal immunoglobulin domain. *Eur J Biochem* **267**, 4372-80.

You, Y., Huang, T., Richer, E. J., Schmidt, J. E., Zabner, J., Borok, Z. and Brody, S. L. (2004). Role of f-box factor foxj1 in differentiation of ciliated airway epithelial cells. *Am J Physiol Lung Cell Mol Physiol* **286**, L650-7.

Zapala, M. A., Lockhart, D. J., Pankratz, D. G., Garcia, A. J., Barlow, C. and Lockhart, D. J. (2002). Software and methods for oligonucleotide and cDNA array data analysis. *Genome Biol* **3**, SOFTWARE0001.

Zariwala, M. A., Knowles, M. R. and Omran, H. (2007). Genetic defects in ciliary structure and function. *Annu Rev Physiol* **69**, 423-50.

Zhang, D., Stumpo, D. J., Graves, J. P., DeGraff, L. M., Grissom, S. F., Collins, J. B., Li, L., Zeldin, D. C. and Blackshear, P. J. (2006). Identification of potential target genes for RFX4_v3, a transcription factor critical for brain development. *J Neurochem* **98**, 860-75.

Zhang, J., Houston, D. W., King, M. L., Payne, C., Wylie, C. and Heasman, J. (1998). The role of maternal VegT in establishing the primary germ layers in Xenopus embryos. *Cell* **94**, 515-24.

Zhang, M., Bolfing, M. F., Knowles, H. J., Karnes, H. and Hackett, B. P. (2004). Foxj1 regulates asymmetric gene expression during left-right axis patterning in mice. *Biochem Biophys Res Commun* **324**, 1413-20.